Assessment of TRAIL sensitisation by IAP antagonist TL32711 in malignant melanoma and development of a framework for response prediction

Von der Fakultät Energie-, Verfahrens- und Biotechnik der Universität Stuttgart
zur Erlangung der Würde eines Doktors der Naturwissenschaften (Dr. rer. nat.)
genehmigte Abhandlung

Vorgelegt von

Vesna Vetma

aus Split, Kroatien

Hauptberichter: Prof. Dr. Markus Morrison

Mitberichter: Prof. Dr. Dagmar Kulms

Tag der mündlichen Prüfung: 3.7.2019.

Institut für Zellbiologie und Immunologie der Universität Stuttgart

2020

Table of Contents

TABLE OF CONTENTS

Abbreviations

2D	two dimensional
3D	three dimensional
AIDS	acquired immune deficency syndrome
Alanine-Valine-Proline-Isoleucine	AVPI (sequence)
amp	ampicillin
ANOVA	analysis of variance
Apaf1	apoptotic protease-activating factor 1
APC	allophycocyanin
Apo2L	Apo2 ligand
ATCC	American Type Cell Culture Collections
AU	absorbance unit
BAD	BCL-2 antagonist of cell death
Bak	BCL-2 antagonist or killer
Bax	BCL-2-associated X protein
Bcl-2	B cell lymphoma 2
Bcl-xl	BCL extra large
BH3	BCL-2 homology 3
Bid	BH3-interacting domain death agonist
BIR	baculovirus IAP repeat
BRAF	homolog B1 rapidly accelerated fibrosarcoma
BSA	bovine serum albumin
CAD	Caspase-activated DNase
CARD	caspase activation and recruitment domain
Caspase	aspartate-specific cysteine protease
CD40L	cluster of differentiation 40 ligand
CD95	cluster of differentiation 95
cFLIP	cellular FLICE-like inhibitory protein
cFLIPL	cFLIP-long
cFLIPR	cFLIP-Raji
cFLIPS	cFLIP-short
CI	combination index
cIAP1	cellular IAP1
cIAP2	cellular IAP2
CpG	cytosine-guanine
CTLA-4	Cytotoxic T-lymphocyte antigen
Cyt C	cytochrome C
dATP	deoxyadenosin triphosphate
DcR	decoy receptor
ddH20	bidistilled water
DED	death effector domain
DIABLO	direct inhibitor of apoptosis binding protein with low pI
DISC	death-inducing signaling complex

ABBREVIATIONS

DMSO	dimethyl sulfoxide
DMSZ	German Collection of Microorganisms and Cell Cultures
DNA	deoxyribonucleic acid
DR	death receptor
DTIC	Dacarbazine
DTT	dithiothreitol
e.g.	exempli gratia – for example
EGFR	epidermal growth factor receptor
EGFR	epidermal growth factor
EpCAM	epitellial cell adhesion molecule
et al.	et alii (and others)
FADD	Fas-associated death domain protein
FAMM	familial atypical multiple mole-melanoma syndrome
FAS	fibroblast associated surface antigen, also known as CD95
FasL	Fas ligand
FBS	fetal bovine serum
Fc	fragment crystallizable
FDA	Food and Drugs Administration
FITC	fluorescein isothiocyanate
FLAG-tag	DYKDDDDK-tag
FLICE	FADD-like interleukin-1β-converting enzyme
GFP	green fluorescent protein
glc	glucose
GPI	glycosylphosphatidylinositol (anchor)
HEK	human embryonic kidney
HER	human epidermal growth factor
HPLC	high-performance liquid chromatography
HRP	horseradish peroxidase
i.p.	intraperitoneally
i.v.	intravenously
IAP	inhibitor of apoptosis
IBM	IAP binding motif
Ig	immunoglobulin
ILI	Isolated limb infusion
ILP	Isolated limb perfusion
IRES	internal ribosome entry site
IZI	Institute of Cell Biology and Immunology
IκBα	nuclear factor of kappa light polypeptide gene enhancer in B cells inhibitor alpha
kDa	kilo Dalton
LB	Luria-Bertani
LDA	linear discriminant analysis
LOOCV	leave one out cross-validation
LPS	lipopolysaccharide
LUBAC	linear ubiquitin chain assembly complex
LUBAC	linear ubiquitin chain assembly complex

MAPK	mitogen-activated protein kinase
MAS	melanoma-astrocytoma syndrome
MC1R	Melanocortin 1 receptor
Mcl-1	myeloid cell leukaemia 1
MEK	mitogen activated protein kinase kinase
ML-IAP	melanoma IAP
MOM	mitochondrial outer membrane
MOMP	MOM permeabilisation
NEMO	NF-κB essential modulator
NF-κB	nuclear factor κ-light-chain enhancer of activated B cells
NIAP	neuronal IAP
NIK	NFκβ-inducing kinase
NLR	nucleotide-binding oligomerization domain and leucine-rich repeat-containing receptors
NLRP3	NLR Family Pyrin Domain Containing 3
NRAS	neuroblastoma rat sarcoma
NS	not significant
ODE	ordinary differential equations
OPG	osteoprotegerin
OS	overall survival
PAGE	polyacril amid gel electrophoresis
PARP	poly (ADP-ribose) polymerase
PBA	Phosphate buffered saline (PBS), 2 % (v/v) FBS, 0.02 % (w/v) NaN$_3$
PBS	phosphate buffered saline
PBST	PBS with TWEEN 20
PCA	principal component analysis
PD-1	programmed death-1
PDE	partial differential equations
PD-L1	programmed death ligand
PD-L1	Programmed death ligand -1
PEI	polyetilenimin
PFS	progression-free survival
PI	propidium iodide
QVD OPh	5-(2,6-Difluorophenoxy)-3-[[3-methyl-1-oxo-2-[(2-quinolinylcarbonyl) amino] butyl] amino]-4-oxo-pentanoic acid hydrate
RAF	rapidly accelerated fibrosarcoma
rh	Recombinant human
RING	really interesting new gene finger domain
RIP1/3	receptor-interacting protein 1/3
RPMI	Roswell Park Memorial Institute
s.c.	subcutaneously
sc	single-chain
SCID	severe combined immunodeficiency disease
SD	standard deviation
SDS	sodium dodecyl sulfate

ABBREVIATIONS

SEC	size exclusion chromatography
SMAC	second mitochondria-derived activator of caspases
SYS ACT	Systems simulations for the personalization and optimization of anti-cancer treatments
TAA	tumour-associated antigens
TAK1	TGF-β-activated kinase 1
TAK1	transforming growth factor β-activated kinase 1
tBid	truncated BID
TBST	tris-buffered saline and Tween
TGF β	transforming growth factor β
TNF	tumour necrosis factor
TNF-R	TNF receptor
TNFRSF	TNF receptor superfamily
TNFSF	TNF superfamily
TRADD	TNF receptor-associated death domain protein
TRAF2	TNF receptor-associated factor 2
TRAIL	tumour necrosis factor-related apoptosis-inducing ligand
TRAIL-R	TRAIL receptor
Tris	Tris(hydroxymethyl)aminomethane
TWEAK	tumour necrosis factor-like weak inducer of apoptosis
USP	ubiquitin specific protease
UV	ultraviolet light
v/v	volume/volume
VH	variable domain of the heavy chain
VL	variable domain of the light chain
w/v	weight/volume
WT	wild type
XIAP	X-linked inhibitor of apoptosis protein

Abstract

Despite the availability of different therapeutic options, large numbers of melanoma patients still do not respond to treatment or experience disease recurrence. Therefore, there is a need to develop novel therapeutics and identify those patients who would benefit most from such therapies. Inducing apoptosis with the cytokine tumour necrosis factor (TNF)-related apoptosis-inducing ligand (TRAIL) is a promising way of eliminating cancer cells as it solely activates cell death in malignant tissue. Due to this specificity, recombinant TRAIL and agonistic antibodies against TRAIL receptor 1 and 2 have been tested in clinical trials, however only with limited success. Besides low stability in serum and low efficacy in crosslinking receptors, TRAIL-based therapy also failed due to the intrinsic resistance of cancer cells caused by upregulation of anti-apoptotic proteins. Therefore, in this study, a novel 2nd generation TRAIL receptor agonist, IZI1551, with improved stability and increased valency was used to investigate apoptosis induction in melanoma cell lines. In addition, to sensitise cells to TRAIL-induced apoptosis, IZI1551 was combined with Birinapant, a SMAC mimetic designed to degrade anti-apoptotic IAP proteins. The combination treatment was tested in a large melanoma cell line panel, covering different mutation status and different disease stages. Furthermore, results of these experiments together with data about the expression of apoptosis-related proteins were used to predict the responsiveness of melanoma to the treatment. Across the cell line panel, high heterogeneity in responsiveness was observed, ranging from complete resistance against the combination treatment with TRAIL and Birinapant to pronounced synergies between the two drugs. More specifically, the combination treatment induced apoptosis in 12/16 melanoma cell lines, 4/5 3D spheroids and 3/5 patient-derived melanoma cell lines.

It was shown in this work that Birinapant efficiently depleted cIAP1 in the first hour of treatment and that depletion lasted for at least 24 h. This, in consistency with current literature available, most likely caused synergistic cell death in melanoma cell lines when treated with Birinapant in combination with IZI1551. Previous studies showed that the responsiveness of the cell lines to TRAIL could not be concluded from the expression of individual apoptosis proteins. Therefore, in this study, a data-driven modelling strategy was devised with the aim to classify cells according to their responsiveness to the combination

ABSTRACT

treatment with IZI1551 and Birinapant. For that, the basal expression of 19 cell death regulators, known to be relevant for the responsiveness to IZI1551 was determined and included in the model. Indeed, by using multivariate statistics, responsive cell lines could be separated from low-responding cell lines with 87.5% accuracy while responsiveness predictions achieved 81.25% accuracy. Predictive capacity of the model was validated for 3D growth conditions (80% accuracy, n=5), patient-derived melanoma cell lines (100%, n=5) and melanoma cell lines grown as xenografts (100%, n=4). Taken together, the combination treatment with IZI1551 and Birinapant induced apoptosis in the majority of melanoma cell lines, 3D melanoma spheroids and patient-derived melanoma cell lines. Moreover, responders and non-responders were successfully identified based on their apoptosis protein expression profiles by using data-driven modelling. In conclusion, the capability to predict responsiveness to combinations of TRAIL receptor agonists and SMAC mimetics might provide an avenue for the future development of personalized treatment strategies based on these targeted therapeutics.

Zusammenfassung

Trotz der Verfügbarkeit verschiedener Therapiemöglichkeiten spricht eine große Anzahl von Melanompatienten noch immer nicht auf eine Behandlung an oder erleidet ein Rezidiv. Daher besteht eine große Notwendigkeit, neuartige Therapeutika zu entwickeln und diejenigen Patienten zu identifizieren, welche von solchen Therapien am meisten profitieren würden. Die Induktion von Apoptose mittels des Zytokins „tumour necrosis factor (TNF)-related apoptosis-inducing ligand (TRAIL)" stellt einen vielversprechenden Weg dar Krebszellen zu eliminieren, da TRAIL ausschließlich den Zelltod in malignen Geweben aktiviert. Aufgrund dieser Spezifität wurde rekombinantes TRAIL und agonistische Antikörper gegen die TRAIL-Rezeptoren 1 und 2 in klinischen Studien gegen solide Tumoure getestet, jedoch nur mit begrenztem Erfolg. Neben einer geringen Stabilität im Serum und einer geringen Wirksamkeit bei der Vernetzung von Rezeptoren versagte die Therapie auf TRAIL-Basis auch aufgrund der intrinsischen Resistenz von Krebszellen, welche durch die Hochregulierung von anti-apoptotischen Proteinen verursacht wird. Daher wurde in dieser Studie ein neuartiger TRAIL-Rezeptor-Agonist der zweiten Generation, IZI1551, mit verbesserter Stabilität und erhöhter Valenz verwendet, um Apoptose in Melanomzelllinien zu induzieren. Außerdem wurde IZI1551 mit Birinapant kombiniert, einem SMAC-Mimetikum, das entwickelt wurde, um Anti-Apoptose-IAP-Proteine abzubauen, wodurch Melanomzellinien für IZI1551-induzierte Apoptose sensibilisiert werden können. Die Kombinationstherapie wurde in einem großen Melanomzelllinien-Panel getestet, das die unterschiedlichen Mutationsstatusse sowie verschiedene Krankheitsstadien abdeckt. Darüber hinaus wurden Ergebnisse dieser Experimente zusammen mit Daten zur Proteinexpression verwendet, um die Sensitivität von Melanomen auf die Behandlung vorherzusagen. Innerhalb des gesamten Zelllinienpanels wurde eine hohe Heterogenität in der Sensitivität beobachtet, welche von vollständiger Resistenz gegen die Kombinationsbehandlung mit IZI1551 und Birinapant bis zu ausgeprägten Synergien zwischen den beiden Arzneimitteln reichte. Es wurde gezeigt, dass die Synergie zwischen IZI1551 und Birinapant auf den schnellen Abbau von cIAP1 durch Birinapant zurückzuführen ist, wodurch Melanomzellen für IZI1551-induzierte Apoptose sensibilisiert werden. Da aus der Expression einzelner Apoptoseproteine nicht auf die Reaktionsfähigkeit der jeweiligen

ZUSSAMMENFASSUNG

Zelllinien geschlossen werden konnte, wurde eine datenbasierte Modellierungsstrategie entwickelt, mit dem Ziel Antwortsynergien vorherzusagen. Dazu wurde die basale Expression von 19 Zelltodregulatoren bestimmt, welche bekanntermaßen für die Reaktion auf TRAIL und Birinapant relevant sind, und in das Modell aufgenommen. Durch die Verwendung von multivariater Statistik konnten sensitive Zelllinien mit 87.5% Genauigkeit von nicht reagierenden Zelllinien getrennt werden, während Synergievorhersagen eine Genauigkeit von 81.25% erreichten. Die Vorhersagefähigkeit des Modells wurde für 3D-Wachstumsbedingungen (80% Genauigkeit, n = 5), von Patienten erhaltene Melanomzelllinien (100%, n = 5) und Melanomzelllinien, die als Xenotransplantate gezüchtet wurden (100%, n = 4), validiert. Zusammenfassend kann gesagt werden, dass die Fähigkeit Sensitivität auf Kombinationen von TRAIL-Rezeptor-Agonisten und SMAC-Mimetika vorherzusagen, einen Weg für die zukünftige Entwicklung personalisierter Behandlungsstrategien auf der Grundlage dieser zielgerichteten Therapeutika bieten kann.

1 Introduction

1.1 Melanoma

Melanocytes are cells of neural crest origin that can be found in the basal epidermis, hair follicles, mucosal surfaces, meninges and in the choroidal layer of the eye. In response to UV-light, melanocytes produce and release the pigment melanin that absorbs visible and ultraviolet light and therefore serves as a protection from UV-induced deoxyribonucleic acid (DNA) damage (D'Mello et al. 2016). Acquiring mutations in melanocytes can result in uncontrollable proliferation, avoiding apoptosis and consequently gives rise to melanoma (reviewed in Bertolotto 2013). The worldwide incidence of cutaneous melanoma has been increasing annually, more rapidly than any other type of cancer. Unlike other tumours, melanoma mostly affects young and middle-aged individuals, with women prevailing in younger age groups and men from the age of 55 onwards (Charbel and Al-Kawas 2011). The incidence of melanoma varies between countries and correlates with racial skin phenotype and sun exposure (ultraviolet (UV) light)(Gilchrest et al. 2002). Polymorphisms of the melanocortin 1 receptor (MC1R) are responsible for the different skin-color phenotypes in humans (Rana et al. 1999). Individuals with red hair, light complexion, and light eyes exhibit a low pigmentation and therefore a heightened sensitivity to UV exposure. The increased risk of melanoma due to sun exposure is directly associated with the UV level, particularly in the UV-B spectrum. Intense and sporadic sun exposure, typical for sunburns, is associated with a higher risk for melanoma development compared to chronic continuous sun exposure that is more associated with non-melanoma skin cancers (Kütting and Drexler 2010). Also, exposure to artificial UV-A rays has been connected to increased risk of melanoma. This mostly includes the use of sunbeds and at a smaller percentage, the case of psoriasis patients receiving UV-A radiation phototherapy (Lazovich et al. 2010; Archier et al. 2012). Indeed, the World Health Organisation (WHO) officially classified the UV light from sunbeds as a human carcinogen. Additionally, the number of congenital and acquired melanocytic nevi and family history also plays a role in the development of melanoma and their numbers, sizes, and types are connected to increased risk at an individual level (Venturini et al. 2017).

Interestingly, 7-15% of melanoma cases occur in patients with a family history of specific malignancies, such as familial atypical multiple mole-melanoma syndromes (FAMM), melanoma-astrocytoma syndrome (MAS), xeroderma pigmentosum, familial retinoblastoma, Lynch syndrome type II and Li-Fraumeni cancer syndrome (reviewed in Leonardi et al. 2018). Interestingly, cutaneous melanoma is one of the most immunogenic cancers with heterogeneous histological and clinical features. It is characterized by a significant number of mutations which are connected to the low rate of tumour regression, multi-drug resistance to targeted therapies, and reduced survival rate (reviewed in Coricovac et al. 2018).

1.1.1 Pathogenesis of driver mutations in melanoma

Melanoma is a highly heterogeneous cancer. The group around Hodis, for example, identified 262 driver mutations in a total of 21 genes in melanoma by analyzing 121 pairs of a tumour and normal samples (Hodis et al. 2012). The most common driver mutations of the malignant phenotype are mutations in rapidly accelerated fibrosarcoma (BRAF), neuroblastoma ras viral oncogene homolog (NRAS), neurofibromin (NF)-1 and KIT genes (reviewed in Mehnert and Kluger 2012). BRAF and NRAS are serine-threonine kinases involved in the mitogen-activated protein kinase (MAPK) pathway that controls cell cycle and proliferation. BRAF is mutated in 50% of melanomas, with V600E being the most frequent mutation, while NRAS is mutated in 15-30% of melanomas. Both mutations result in constitutionally active MAPK and phosphoinositide 3-kinase (PI3K) pathways, leading to cell proliferation and survival. NF1 is a tumour suppressor gene mutated in 10-15% of melanoma cases. NF1 regulates RAS activation and mutations in NF1 cause hyper activation of the NRAS protein. Mutations in the receptor tyrosine-kinase KIT are found in 2-8% of melanoma cases and can affect melanoma survival and proliferation through modulation of the RAS/RAF and PI3K/AKT pathways. Beside the mentioned gene alterations, a great number of other mutations are also responsible for invasive and metastatic melanoma phenotypes.

1.1.2 Therapeutic strategies for the treatment of unresectable and metastatic melanoma

Depending on the location, stage or genetic profile of melanoma, the therapeutic options include surgical resection, chemotherapy, radiotherapy, immunotherapy or targeted therapy. For patients with stage II-IV melanoma, surgery is the primary treatment often followed by adjuvant therapy, such as targeted therapy or immunotherapy. Chemotherapy is considered only as a second or third-line treatment after failure of immunotherapy or targeted therapy (Lee et al. 2014). Radio therapy is rarely applied for primary tumour treatment, but it can be used for the treatment of skin, bone or brain metastases.

Dacarbazine (DTIC), an alkylating agent approved in 1974 by the food and drug administration (FDA) remained the standard chemotherapeutic for metastatic melanoma for the last 35 years although a complete response was achieved in less than 5% of all patients. Even though many other single agents or combinations of chemotherapeutics were tested on melanoma, none of these treatment strategies improved overall survival (OS) of the patients. During systemic chemotherapy, DTIC serum concentrations can reach up to 29 µg/mL, while higher concentrations are achieved only during isolated limb perfusion (ILP) or infusion (ILI), procedures that have been developed to treat locoregionally advanced malignancies in an extremity (O'Donoghue et al. 2017; Moreno-Ramirez et al. 2010).

The discovery that 40-60% of melanomas harbor activating mutations in the serine/threonine kinase gene BRAF led to the development of specific drugs targeting the V600E mutation of the protein. One of these drugs, Vemurafenib, was approved by the FDA in 2011 and was found to improve clinical response rates and progression-free survival (PFS) in patients with metastatic melanoma. However, unfortunately, the clinical benefit of Vemurafenib and similar drugs (Dabrafenib, Encorafenib) is limited due to the rapid development of resistance in melanoma. This resistance is mediated by the reactivation of the MAPK pathway or amplification of BRAF and NRAS genes. To bypass that problem, different combination therapies were tested on melanoma. In 2014, the combination of a BRAF-inhibitor, Dabrafenib, and a MEK-inhibitor, Trametinib, was approved by the FDA as a treatment for unresectable and metastatic melanoma harboring a BRAF mutation (reviewed

in Domingues et al. 2018). Interestingly, it was observed that patients with acquired tumour resistance to BRAF inhibitors can respond when re-challenged with combination treatment with Dabrafenib and Trametinib (Schreuer et al. 2017). Additionally, novel BRAF inhibitors that can circumvent the activation of the MAPK pathway upon monotherapy are currently being developed (Tutuka et al. 2017; Roskoski 2018).

Tumours bearing NRAS mutations are highly aggressive and NRAS mutations correlate with shorter patient survival (Heppt et al. 2017). RAS proteins in general are considered "undruggable" targets as it is challenging to identify small molecules that bind directly to RAS due to lack of hydrophobic pockets on its surface. However, patients with NRAS mutations have been reported to benefit from immunotherapy, but not from the combination of BRAF and MEK inhibitors (reviewed in Echevarría-Vargas and Villanueva 2017). Up to date, no selective inhibitors of NRAS have been identified.

Immunomodulating drugs such as the anti-programmed death (PD)-1 antibodies Nivolumab and Pembrolizumab or the anti-cytotoxic T-lymphocyte antigen (CTLA)-4 antibody Ipilimumab are currently revolutionising the field of melanoma therapeutics. Cancer cells can upregulate the expression of PD1 and thus avoid the detection by the immune system. Applying anti-PD1 inhibitors enables the activity of the immune system by disrupting the bond between PD-1 on T-cells and programmed death ligand (PDL-1) on tumour cells, exposing cells to the immune system. On the other hand, inhibition of CTLA-4 enhances T-cell activation, amplifies their proliferation and indirectly acts as an anti-cancer therapeutic by upregulating the immune system. Indeed, immunotherapy exhibited improved properties in extending PFS and OS when compared to DTIC and the combination of different immunotherapies showed superior properties when compared to the single treatments. For example, the combination of Ipilimumab and Nivolumab resulted in a 3-year overall survival rate of 63% and the combination of Pembrolizumab and Nivolumab exhibited a 44% overall survival rate in patients with unresectable stage III or IV melanoma (Albertini 2018; Hogan, Levesque, and Cheng 2018).

However, approximately 50% of all patients do not qualify for targeted therapy or do not respond to immunotherapy (reviewed in Hogan, Levesque, and Cheng 2018). Furthermore, immunotherapy can trigger autoimmune diseases and other severe side effects (Beer, Hochmair, and Prosch 2018). Additionally, immunotherapy is expensive and careful patient

selection is crucial in terms of cost-effectiveness, but unfortunately, predictive biomarkers for immunotherapy responsiveness have not been identified yet (Verma et al. 2018). Taken all facts together, investigating novel treatments against melanoma is still of relevance.

1.2 Apoptosis

Apoptosis, an evolutionary highly conserved type of programmed cell death, is a crucial process involved in the development of multicellular organisms, immunity and tissue homeostasis. It is characterized by cytoplasmic shrinkage, chromatin condensation (pyknosis) and nuclear fragmentation (karyorrhexis) followed by plasma membrane blebbing. Subsequently, the cell is broken down into smaller apoptotic bodies and afterwards taken up by cells exhibiting phagocytic activity (efferocytosis)(Galluzzi et al. 2018). Every day, the human body generates 10-100 billion cells and the same number of cells die to maintain homeostasis (reviewed in Nagata 2018). Therefore, dysregulation of apoptosis carries serious consequences for the organism, leading to malformations, autoimmune diseases, and cancer. On the other hand, removal of healthy cells by apoptosis can result in infection, hypoxic-ischaemic injury, neurodegenerative or neuromuscular diseases and the acquired immune deficiency syndrome (AIDS)(reviewed in Mazarakis, Edwards, and Mehmet 1997; Roshal, Zhu, and Planelles 2001; Mehrbod et al. 2019). Evading apoptosis contributes to carcinogenesis by creating a permissive environment for genetic instability and accumulation of gene mutations. Thereby, damaged cells avoid the immune surveillance and cell cycle checkpoints which can confer resistance to anti-cancer drugs (Fulda 2010). Since apoptosis is regulated at many levels, there is a multitude of opportunities for dysregulation of signaling that can contribute to the survival of the damaged cell and the subsequent rise of cancer. Therefore, a deep knowledge of apoptosis signalling is indispensable for the development of new anti-cancer agents targeted against these dysregulated proteins.

1.2.1 TRAIL-mediated apoptosis signalling

The extrinsic pathway of apoptosis is activated by binding of death ligands like tumour necrosis factor (TNF), fibroblast associated surface antigen (Fas) ligand (FasL), and TNF-related apoptosis-inducing ligand (TRAIL) to their respective death receptors (DRs): tumour necrosis factor receptor 1 (TNF-R1), Fas receptor (FasR) and TNF-related apoptosis-inducing receptor 1/2 (TRAIL - R1/2). TRAIL can bind five different receptors: TRAIL- R1 (DR4, tumour necrosis factor receptor superfamily member 10A (TNFRSF10A)), TRAIL-R2 (DR5, TNFRSF10B), TRAIL-R3 (decoy receptor 1 (Dc-R1)), TRAIL-R4 (Dc-R2) and Osteoprotegerin (OPG). TRAIL-R1 and TRAIL-R2 comprise a C-terminal cytoplasmic death domain necessary for induction of apoptosis. TRAIL-R1 can be activated by binding of soluble TRAIL and membrane-bound TRAIL, while TRAIL-R2 requires high order receptor clustering induced by binding of a membrane-bound ligand (Pan et al. 1997; Mühlenbeck et al. 2000). TRAIL-R3 lacks a transmembrane and cytoplasmic domain and is linked to the cell surface via a glycosylphosphatidylinositol (GPI) anchor. TRAIL-R4 contains a transmembrane domain, but only a truncated cytoplasmic domain. Thus, TRAIL-R3 and TRAIL-R4, cannot mediate apoptosis signalling and are considered to negatively regulate apoptosis by competing with TRAIL-R1 and TRAIL-R2 for ligand binding or forming heteromeric receptor complexes with TRAIL-R1 and TRAIL-R2 that are not able to induce apoptosis (Merino et al. 2006; Neumann et al. 2014). The function of Osteoprotegerin in TRAIL signalling, a soluble receptor, is still unclear (Reid and Holen 2009).

Upon binding of TRAIL to TRAIL-R1 and TRAIL-R2, death receptors trimerize resulting in a conformational change at their cytoplasmic side that exposes the death domain (DD).The adaptor protein Fas-associated protein with death domain (FADD) associates with death receptors via interactions of their death domains. The stoichiometry of FADD to death receptor is still not elucidated as studies suggest either one FADD or three FADDs per trimer (Dickens et al. 2012; Schleich et al. 2016; Majkut et al. 2014). FADD recruits the proform of aspartate-specific cysteine protease (Caspase) 8 or Procaspase 10 via interactions with their death effector domains (DED) leading to the formation of an intracellular multiprotein complex called death-inducing signaling complex (DISC). Recruited Procaspase 8 proteins form a large filament in which the cleavage and activation is carried out. Different isoforms of cellular FADD-like interleukin-1β-converting enzyme (FLICE)-like inhibitory protein (cFLIP)

are also recruited at the DISC, cFLIP long (cFLIP$_L$) and cFLIP short (cFLIP$_S$). Procaspase 8 is required for recruitment of cFLIP to the DISC, as suggested in the hierarchal binding model of the DISC formation (Hughes et al. 2016). The short isoform of cFLIP is reported to inhibit and the long isoform to activate Procaspase 8 by modulating its oligomerization. However, elevated expression of cFLIP$_L$ was also shown to inhibit extrinsic apoptosis by disrupting Caspase 8 maturation (reviewed in Tsuchiya, Nakabayashi, and Nakano 2015). Type I cells can activate executioner Caspase 3 and Caspase 7 by the activation of Caspase 8 and Caspase 10 (reviewed in Özören and El-Deiry 2002). In contrast to that, in type II cells the activation of Caspase 3 and 7 is blocked by the X-linked inhibitor of apoptosis protein (XIAP), thus these cells require an additional amplification loop that links the extrinsic to the intrinsic apoptosis pathway. In this amplification loop, the protein BH3- interacting domain death agonist (Bid) is proteolytically cleaved by Caspase 8 to truncated Bid (tBid) that can translocate to the outer mitochondrial membrane. There, tBid mediates the insertion of Bcl-2 associated X protein (Bax) and Bcl-2 antagonist or killer (Bak) into the outer mitochondrial membrane which in turn permeabilizes the membrane and causes the release of Cytochrome C and second mitochondrial activator of caspases (SMAC) into the cytosol (reviewed in Dewson and Kluck 2009). Mitochondrial outer membrane permeabilization (MOMP) is antagonized by anti-apoptotic members of the B cell lymphoma (Bcl-2) family, including Bcl-2, BCL extra large (Bcl-xl) and myeloid cell leukemia (Mcl)-1 (reviewed in Cory and Adams 2002). Released Cytochrome C binds to apoptotic peptidase activating factor 1 (Apaf1) and Procaspase 9 in a deoxyadenosine triphosphate (dATP) dependent manner to form a complex called apoptosome. Procaspase 9 is activated on the apoptosome and can catalyze the proteolytic activation of Procaspase 3 and Procaspase 7. Additionally, Cytosolic SMAC can promote apoptosis by sequestrating XIAP from executioner Caspases (Figure 1). Active executioner Caspases are involved in DNA fragmentation, phosphatidylserine (PS)

exposure and the formation of apoptotic bodies (reviewed in Galluzzi et al. 2018).
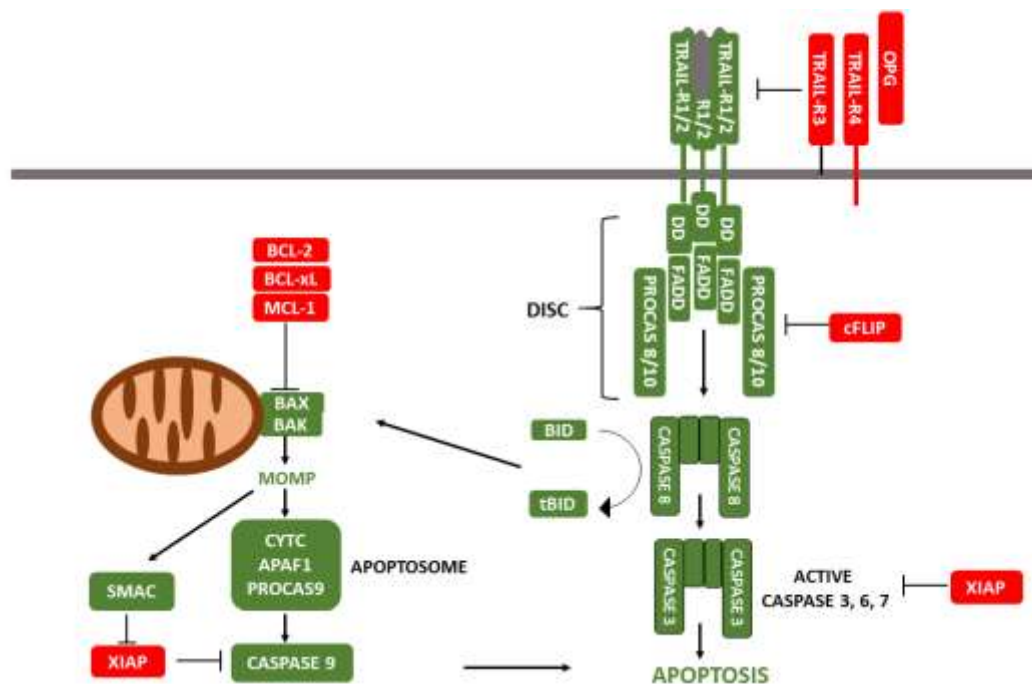
Figure 1. Simplified scheme of TRAIL-induced apoptosis. Apoptosis is regulated by more than 50 pro- and anti-apoptotic proteins. TRAIL induces the extrinsic apoptosis pathway that is linked to the intrinsic pathway through cleavage of the protein Bid. Pro-apoptotic proteins are shown in green, while anti-apoptotic are depicted in red colour. The figure is modified based on Hutt 2017 and Galluzzi et al. 2018.

1.2.2 TRAIL in cancer therapy

Triggering the extrinsic apoptotic pathway is a promising way to induce cell death in tumour cells independent of their p53 status. In 1891, William Coley administered extracts of gram-negative bacteria to treat sarcoma patients, marking the first time this principle was exploited (Coley 1891). A century later, anti-tumoural properties of the extracts were attributed to lipopolysaccharide (LPS)-induced TNF expression (Carswell et al. 1975). TNF caused severe toxicity when applied for tumour therapy, while TRAIL, discovered in 1995, selectively induced cell death exclusively in malignant cells, thus sparing healthy tissue (van Horssen 2006; Ashkenazi 2002; Walczak et al. 1999). Because of this feature, TRAIL was intensively investigated as an anti-cancer therapeutic.

In recent years, recombinant TRAIL, as well as monoclonal antibodies against TRAIL-R1 or TRAIL-R2, have been developed and evaluated in phase I clinical studies, however, to date with only limited success. TRAIL-based therapeutics showed good tolerability in the patients, but also a limited activity (den Hollander et al. 2013). These results were partially attributed to the ligand itself. Soluble trimeric TRAIL, tested in clinical trials, exhibited a short serum half-life and limited capacity to induce clustering of death receptors. Furthermore, besides activating apoptosis, TRAIL is also able to induce pro-survival signalling (Fulda 2013). As cancer cells can also develop resistance to TRAIL monotherapy by upregulating anti-apoptotic proteins, TRAIL can be combined with sensitizing agents like Bcl-2 or IAP antagonists (Lemke et al. 2014). Finally, careful selection of patients that would benefit from TRAIL-therapy is needed to spare the patients from potentially unnecessary treatment.

1.2.3 2nd generation TRAIL-receptor ligands as cancer therapeutics

2nd generation TRAIL-receptor ligands were created to improve the activity, stability, and half-life of TRAIL as a therapeutic. First, the stability of TRAIL molecules was improved by generating single-chain variants of TRAIL (scTRAIL) by fusion of the extracellular part via short peptide linker and thus preventing the dissociation of the fusion protein into monomeric subunits (Schneider et al. 2010). Second, increasing the half-life of TRAIL molecules can be achieved by fusing them to antibody fragments. For example, fusing TRAIL to a fragment crystallizable (Fc) of IgG antibody increased its half-life by taking advantage of the recycling of the antibody via the neonatal fragment crystallizable (FcRn) receptor (Pyzik et al. 2015). Third, the activity of the molecule was improved by increasing the valency of TRAIL thus inducing higher order clustering of TRAIL receptors. The concept of improving TRAIL-based therapeutics by increasing valency came from the observation that the members of the TNF-receptor superfamily (TNFRSR) require cross-linking for optimal activation (Wajant et al. 2015). Emphasizing this assumption, it was shown in a study by Tuthill and colleagues, that soluble TRAIL and a TRAIL-R2 specific antibody synergized in

killing cancer cells by clustering receptors and activating the DISC (Tuthill et al. 2014). Moreover, a fusion of scTRAIL to dimerization modules in studies by Gieffers and Seifert resulted in tetravalent or hexavalent molecules that exhibited enhanced apoptosis induction compared to soluble TRAIL (Gieffers et al. 2013; Seifert et al. 2014). Moreover, another approach to improve the efficacy of a drug is to target it actively or passively to the tumour. To actively target TRAIL-R agonists to the tumour site it is possible to fuse TRAIL to tumour-associated antigens (TAA) (Hutt et al. 2017). Binding partners can be used to support the anti-tumour effect by activation or inhibition of signalling pathways. Besides the advantage of targeting the drugs to a tumour, this also mimics membrane-bound TRAIL and thus facilitate the activation of TRAIL-R2. For example, in work by Hutt and colleagues, scTRAIL was targeted to the epidermal growth factor receptor (EGFR), the human epidermal growth factor 2 (HER2), the human epidermal growth factor 3 (HER3) or epithelial cell adhesion molecule (EpCAM). Beside targeting the drug to the tumour, this enabled the inhibition of the EGFR pathway or the cleavage of EpCAM, thus hindering the transcription of genes involved in tumour growth and proliferation (Hutt et al. 2017). It is also possible to generate molecules with both increased valency and active targeting (Siegemund et al. 2012; Seifert et al. 2014). Besides actively, drugs can be passively targeted to the tumour site. Passive targeting relies on leaky blood vessels, easing the access of bigger proteins to the inside of the tumour (Iyer et al. 2006). Also, poor drainage of the tumour can trap big macromolecules like TRAIL-fusion proteins in the inside of the tumour. Additionaly, TRAIL molecules can also be encapsulated in or attached to the surface of nanoparticles. In this way TRAIL can be delivered directly to the tumour site or surface-attached TRAIL can exhibit increased bioactivity by mimicking the membrane-bound form (reviewed by De Miguel et al. 2016; Iyer et al. 2006).

The TRAIL-R agonist used in this study, IZI1551, is a non-targeted dimeric scTRAIL molecule generated by fusing scTRAIL to the C-terminus of the human IgG1 Fc part, resulting in a dimeric protein covalently linked via disulfide bonds in the Fc region (Figure 2). This dimeric fusion protein comprises six TRAIL receptor binding sites and exhibits high stability in human plasma. Additionally, terminal half-life measured in serum of CD-1® mice was calculated to be 14.5 h (Hutt et al. 2017).

Of note, a similar molecule, hexavalent TRAIL ABV-621 by Abbvie, is currently being examined in clinical trials in patients with previously treated solid tumours and hematologic malignancies (NCT03082209)(Morgan-Lappe 2017).
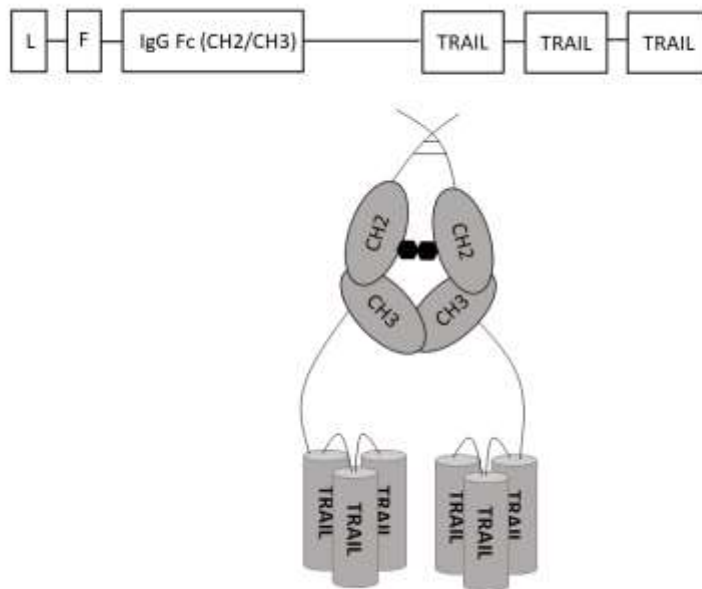
Figure 2. Structure of IZI1551. IZI1551 is generated by fusing the Fc part of a human IgG antibody to scTRAIL. Dimerization is achieved via disulfide bonds. CH=constant domain of the heavy chain; F= FLAG tag; L= Igκ chain leader sequence. The figure is modified based on Hutt et al. 2017.

1.3 Inhibitor of Apoptosis Protein (IAP) family

1.3.1 Structure

IAP proteins were first discovered in baculoviruses in 1993 as potent apoptosis inhibitors in infected insect cells (Crook et al. 1993). Since then, eight members of the family were identified in humans: cellular IAP 1 and 2 (cIAP1, cIAP2), X-chromosome linked IAP (XIAP), melanoma IAP (ML-IAP or Livin), Apollon (BRUCE), survivin, neuronal apoptosis inhibitory protein (NIAP) and IAP-like protein 2. All proteins are characterized by the presence of one to three highly conserved protein motifs called baculoviral IAP repeats (BIR), a zinc-binding fold made of approximately 70 amino acid residues that mediate protein-protein interactions. CIAP1, cIAP2, and XIAP contain one type I (BIR1) and two type II BIR domains (BIR2 and BIR3) located at the N-terminus of the proteins. Although the BIR domain itself is

highly conserved, small sequence differences allow for binding of different partners. For example, the BIR1 domain of the cIAPs interacts with TNFR-associated factor 1 (TRAF 1) and TRAF2 while the BIR1 domain of XIAP mediates interaction with transforming growth factor-β (TGFβ) activated kinase (TAK1) binding protein TAB1. Type II BIR domains in IAP proteins carry a distinctive hydrophobic cleft through which they bind to N-terminal tetrapeptides called IAP-binding motifs. These IAPs also contain a Really Interesting New Gene (RING) domain at the C-terminus that provides them with ubiquitin (Ub) ligase activity (E3) and a Ub-associated (UBA) domain through which they interact with ubiquitin chains including K63, K48, K11, linear chains as well as mono-ubiquitin. Furthermore, cIAP1 and cIAP2 also posses a caspase-recruitment domain (CARD) positioned between the BIR domains and the RING domain. CARD domains typically mediate oligomerization with other CARD-containing proteins, similar to death domains and death effector domains. However to date, the function of the CARD domain in IAPs is not fully elucidated (reviewed in De Almagro and Vucic 2012; Hunter et al. 2007).

1.3.2 cIAPs in cancer: regulating cell survival via the NFκB pathway

IAP proteins were found to be overexpressed in cancer and are hereby connected to increased proliferation, motility and migration. IAP proteins can regulate cell survival in two distinct ways. First, by modulating the nuclear factor kappa-light-chain-enhancer of activated B cells (NFκB) survival pathway through their E3 ligase activity or second, by directly binding and inhibiting caspases (reviewed in De Almagro and Vucic 2012).

The NFκB pathway plays an important role in cell survival and immunity. It is tightly controlled by the interplay of phosphorylation and ubiquitination of crucial signaling transducers. Two branches can be differentiated based on the timing of activation and signalling proteins involved in the initiation of the pathway. The canonical NFκB pathway is activated by binding of TNFα to TNF-R1. This leads to the assembly of a receptor-associated complex consisting of tumour necrosis factor receptor-associated death domain protein (TRADD), TRAF2, cIAP1, cIAP2, and receptor interacting protein 1 (RIP1). CIAP1 and cIAP2 bind the complex through the interaction with TRAF2 in a way that one cIAP protein binds

three TRAF2 molecules. The aggregation of activated receptors causes recruitment of multiple TRAF2 trimers, resulting in cIAP dimerization and activation of their E3 ligase activity, leading to ubiquitination of the kinase RIP1. This furthermore allows the binding of nuclear factor kappa-B kinase subunit alpha (IKKα), inhibitor of nuclear factor kappa-B kinase subunit beta (IKKβ), NF-kappa-B essential modulator (NEMO), transforming growth factor β-activated kinase 1- binding protein (TAK1-TAB) complex and linear ubiquitin chain assembly complex (LUBAC) and subsequent ubiquitination of NEMO by LUBAC. The proximity of the IKK complex to TAK1 kinase leads to phosphorylation and activation of IKKβ which triggers the phosphorylation of IκBα. This, in turn, results in ubiquitination of IκBα and subsequent proteasomal degradation as well as the release of transcription factors p65 and RelA which can translocate to the nucleus and induce the transcription of genes. In the presence of IAP antagonists, cIAP1 and cIAP2 are degraded, which allows the dissociation of RIP1 from the complex and forming the cytoplasmic complex together with FADD and Caspase 8 that initiates apoptosis.

The non-canonical NFκB pathway differs from the canonical branch in signalling components and biological function. It is mainly involved in lymphoid organogenesis as well as B cell survival and maintenance (Cildir et al. 2016). Deregulation and defects of the non-canonical pathway have been associated with severe immune deficiencies, autoimmune and inflammatory diseases (reviewed in Sun 2017). IAP proteins can negatively regulate non-canonical NFκB signalling through their association with the key regulator NFκB inducing kinase (NIK). In unstimulated cells, cIAPs are associated with NIK, constitutively ubiquitinating and tagging it for proteasomal degradation. Upon stimulation of receptors fibroblast growth factor-inducible 14 (Fn14), CD40 or treatment with IAP antagonists, cIAPS are degraded and NIK can accumulate. NIK accumulation is a result of stabilization and *de novo* synthesis, a hallmark of the NFκB non-canonical pathway (Sun 2011). In turn, NIK phosphorylates IKKα dimers and p100 which leads to partial proteasomal truncation of p100, yielding the p52 fragment. This fragment then dimerizes with RelB and translocates into the nucleus to activate the transcription of non-canonical pathway-related NFκB genes. Of note, the activation of the non-canonical pathway is slower than the canonical pathway due to the requirement for new protein synthesis (reviewed in Silke and Meier 2013; Gyrd-Hansen and Meier 2010; De Almagro and Vucic 2012) (Figure 3).
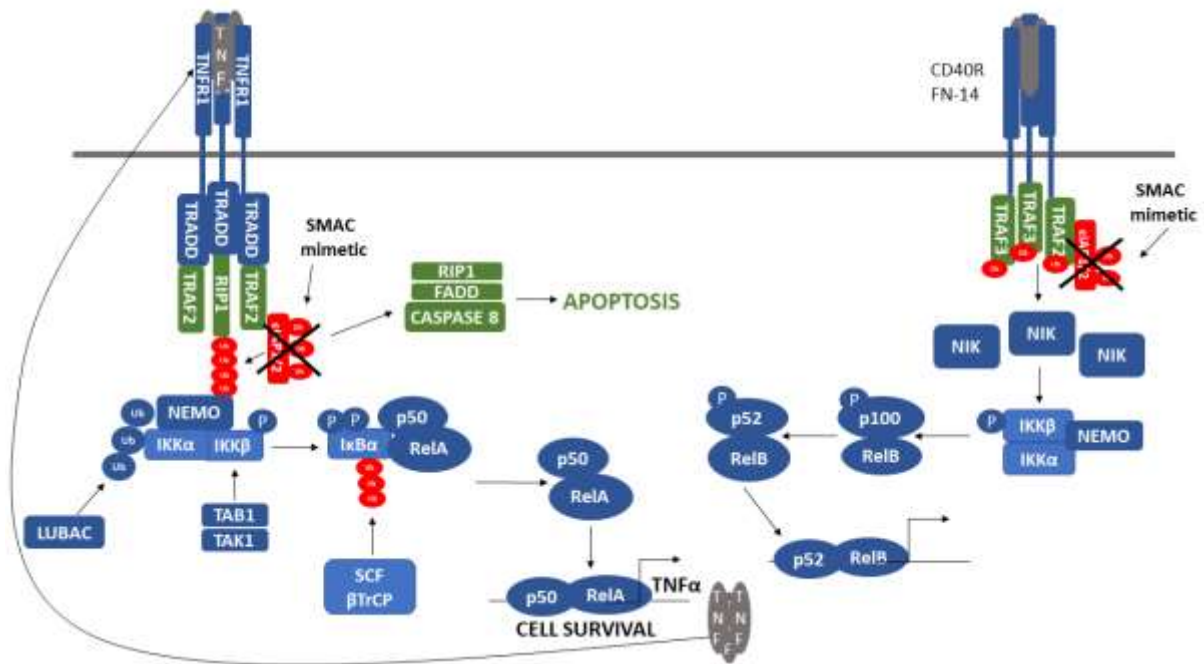
Figure 3. Canonical and non-canonical NFκB signalling pathway modulated by SMAC mimetics. NFκB family of transcription factors transduces the signals of various stimuli that lead to the transcription of a broad spectrum of genes. SMAC mimetics (IAP antagonists) can regulate both the canonical and non-canonical branch of the pathway. The figure is modified based on (De Almagro and Vucic 2012; Darding and Meier 2012)

1.3.3 XIAP as an inhibitor of caspases

XIAP is the only IAP family member with the ability to directly bind and inactivate Caspases. This was shown in many studies where overexpression of XIAP inhibited apoptosis and vice versa, inhibition of XIAP sensitised cells to apoptosis (Holcik et al. 2000; McManus et al. 2004; Shaw et al. 2008; Obexer and Ausserlechner 2014). XIAP can directly bind Caspase 3, Caspase 7 and Caspase 9. Thereby, amino acid residues belonging to the linker region between the BIR2 and the BIR3 domains of XIAP bind to the active site of Caspases resulting in the inhibition of their catalytic activity. Furthermore, the BIR2 domain of XIAP binds to an IBM motif at the neo-amino terminus of the caspase subunit thereby strengthening the binding between the two proteins which contributes to the inhibition of caspase activity (Scott et al. 2005). In case of the inhibition of Caspase 9, the BIR3 domain of XIAP binds to the homodimerization surface of the enzyme, thus blocking the dimerization and

dimerization-induced conformational change that exposes the catalytic pocket (Srinivasula et al. 2001).

1.3.4 TRAIL-mediated activation of NFκB signalling

Stimulation with TRAIL can induce several outcomes in cells, ranging from apoptosis, necroptosis and gene activation to cytokine production and migration. Apoptosis is characterized by the assembly of the DISC and subsequent activation of caspases, while necroptosis is caspase-independent and involves RIPK1, RIPK3 and mixed lineage kinase domain-like protein (MLKL). Gene activation is thought to originate from complex II, a secondary cytoplasmic signalling complex consisting of RIPK1, NEMO, TRAF2, FADD and Caspase 8. Even though the molecular basis for different outcomes upon TRAIL-treatment is still not clearly defined, yet two recent studies suggest the mechanism of gene activation upon TRAIL stimulation. First, a group around Lafont described the role of complex I in gene-activation, thus extending and revising the current model that describes complex II as the only mediator of gene activation in the TRAIL-induced pathway. More precisely, the protein complex LUBAC was shown to be a crucial regulator of different outcomes of TRAIL-induced signalling. It was found present in both complex I and complex II with RIPK1 and Caspase 8 upon TRAIL stimulation. Within both complexes, LUBAC limited activation of Caspase 8 by ubiquitination and promoted IKK complex recruitment, thereby inhibiting apoptosis and enabling pro-inflammatory cytokine production (Figure 4A). Additionally, IAP antagonists were found to limit LUBAC activity, thus stimulating TRAIL-induced apoptosis and moreover, restricting surviving cells from producing tumour-promoting cytokines (Lafont et al. 2017).

In a second study, by Henry and Martin, it was also demonstrated that TRAIL receptor stimulation can induce NFκB-dependent pro-inflammatory cytokine production (Henry and Martin 2017). In this work, Caspase 8 was found to be an important mediator of the pro-inflammatory signalling, functioning as a scaffold for recruitment of RIPK1 to the TRAIL-R signalling complex (Figure 4B). The pro-inflammatory FADD/RIPK1 complex named 'FADDosome' was also found downstream of other death receptors such as Fas/CD95 which may explain why the expression of TRAIL receptors failed to serve as a predictive biomarker for TRAIL-induced apoptosis by anti-cancer agents. Moreover, these studies emphasize the

benefit from applying IAP antagonists together with TRAIL. IAP antagonists deplete cIAP1 and cIAP2 which results in an un-ubiquitinated RIP1 and as a consequence, NEMO cannot bind to the complex. Therefore, pro-survival signalling is blocked and apoptosis is initiated.
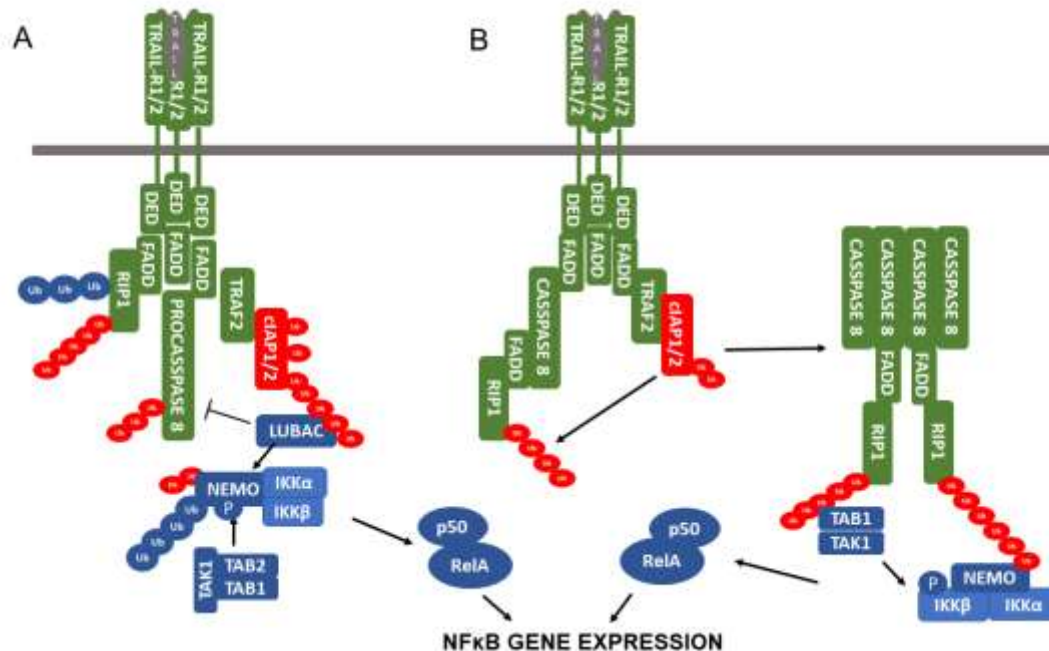
Figure 4. TRAIL-induced pro-inflammatory signalling. Binding of TRAIL to TRAIL-Rs can initiate a signalling cascade that results in the transcription of pro-inflammatory genes. A) Lafont and colleagues point out a crucial role of LUBAC in promoting non-apoptotic signalling by inhibiting the maturation of Caspase 8 and recruiting the IKK complex to the receptor. B) Henry and Martin demonstrated non-enzymatic, but rather scaffolding activity of Caspase 8 resulting in the formation of the 'FADDosome' and activation of NFκB-related genes. Ubiquitin chains generated by LUBAC are depicted in blue, while the ones generated by cIAPs are shown in red. The figure is modified according to Lafont et al. 2017 and Henry and Martin 2017.

1.3.5 SMAC mimetics act as anti-cancer therapeutics through antagonising IAPs

SMAC mimetics are a class of pharmacological inhibitors that mimic the IAP binding motif (IBM) AVPI (Ala-Val-Pro-Ile) of the mature SMAC/ direct IAP binding protein with low PI (DIABLO). SMAC is released from the mitochondria during apoptosis via Bax/Bak channels in the mitochondrial membrane. Subsequently, the AVPI sequence of released SMAC binds to the shallow groove of the BIR2 and BIR3 domain of XIAP and the BIR3 domain of cIAP1,

inhibiting their function (Sun et al. 2014). Binding of SMAC mimetics to the BIR3 domain of cIAPs causes a conformational change in cIAPs, allowing RING domain dimerization, auto-ubiquitylation and subsequent proteasomal degradation. This sensitises cancer cells to TNF-mediated apoptosis through the stabilization of RIP1 and activation of ripoptosome (reviewed in Silke and Meier 2013).

So far, monovalent and bivalent SMAC mimetics have been synthesised. Although both types of SMAC mimetics, were shown to sensitise cancer cells to apoptosis, bivalent SMAC mimetics are considered the better option, due to their more efficient degradation of TRAF2-bound cIAPs and inhibition of TNF-stimulated p65/NFκB gene transcription (Mitsuuchi et al. 2017). The first generation SMAC mimetic, Compound A, was connected to poor tolerability in patients due to its pan-IAP antagonism that led to the activation of nucleotide-binding oligomerization domain and leucine-rich repeat-containing receptors (NLR) Family Pyrin Domain Containing 3 (NLRP3)-caspase-1 inflammasome-dependent IL-1β secretion, responsible for systemic inflammation (Condon et al. 2014; Lawlor et al. 2017). In contrast to that, Birinapant (TL32711), a 2nd generation bivalent SMAC mimetic, displayed preferential binding to cIAP1 rather than cIAP2 and XIAP, suppressed IL-1β secretion and exhibited better tolerability in the patients (Benetatos et al. 2014). Furthermore, Birinapant showed significant anti-tumour activity in preclinical models of ovarian, colorectal, head and neck squamous cell carcinoma as well as leukemia and melanoma (Eytan et al. 2016; Allensworth et al. 2013; Carter et al. 2014; Amaravadi et al. 2015). Besides that, it also exhibited synergistic pre-clinical anti-tumour activity with multiple chemotherapies (Janzen et al. 2015; Crawford et al. 2018; Eytan et al. 2015). Currently, Birinapant is investigated in clinical trials as a combination treatment with the PD-1 inhibitor Pembrolizumab in solid tumours (NCT02587962). Beside Birinapant also other SMAC mimetics are at the moment investigated in clinical settings. Debio1143 is combined with the anti-PD-1 antibody Avelumab to treat solid malignancies (NCT03270176). LCL161 is being tested in combination with an anti-interleukin 17A (IL17A) monoclonal antibody CJM112 and anti-PD1 monoclonal antibody in multiple myeloma (NCT03111992). SMAC mimetic APG-1387 is investigated as a single treatment for advanced solid tumours or hematological malignancies (NCT03386526).

1.4 Computational modeling in apoptosis

Systems biology combines experimental approaches of investigating biological systems with mathematical modelling, in a way that a computational model is compared to experimental results in an iterative procedure (reviewed in Hantusch et al. 2018). There are several approaches in investigating signalling networks by systems analysis. Some of them include ordinary differential equations (ODE)-based models, partial differential equations (PDE)-based models, Boolean networks, agent-based modelling, and statistical modelling. The purpose and the amount and quality of data available for parametrizing the model determines which approach should be used. For example, ODE models are very often used in analysing extrinsic and intrinsic apoptosis (reviewed in Spencer and Sorger 2011).

The first model of apoptosis was developed in 2000 by a group around Fussenegger. Even though it was not yet parametrized with experimental data, it still greatly influenced the subsequent work in the field (Fussenegger et al. 2000). Many important discoveries in both extrinsic and intrinsic apoptosis were made by using ODE modelling (reviewed in Schleich and Lavrik 2013). For example, Bentele and colleagues demonstrated that the assembly of the DISC is the central point of extrinsic apoptosis upon stimulation with FasL (Bentele et al. 2004). Furthermore, activation of Caspase 8 was described as a stage-limiting step in extrinsic apoptosis of type I cells. Additionally, the same group demonstrated the importance of the amount of cFLIP$_L$ in defining life or death of a cell (Fricker et al. 2010; Lavrik et al. 2007). Intrinsic apoptosis was also studied by ODE modelling. Rehm and colleagues described swift apoptosis execution upon activation of caspases and highlighted the crucial role of XIAP in caspase activation via the apoptosome. It was further demonstrated that in Hela cells XIAP inhibits Caspase activation at concentrations above 0.3 μM, while at 0.15 μM the activation is enabled (Rehm et al. 2006). In another study, the dynamics of initiator and executioner caspase activation pre- and after MOMP were investigated by Albeck and colleagues. This study identified the activity of initiator caspases (e.g. Caspase 8) before the event of MOMP and the activity of executioner caspases (e.g. Caspase 3) exclusively after MOMP (Albeck et al. 2008; reviewed in Schleich and Lavrik 2013). Fundamentals of apoptosis signalling were also analysed by other types of computational modelling. For example, agent-based modelling was used to elucidate the role of cFLIP and Caspase 8 in DED chains of the DISC and subsequent activation of apoptosis

(Schleich et al. 2016). Furthermore, the Boolean model developed by Calzone and colleagues demonstrated the decision switch between apoptosis, necroptosis and survival (Calzone et al. 2010; Schleich and Lavrik 2013).   Besides investigating mechanisms of apoptosis, ODE modelling was also used to predict the response of cell lines and tissues to genotoxic agents. Lindner and colleagues developed an ODE-based model dose response medicinal outcome model predictor (DR_MOMP) which categorized colorectal cancer patients as responders or non-responders to genotoxic stress based on Bcl-2 family protein interactions (Lindner et al. 2013). DR_MOMP was also used to classify breast cancer cell lines as responsive or non-responsive to cisplatin or paclitaxel (Lucantoni et al 2018). In both studies, DR_MOMP successfully predicted the outcomes. The model consists of 126 reactions and 71 proteins and it requires a great amount of data for parameterization, including protein concentrations, protein production rates, binding kinetics, dissociation constants, and information about drug degradation. In the study by Lucantoni and colleagues, some parameters were measured (Bcl-2 protein profiling), while others were taken from the literature (binding kinetics, dissociation constants) or modelled computationally with a mathematical function (protein production rates).

In contrast, data-driven modelling does not require a-priori knowledge and it is applied when a larger amount of experimental data is available. It is performed by applying multivariate statistical methods or pattern recognition algorithms to sets of data, allowing feature selection and prediction (Janes and Yaffe 2006). This approach can also be used to predict the response of patients or cell lines to therapeutics, as it was demonstrated in several studies with the aim to identify melanoma or glioma cells that respond to apoptosis-inducing treatments (Passante et al. 2013; Weyhenmeyer et al. 2016; Rožanc et al. 2018). As described before, melanoma can be resistant to apoptosis-inducing agents due to the deregulation of apoptosis proteins. Despite the detailed knowledge of the regulators involved in apoptosis attenuation, individual proteins could not be validated as predictive biomarkers in melanoma. Many individual proteins of the apoptosis signalling were suggested as possible biomarkers in cancer, particularly Bcl-2 family members, XIAP, Apaf1, cFLIP, however none of them were validated in a large and independent study aimed at discovering biomarkers (Anvekar et al. 2011; Raisova et al. 2001; Trisciuoglio et al. 2017; Campioni et al. 2005; Thayaparasingham et al. 2009; Tian and Lee 2010). As it was pointed

out in a study by Manfredi and colleagues, there is a high occurrence of false positive biomarkers in these studies due to chance correlation (Manfredi 2015). Furthermore, due to the complexity and non-linearity of apoptosis signalling, predicting the response to therapeutics based on the expression of individual proteins might be impossible. However, analysing all critical regulators of a disease-related pathway with systems levels approaches might outperform classical statistical biomarker identification (Charles and Rehm 2014). Several studies confirm this hypothesis. A study by Passante and colleagues successfully identified melanoma cell lines that responded to treatment with DTIC or TRAIL based on the quantity of proteins involved in apoptosis by using data-driven modelling. Similarly, a study by Weyhenmeyer identified glioblastoma cell lines responsive and resistant to the treatment with temozolomide, a standard-of-care chemotherapeutic, and TRAIL, based on the expression of apoptosis protein. Using the same methodology, Rožanc and colleagues successfully predicted the responsiveness of melanoma cell lines to Trametinib, a MEK inhibitor, based on a phosphoproteomic signature. Additionally, a sensitization approach guided by multivariate statistics and data-driven modelling was successfully implemented in cells resistant to Tramentinib (Rožanc et al. 2018). Taken together, these studies imply that systems biology is a valuable tool for studying apoptosis, both mechanistically and in the context of identifying the responsiveness to therapeutics.

1.5 Aims of the thesis

Melanoma is a highly heterogeneous and aggressive cancer and patients often suffer from inefficacy of available therapeutics or reoccurrence. Therefore, there is a need to develop novel drugs against melanoma and additionally, to identify the patients who would benefit most from such therapeutics. It was suggested in many studies that inducing apoptosis with TRAIL is a promising way of eliminating cancer cells, however recombinant TRAIL and TRAIL receptor agonists tested in the clinical trials have not been successful yet, due to the low efficacy and bioavailability. Additionally, cancer cells can upregulate anti-apoptosis proteins which renders them resistant to TRAIL-induced apoptosis. Therefore, a first major aim of this study was to investigate the susceptibility of melanoma cell lines to apoptosis-inducing IZI1551, a novel 2nd generation TRAIL receptor agonist with improved potency and half-life compared to recombinant human TRAIL. In addition, to sensitise TRAIL-resistant melanoma

cell lines, IZI1551 was combined with Birinapant, a SMAC mimetic that depletes anti-apoptotic IAP proteins. For comparison purposes, Birinapant was also applied together with the FDA-approved chemotherapeutic against melanoma, Dacarbazine. In order to reflect the heterogeneity of the disease, both combination treatments were tested on a large panel of melanoma cell lines covering different mutation statuses and points of origin. However, previous studies showed that culturing cell lines on a rigid plastic dish can change cell morphology and physiology. Furthermore, using over-subcultured cell lines can drastically change gene and protein expression in a way that cell lines no longer reflect source material. Therefore, the efficacy of the combination treatment was additionally tested in a set of freshly isolated patient-derived melanoma cells and in melanoma cell lines grown as three-dimensional (3D) spheroids which better represent the natural physiology of a tumour. Finally, to validate results obtained *in vitro*, the combination treatment was also tested in melanoma cell lines grown as xenografts. Combination treatment induced apoptosis in the majority of the cell lines, while part of the cells exhibited low response. Therefore, there was a need to identify responders before the treatment was applied. Previous studies have tried to make the connection between the TRAIL responsive cell lines and the expression of individual apoptosis proteins, but without success. Therefore, the second aim of this thesis was to predict the responsiveness of the investigated melanoma cell lines to the combination treatment with IZI1551 and Birinapant by analysing the expression of 19 proteins involved in apoptosis using multivariate statistics.

2 Materials

2.1 General consumables

Laboratory plastic was bought from Greiner Bio-One (Frickenhausen, Germany). Chemicals were bought from Sigma-Aldrich, Munich, Germany, Thermo Fisher Scientific Inc., Waltham, USA, Carl Roth GmbH & Co. KG, Karlsruhe, Germany, Merck, Roche Diagnostics AG, Basel, Switzerland, Dako, Agilent Technologies, Santa Clara, USA.

2.2 Prokaryotic and Eukaryotic Cell lines

Cell line	Description	Source
WM115	Human melanoma cell line	American Type Culture collection (ATCC)
SkMel1	Human melanoma cell line	ATCC
SkMel2	Human melanoma cell line	ATCC
MeWo	Human melanoma cell line	ATCC
Malme 3M	Human melanoma cell line	ATCC
SkMel5	Human melanoma cell line	ATCC
WM35	Human melanoma cell line	WISTAR
WM3060	Human melanoma cell line	WISTAR
WM1791c	Human melanoma cell line	WISTAR
WM1366	Human melanoma cell line	WISTAR
WM3211	Human melanoma cell line	WISTAR
Mel Juso	Human melanoma cell line	German collection of Microorganisms and Cell cultures (DSMZ)
SkMel147	Human melanoma cell line	Prof. Dr. Dagmar Kulms
WM793	Human melanoma cell line	Prof. Dr. Dagmar Kulms
WM852	Human melanoma cell line	Prof. Dr. Dagmar Kulms
WM1346	Human melanoma cell line	Prof. Dr. Dagmar Kulms

WM3248	Human melanoma cell line	Prof. Dr. Dagmar Kulms
M10	Patient-derived melanoma cells	BRAF V600E mutated
M20	Patient-derived melanoma cells	NRAS Q61H mutated
M32	Patient-derived melanoma cells	NRAS Q61R mutated
M34	Patient-derived melanoma cells	NRAS Q61L mutated
M45	Patient-derived melanoma cells	BRAF V600E mutated
HEKP2	Suspension HEK293 with DR5 KO	Generated by Dr. Martin Siegemund
DH5α	E. coli strain	

Patient-derived metastatic melanoma cells M10, M20, M32, M34 and M45 were a generous gift from Prof. Dr. Dagmar Kulms and Prof. Dr. Friedegund Meier, Technical University of Dresden, Germany. Mutation status of other cell lines can be found in chapter 4, Results, Figure 8.

2.3 Antibodies and proteins

Antibodies were bought from Cell Signalling Technologies (CST), Abcam, Thermo Fisher, BD Transduction Laboratories, R&D Systems, BioLegend and Enzo.

Table 1. Antibodies used in flow cytometry

Antibody	Isotype	Application	Source
Anti-human TRAIL R1	Mouse IgG1	Flow cytometry (1:100)	R&D Systems
Anti-human TRAIL R2	Mouse IgG2b	Flow cytometry (1:100)	R&D Systems
Anti-human TRAIL R3	Mouse IgG1	Flow cytometry (1:100)	R&D Systems

Anti-human TRAIL R4	Mouse IgG1	Flow cytometry (1:100)	R&D Systems
Mouse IgG1 control	Mouse IgG1	Flow cytometry (1:100)	BD Transduction Laboratories
Mouse IgG2b control	Mouse IgG2b	Flow cytometry (1:100)	BD Transduction Laboratories
Anti-human HLA-ABC FITC conjugated	Mouse IgG1	Flow cytometry (1:50)	BD Transduction Laboratories
Mouse IgG1-FITC conjugated control	Mouse IgG1	Flow cytometry (1:50)	BD Transduction Laboratories

Table 2. Primary antibodies used in Western blotting and co-immunoprecipitation

Antibody	Host animal	Application	Source
Anti-human Apaf-1	Mouse	WB (1:1000)	BD Transduction Laboratories
Anti-human Actin	Mouse	WB (1:10 000)	CST
Anti-human Actin	Rabbit	WB (1:10 000)	CST
Anti-human Bak	Rabbit	WB (1:1000)	CST
Anti-human Bax	Rabbit	WB (1:1000)	CST
Anti-human Bcl-2	Rabbit	WB (1:1000)	CST

Anti-human Bcl-2	Mouse	WB (1:1000)	BD Transduction Laboratories
Anti-human Bcl-xL	Rabbit	WB (1:1000)	CST
Anti-human Bid	Mouse	WB (1:1000)	BD Transduction Laboratories
Anti-human Bid	Rabbit	WB (1:1000)	CST
Anti-human Caspase 3	Rabbit	WB (1:1000)	CST
Anti-human Caspase 8	Mouse	WB (1:1000)	CST
Anti-human Caspase 8	Mouse	Co-IP (1:50)	Thermo Fisher
Anti-human Caspase 8	Mouse	WB (1:1000)	From Martin Leverkus lab
Anti-human Caspase 8	Rabbit	WB (1:1000)	CST
Anti-human Caspase 9	Rabbit	WB (1:1000)	CST
Anti-human cIAP1	Rabbit	WB (1:1000)	Abcam
Anti-human cIAP2	Rabbit	WB (1:1000)	Abcam
Anti-human cFLIP	Mouse	WB (1:1000)	Abcam
Anti-human cFLIP	Mouse	WB (1:500)	Enzo
Anti-human cFLIP	Rabbit	WB (1:500)	CST
Anti-human Cytochrome C	Mouse	WB (1:1000)	BD Transduction Laboratories

Anti-human DR4	Mouse	Co-IP (1:100)	CST
Anti-human DR5	Mouse	Co-IP (1:100)	CST
Anti-human FADD	Rabbit	WB (1:1000)	Santa Cruz
Anti-human PARP	Mouse	WB (1:1000)	BD Transduction Laboratories
Anti-human SMAC	Mouse	WB (1:1000)	BD Transduction Laboratories
Anti-human XIAP	Mouse	WB (1:1000)	BD Transduction Laboratories
Anti-human XIAP	Rabbit	WB (1:1000)	CST

Table 3. Secondary antibodies used in Western blotting and co-immunoprecipitation

Antibody	Host animal	Application	Source
Anti-mouse IgG	Goat	WB (1:10 000), HRP	Thermo Fisher
Anti-rabbit IgG	Goat	WB (1:10 000), HRP	Thermo Fisher
Anti-mouse IgG	Goat	WB (1:10 000), IRDeye 800	Licor
Anti-rabbit IgG	Goat	WB (1:50 000), IRDeye 680	Licor
Anti-mouse FITC	Goat	Flow cytometry	DAKO
Veriblot mouse and rabbit IgG	Mouse and rabbit	WB (1:40), HRP	Abcam

Table 4. Recombinant proteins

Protein	Application	Source

Recombinant human cIAP1	WB	R&D Systems
Recombinant human cIAP2	WB	R&D Systems

2.4 Markers and kits

Alanine Transaminase Activity Assay kit	Abcam, Cambridge, UK
DAKO QIFIKIT	Agilent, CA, USA
Mouse TNFα ELISA MAXTM Standard	BioLegend
NucleoBond® Xtra Midi	Macherey-Nagel, Düren, Germany
PageRuler™	Prestained Protein Ladder (Thermo Fisher Scientific, Waltham, MA, USA)
SuperSignalTM West Dura Extended Duration Substrate	Thermo Fisher Scientific Inc., Rockford, USA
SuperSignalTM West Pico Chemiluminescent Substrate	Thermo Fisher Scientific Inc., Rockford, USA
Tumour Dissociation kit, human	Milteny Biotech

2.5 Plasmids

Plasmid was developed at the Institute of Cell Biology and Immunology (University of Stuttgart, Germany) and kindly provided by Prof. Dr. Roland Kontermann.

Flag/Fc (Q, G)-scTRAIL-pSecTag	Fc-sc TRAIL

2.6 Chemicals, buffers, solutions and cell culture reagents

Agarose	Carl Roth GmbH & Co, Karlsruhe, Germany
Fetal calf serum (FCS) (P30-3309)	PAN-Biotech GmbH, Aidenbach, Germany

MATERIALS

10 × trypsin/ ethylenediaminetetraacetic acid (EDTA)	Life technologies, Gibco, Karlsruhe, Germany
Annexin V binding buffer (10 x concentrated)	BD Pharmingen, BD Biosciences, San Diego, USA
Annexin V-EGFP	manufactured by Dr. Fabian Richter, Institute for Cell Biology and Immunology, University of Stuttgart
Annexin V-EGFP	Produced in house by Nathalie Peters
Blocking Reagent Roche (10x)	Roche Diagnostics AG, Basel, Switzerland
Bradford reagent (5x)	Bio-Rad protein assay (Bio-Rad, Munich, Germany)
Coomassie staining solution	0.008% (w/v) Coomassie Brilliant Blue G-250 (SERVA Electrophoresis, Heidelberg, Germany), 35 mM HCl
Crystal violet staining solution	0.5% (w/v) crystal violet, 20% (v/v) methanol
PBS (1x)	GIBCO® Dulbecco's phosphate-buffered saline (Thermo Fisher Scientific, Waltham, MA, USA)
ELISA blocking buffer (MPBS)	2% (w/v) non-fat dry milk powder in 1x PBS
ELISA substrate solution	100 mM sodium acetate pH 6.0, 0.1 mg/ml TMB, 0.006% (v/v) H_2O_2
ELISA wash buffer (PBST)	0.005% (v/v) TWEEN 20 in 1 x PBS
Ethanol	Merck KGaA, Darmstadt, Germany
F17 Freestyle Expression Medium	Thermo Fischer Scientific Inc., Waltham, USA

GlutaMAX	Thermo Fisher Scientific, Inc., Waltham, USA
HPLC running buffer	0.1 M Na_2HPO_4/NaH_2PO_4, 0.1 M Na_2SO_4, pH 6.7
IBlot®2 NC Regular Stacks	Life technologies Corporation, Carlsbad, USA
IMAC elution buffer	250 mM imidazole in 1x sodium phosphate buffer
IMAC wash buffer	25 mM imidazole in 1x sodium phosphate buffer
Isopropanol (70%)	Merck KGaA, Darmstadt, Germany
Koliphor P 188	10% (w/v), Sigma Aldrich, Merck KGaA, Darmstadt, Germany
Laemmli loading buffer (5x)	non-reducing: 25 % (v/v) glycerol, 10 % (w/v) SDS, 0.05 % (w/v) bromophenol blue in 312.5 mM Tris-HCl pH 6.8; reducing: non-reducing, 12.5% (v/v) β-mercaptoethanol
LB medium	% (w/v) peptone, 0.5% (w/v) yeast extract, 0.5% (w/v) NaCl in H_2O
LB $_{amp,glc}$ agar plates	LB medium, 2% (w/v) agar; after autoclaving: addition of 1% (w/v) D-glucose and 100 µg/ml ampicillin
Methanol	Carl Roth GmbH & Co, Karlsruhe, Germany
Methyl Cellulose	20% (w/v) in RPMI, Sigma Aldrich, Merck KGaA, Darmstadt, Germany

NuPAGE MES SDS Running Buffer (20x)	Thermo Fisher Scientific Inc., Waltham, USA
NuPAGE® Novex® Antioxidant	Life technologies Corporation, Carlsbad, USA
NuPAGE® Novex® Bis-Tris Midi Gels	Life technologies Corporation, Carlsbad, USA
NuPAGE® Novex® MES SDS running buffer	Life technologies Corporation, Carlsbad, USA
PageRulerTM Prestained Protein ladder, 10 to 180 kDa, #26616	Thermo Fisher Scientific Inc., Rockford, USA
PBA	2% (v/v) FBS, 0.02% (w/v) NaN_3 in 1x PBS
PBS (10x)	80.6 mM Na_2HPO_4, 14.7 mM KH_2PO_4, 1.37 M NaCl, 26.7 mM KCl; used as 1x PBS pH 7.5
PBST	PBS, 0.05 % (v/v) Tween 20
Penicillin-Streptomycin (100x)	10.000 U/ml penicillin, 10.000 µg/ml streptomycin (Thermo Fisher Scientific, Waltham, MA, USA)
Phosphate buffered saline (PBS)	20 mM Na_3PO_4, 0.7 % NaCl, pH 7.2
Protease inhibitor, cOmplete, EDTA-free	Roche Diagnostics AG, Basel, Switzerland
Puromycin	Sigma Aldrich, Merck KGaA, Darmstadt, Germany
RPMI 1640 medium (+ 2 mM L-glutamine, 21875-034)	Life Technologies, Gibco, Karlsruhe, Germany
TBST	TBS, 0.1% (v/v) Tween 80
Tris-buffered saline (TBS)	0.242% (w/v) Tris, 0.08% (w/v) NaCl
Tween 20	Carl Roth GmbH & Co, Karlsruhe, Germany

Tween 80	Merck KGaA, Darmstadt, Germany
ZnCl$_2$	100 mM in H$_2$O, sterile filtered

2.7 Mice

NMRI nude	Crl: NMRI-Foxn1nu (Charles River, Wilmington, MA, USA)

2.8 Special Implements

Anti-FLAG® M2 affinity gel	Sigma-Aldrich, St. Louis, MO, USA
Bottle Top Filter	CA Low Protein binding, 500 mL, 0.2 µm/0.45 µm (Corning Incorporated, Tewksbury, MA, USA)
Chromatography columns	Poly-Prep® (Bio-Rad, Munich, Germany)
Counting chamber	Neubauer improved (Marienfeld Superior, Paul Marienfeld GmbH & Co. KG, Lauda-Königshofen, Germany)
Dialysis membrane	High retention seamless cellulose tubing, 23 mm, MWCO 12.400 (Sigma-Aldrich, St. Louis, MO, USA)
FLAG peptide	5 mg/ml (peptides&elephants, Potsdam, Germany)
FPLC column	Superdex 200 10/300 GL (GE Healthcare, Little Chalfont, Buckinghamshire, UK)
HPLC column	Yarra™ 3 µm SEC-2000, Yarra™ 3 µm SEC-3000 (Phenomenex, Torrance, CA, USA)
Reaction tubes	1.5 mL, 2 ml Safe-Lock (Eppendorf AG,

Hamburg, Germany)

Syringe filter	Acrodisc® 13 mm, 0.2 µm, HT Tuffryn® Membrane (Pall Corporation, Port Washington, NY, USA)
Ultrafiltration spin columns	Vivaspin 500, 30,000 MWCO PES (Sartorius, Göttingen, Germany)

2.9 Instruments

-20°C freezer	Comfort NoFrost, Liebherr, Bulle, Switzerland
-80°C freezer	HT5786-A, Hettich lab technologies, Tuttlingen, Germany
Cell counter CASY	OLS OMNI Life Science, Bremen, Germany
centrifuge	Eppendorf centrifuge 5415R, Hettich lab technologies, Tuttlingen Germany
centrifuge	Heraeus Multifuge 3-LR, Hettich lab technologies, Tuttlingen, Germany
centrifuge	Eppendorf centrifuge 5810R, Hettich lab technologies, Tuttlingen, Germany
ECL imager	Amersham Imager 600, GE Healthcare Europe GmbH, Freiburg, Germany
electrophoresis power supply EPS 301	Amersham Pharmacia Biotech; GE Healthcare Europe GmbH, Freiburg, Germany
electrophoresis power supply EPS 601	Amersham Pharmacia Biotech; GE Healthcare Europe GmbH, Freiburg, Germany
flow cytometer	MACSQuant Analyser 10, Militneyi Biotec, Bergisch Gladbach, Germany

heat block	HBT-1-131, Haep Labor Consult, Bovenden, Germany
heat block	Eppendorf Thermomixer compact, Merck KGaA, Darmstadt, Germany
iBlot 2	Dry Blotting System Thermo Fisher Scientific Inc., Waltham, USA
incubator	Varocell, Varolab GmbH, Giesen, Germany
incubator	Forma Reach-In CO2 Incubator, Thermo Fisher Scientific Inc., Waltham, USA
infrared imager	LI-COR Odyssey, LI-COR Biosciences GmbH, Bad Homburg, Germany
microplate reader	SPARK, Tecan, Meannedorf, Switzerland
microplate reader	Infinite M200, Tecan, Meannedorf, Switzerland
Mini Gel Tank	Thermo Fisher Scientific Inc., Waltham, USA
nitrogen tank	K SERIES cryostorage system, tec-lab GmbH, Taunusstein, Germnay
sonifier	SONOPLUS HD 200, BANDELIN electronic GmbH & Co. KG, Berlin, Germany

2.10 Software

Fiji	distribution of ImageJ
Flowing software 2.5.1	Cell Imaging Core, Turku Centre for Biotechnology, University of Turku and Åbo Akademi University
FlowJo	7.6.1 Tree Star Inc., Ashland, Oregon, USA
GraphPad Prism 5	GraphPad Software Inc., San Diego, CA, USA
MACSQuantify	MACS Miltenyi Biotec, Bergisch Gladbach,

Germany

Matlab R2016b	The Mathworks Inc. MA, US
Odyssey	LI-COR Odyssey, LI-COR Biosciences GmbH, Bad Homburg, Germany

3 Methods

All described methods are commonly used in the Morrison Lab at the Institute of Cell Biology and Immunology, Stuttgart, Germany.

3.1 Cell culture

3.1.1 2D cell culture and passaging

Cell lines were cultivated in RPMI 1640 medium with 2 mM L-glutamine and supplemented with 10% (v/v) fetal bovine serum (FBS, NCI-H460). The cell lines were grown adherently on various culture flasks at 5% CO_2 and 96% relative humidity in an incubator (Varocell, Varbolab GmbH; Forma Reach-In CO2 Incubator, Thermo Fisher Scientific Inc.) and were passaged every other day to maintain a healthy and proliferative cell culture. Passaging was performed by washing the cells with pH 7.4 phosphate buffered saline (PBS) and detaching them from the surface by applying 1 x trypsin (10 x trypsin/ethylenediaminetetraacetic acid (EDTA) in PBS) for approximately 5 minutes. Afterwards, the reaction was stopped by adding at least the equal amount of cell culture medium to inactivate the trypsin. The suspension was gently but thoroughly mixed and cell were diluted as necessary (from 1:2 to 1:10, depending on the cell line) or prepared for counting, further seeding or preparing protein lysates for Western blotting. For long term storage of the cell lines, approximately 2×10^6 cells were pelleted by centrifugation (300 g for 5 min, Eppendorf centrifuge 5810R, Hettich lab technologies), supernatant was removed, and the cells were re-suspended in the 500 µL of RPMI 1640 medium and 500 µL of freezing medium (20% (v/v) dimethyl sulfoxide (DMSO) in FBS). This suspension was then transferred to a sterile cryo vial and frozen at - 80°C (HT5786-A, Hettich lab technologies). After at least 24 h, frozen vials were transferred to a liquid nitrogen tank (K-series, tec-lab GmbH).

3.1.2 Cell counting and seeding for various assays

Cell counting was performed using a Neubauer counting chamber (haemocytometer). The cells were trypsinised from the plastic and 10 µl of the suspension was mixed with 10 µl of

trypan blue solution to exclude the dead cells from the count. 10 µl of the solution was loaded onto the counting chamber. The cell number was then obtained by calculating the mean number of cells counted multiplied by the volume cell suspension loaded onto the haemocytometer, multiplied by 10^4 (conversion factor to achieve a number of cells per millilitre). Depending on the size of the plastic dish needed for the experiment, a different number of cells were seeded. For cell death assays performed in a 96-well plate, approximately 1 x 10^4 cells in 100 µl of the medium was seeded per well. For assays performed in a 6-well plate, approximately 1 x 10^5 cells were seeded in 2 mL of the feeding medium. For assays performed in a 6 mm Petri dish, approximately 1 x 10^6 cells were seeded in 10 mL of the feeding medium. Afterwards, the cells were evenly distributed over the surface by gently swirling the dish and were left to attach overnight in an incubator at 37°C and 5% CO_2.

3.1.3 3D cell culture

The desired cell line was grown until the confluency reached 80-90%. The cells were washed with 5 mL 1 x PBS and afterwards trypsinised with 5 mL 1 x trypsin for 5 min. The reaction was stopped by adding 10 mL of medium and the cells were gently re-suspended and collected in a Falcon tube. The cells were spun down at 500 g for 5 min and the supernatant was aspirated. The cells were re-suspended in 5 mL of the fresh medium. Next, the cells were counted with a haemocytometer and diluted to the final concentration of 10^4 cells/mL in RPMI with the addition of 20% of Methyl Cellulose (Sigma Aldrich, Germany) solution. Approximately 40 spheroids could fit on the lid of a Petri dish, making the calculation enough to seed 40 spheroids of 25 µL of suspension and containing ~ 250 cells per spheroid. The Petri dish was filled with 1 x PBS so the spheroids would not dry during the incubation period. The spheroids were left to form for 4 days at 37°C and 5% CO_2. On the fifth day, 10 µL of fresh RPMI + 20% Methyl Cellulose was added to the spheroids. The medium was exchanged every second day until the spheroids were 10 days old.

3.1.4 Preparing IZI1551 for treatment

IZI1551 was initially supplied by Roland Kontermann and the same batch was used for all *in vitro* experiments. For the purpose of xenograft experiments (*in vivo* experiments), IZI1551 was produced and purified by Vesna Vetma (as described in section Methods 3.4). Recombinant protein was supplied in PBS. Protein concentration (mg/mL) was determined by measuring the absorption at 280 nm using NanoDropTM ND-1000 spectrophotometer. Beer-Lambert equation was used to calculate the concentration of protein:

$$c = \frac{A280 \cdot Mw}{\varepsilon \cdot d}$$

where:

A280 – absorption at 280 nm

Mw – molecular weight of the protein (g/mol)

Ɛ – extinction coefficient

d – path length (cm)

Afterwards, the protein concentration (g/L) was divided with molecular weight (g/mol) to convert the units from mg/mL to mol/L, and then multiplied by 10^9 to get nanomolar values.

The cell lines were treated with different drug combinations or single treatments and incubated at 37 °C for different durations.

3.2 Flow cytometry

3.2.1 Measuring the expression of surface death receptors

The cells were cultivated in cell culture flasks until they reached 80-90% confluency and afterwards washed with PBS and harvested with 1 x trypsin for 10 min. The cells were then

counted and 1 x 10^5 cells per sample were spun down with 500 g for 5 min. Subsequently, the pellet was re-suspended in ice-cold PBA (0.05% (w/v) bovine serum albumin (BSA) + 0.02% (w/v) NaN_3 in PBS) and spun again. The supernatant was removed, and the pellet was re-suspended in 100 μL ice-cold PBA containing the primary antibody (dilution 1:100) and incubated on ice for 1 h. Afterwards, the cells were washed again with PBA and re-suspended in 50 μL of secondary antibody (dilution 1:50) in PBA. The cells were left to incubate for 45 min on ice and in the dark. Afterwards, the cells were washed again with ice-cold PBA, re-suspended in 100 μL of fresh ice-cold PBA and transferred to a 96-well plate (U bottom). The fluorescence was measured by flow cytometry (MACSQuant Analyser 10, Miltenyi Biotec; LSRFortessa, BD Biosciences) by using the 488 nm excitation laser. Emission was recorded at 500-550 nm. Surface expression of death receptors was calculated with quantification beads QIFIKIT (Biozol, Germany) by comparing the mean FITC signal of the cells to the calibration beads.

3.2.2 High-throughput cell death measurement

10000 cells/well were seeded in a 96-well plate and left to attach overnight at 37°C and 5% CO_2. The next day, treatments were prepared as necessary. The medium was removed from the cells and the previously prepared treatment was transferred to the cells (100 μL). Treated cells were left to incubate at 37°C and 5% CO_2 for 24 or 72 h. After the desired incubation period, the treatments were removed and kept in a separate 96-well plate. The cells were washed with 50 μL PBS (transferred to an additional plate) and afterwards harvested with 50 μL 1 x trypsin for 5-10 min. The reaction was stopped by adding the medium from the separate 96-well plate to the trypsinised cells. 50 μL of PI (propidium iodide) (1 μg/mL) was added to each well in a plate. The plate was incubated for 10 min with gentle shaking before starting the measurement on a flow cytometer. The measurements were done on a high throughput flow cytometer (BD LSRII SORP) using 488 nm lasers for excitation and emission was recorded at 617 nm wavelength.

3.2.3 Apoptotic cell death measurements by Annexin V/ PI staining

The cells were seeded in a 6-well plate and left to attach overnight at 37°C and 5%. Alternatively, 3D spheroids were collected (approx. 40 spheroids per treatment) in a Falcon tube and spun down at 500 g for 5 min and placed in an agar-coated 6-well plate.

The cells were treated with IZI1551, Birinapant, their combination or their combination with the addition of the pan-caspase inhibitor QVD OPh for 24, 48 or 72 h. The spheroids were treated for 24 or 72 h.

On the day of the measurement, the supernatant was collected in a separate tube, in order to collect both the dead cells and alive cells. Attached cells were washed with 1 mL 1 x PBS and trypsinised with 1 x trypsin for 5 min. The reaction was stopped by adding 2 mL of the medium. Trypsinised cells and the supernatant with dead cells were combined and spun down at 500 g for 5 min. The supernatant was removed and the cells were washed with 500 µL of Annexin V Binding Buffer (BioLegend Germany). The cells were again spun down at 500 g for 5 min and the binding buffer was removed. Separately, the mixture of Annexin V-APC (Biolegend, Germany) (0.1%) or Annexin V-GFP (made in-house, 0.1%) and PI (Biolegend, Germany or Sigma Aldrich, Germany) (1 µg/mL) was prepared as a master mix. The cells were resuspended in 100 µL of the master mix. Measurements were done on a BD FACS Canto II flow cytometer using a yellow-green laser with 561 nm excitation wavelength (emission from 600 to 620 nm; PI) or red laser with 640 nm excitation wavelength (emission from 655 to 685 nm; APC). Alternatively, measurements were done on the MacsQuant flow cytometer using the blue 488 nm laser for excitation (emission from 655-730 nm; PI) and blue 488 nm laser for excitation (emission from 500-550 nm; GFP). Compensation was performed as required.

3.2.4 Analysis of flow cytometric data

To analyse the data generated by flow cytometry, following software were used: the software FlowJo 7.6.1 (Tree Star Inc.), MACSQuantify (MACS Miltenyi Biotec), Flowing

software 2.5.1 and Cyflogic (Cell Imaging Core, Turku Centre for Biotechnology, University of Turku and Åbo Akademi University).

3.2.5 Calculating the synergy scores by Webb's fractional product

Webb's fractional product method was used to calculate the synergy between IZI1551 and Birinapant. The calculation was done based on cell death data generated by flow cytometry. Percentage of cell death for each treatment was calculated as a mean of n=3 independent repeats. CI (combination index) was calculated according to the formula:

$$CI = \frac{a x b}{c}$$

Where:

a – Percentage of alive cells after the single treatment with a

b – Percentage of alive cells after the single treatment with b

c – Percentage of alive cells after the combination treatment of drugs a and b

Calculated CI values represent:

CI < 1.0 indicates synergy; the lower the CI value is, the stronger the synergy

CI = 1.0 indicates additive effect

CI > 1.0 indicates antagonistic effect

3.3 Western blotting

3.3.1 Preparation of whole cell extracts for western blotting for 2D and 3D culture

The cells were harvested as described before, either untreated for basal protein quantification or treated, for examining the signalling pathways. After trypsinising the cells

with 5 mL 1 x trypsin and deactivation with 10 mL of medium, the cells were spun down at 500 g for 5 min. The supernatant was aspirated, and the cells were re-suspended in 100 μL of 1 x PBS and transferred to a 1.5 mL reaction tube. The cells were again centrifuged at 500 g for 5 min to remove the PBS. The cell pellet was re-suspended in lysis buffer (150 mM NaCl, 1 mM EDTA, 20 mM TRIS, 1% Triton x-100, pH=7.6) with addition of phosphatase inhibitor (PhosSTOP, 20x, Roche, Germany) and protease inhibitor (cOmplete, 20x, Roche, Germany) and incubated for 1 h on ice. Afterwards, the lysed suspension was centrifuged at 1500 g for 20 min at 4 °C to pellet the crude cell components. The supernatant was transferred to a new 1.5 mL reaction tube and the pellet was discarded.

For 3D spheroids the protocol was similar. The additional step for the spheroids was the sonication (6 pulses, Bandelin Sonoplus HD 200, BANDELIN electronic GmbH & Co. KG) to ease the lysis of the spheroids.

3.3.2 Determining the concentration of proteins by Bradford assay

Generated whole cell lysate was diluted 1:10 with dd H_2O and 2 μL were loaded onto the 96-well plate (F-bottom, clear) in duplicates. Also, the BSA standard was loaded in the same plate (Paesel + Lorei GmbH & Co; 0.0, 0.125, 0.25, 0.5, 0.75, 1.0, 1.5, 2.0 mg/ml BSA diluted in ddH_2O). 200 μL of Bradford reagent (Carl Roth GmbH & Co) was added to the cell lysates. The plate was incubated for 5 min at RT and afterwards, the absorbance was measured at a wavelength of 595 nm with a microplate reader (Infinite M200 or SPARK, Tecan, Meannedorf, Switzerland). The concentration of the protein in a whole cell lysate was determined by comparing the absorbance of the colorimetric signal of the samples of a known concentration to the one of the unknown concentration. The protein samples were either further prepared for Western blotting or stored at -20°C for later analysis.

3.3.3 Protein sample preparation for SDS-PAGE

1 μg/ 1 μL (20 μg in 20 μL) of the protein sample was prepared from the previously prepared whole cell lysate. The protein samples consisted of the required volume of cell lysate containing 20 μg of protein, Laemmli 5 x loading buffer Tris-HCl 27 mM (pH 6.8), glycerol

5%, SDS 1.6%, β-mercaptoethanol 0.83% and bromophenol blue 0.002%) and lysis buffer. The protein samples were incubated for 5 min at 95°C on a heat block (HBT-1-131, Haep Labor Consult, Bovenden, Germany) and finally, either frozen at -20°C or directly loaded onto the gel.

3.3.4 Sodium Dodecyl Sulfate Polyacrylamide gel electrophoresis (SDS-PAGE)

The protein samples, together with protein standard, were loaded on the respective precast gel and ran depending on the gel in the corresponding electrophoresis chamber using the indicated buffers, following the manufacturer's instructions (Table 1).

Table 5. The list of gels and buffers used for SDS-PAGE

Gel	Buffer	Chamber	Conditions
Bolt 4-12% Bis-Tris Plus Gel 1.0 mm x 10 well	1.0 mm x 10 well Bolt MES SDS Running Buffer (20X)	Bolt mini gel tank	150 V, 400 mA, 40 min
Bolt 4-12% Bis-Tris Plus Gel 1.0 mm x 15 well	Bolt MES SDS Running Buffer (20X)	Bolt mini gel tank	150 V, 400 mA, 40 min
Bolt 4-12% Bis-Tris Plus Gel 1.0 mm x 17 well	Bolt MES SDS Running Buffer (20X)	Bolt mini gel tank	150 V, 400 mA, 40 min
NuPAGE 4-12% Bis-Tris Midi Gel 1.0 mm x 20 well	NuPAGE MES SDS Running Buffer + NuPAGE Antioxidant	XCell4 SureLock Midi-Cell	200 V, 400 mA, 40 min

3.3.5 Semi-dry protein transfer

After the SDS-PAGE, proteins were transferred to a nitrocellulose membrane using the iBlot 2 Dry Blotting System following the manufacturer's instructions (transfer settings: 20 V; 7

min, Thermo Fisher Scientific Inc.). Membranes were stained with Ponceau S solution (Ponceau S solution 0.1%, acetic acid 5%) to examine the quality of protein transfer. Next, membranes were incubated for 1 h with blocking reagent (diluted 1:10 in TBST, Roche Diagnostics).

3.3.6 Protein detection

Following the blocking, membranes were incubated with primary antibody diluted in 0.5 x Blocking reagent in TBST, overnight at 4°C. Afterwards, the membranes were washed 3 x 10 min with 1 x TBST at room temperature. Following the washing step, proteins were detected by either directly measuring fluorescence with an infrared imager (LI-COR Odyssey, LI-COR Biotechnology GmbH) or incubating the membrane with an HRP substrate (SuperSignal West Pico ECL Substrate/SuperSignal West Dura Extended, Pierce Protein Research Products; Luminata Forte Western HRP Substrate, Merck Millipore) and detecting the signals with an ECL imager (Amersham Imager 600, GE Healthcare Europe GmbH). In the case of re-probing, membranes were washed three times with TBST before incubating them with additional antibodies.

3.3.7 Densitometry

Densitometry was performed to calculate the absolute amount of apoptotic proteins in melanoma cell lines by analyzing raw western blot images using Odyssey V3.0 software (LI-COR Biosciences). The intensity of the fluorescent signal was measured for each protein and the background was subtracted for each signal (median background; from top to bottom). The signal was then adjusted to the loading control for each sample. In the end, the signal of the unknown sample was compared to the signal from HeLa cells. The absolute concentrations of apoptotic proteins in HeLa cells were taken from the literature (Lindner et al. 2013; Rehm et al. 2006; Laussmann et al. 2012) except for cIAP1 and cIAP2, which were determined in this study.

3.3.8 Determining the concentration of cIAP1 and cIAP2 in HeLa cells

cIAP1 and cIAP2 recombinant proteins were bought from R&D (Wiesbaden, Germany). cIAP1 (250 ng/µL) was diluted in lysis buffer to the final concentrations of 2.5, 0.025 and 0.0025 ng/µL. cIAP2 (150 ng/µL) was diluted in lysis buffer to the final concentrations of 1.5, 0.015 and 0.0015 ng/µL. cIAP1 recombinant protein was diluted with lysis buffer and 5 x Laemmli buffer to contain 25, 12.5, 6.25, 3.125, 1.56, 0.78, 0.39, 0.19, 0.9 ng of protein to be loaded on the gel. cIAP2 recombinant protein was diluted with lysis buffer and 5 x Laemmli buffer to contain 15, 7.5, 3.75, 1.875, 0.93, 0.46, 0.23 ng.

HeLa cells were grown to the confluency of 80 – 90%. The cells were washed with 5 mL of 1 x PBS and harvested by 5 mL of 1 x trypsin for 5 min. The reaction was stopped by adding 10 mL of the medium. The cell suspension was centrifuged at 500 g for 5 min. The supernatant was aspirated, and the pellet was dissolved in 10 mL of PBS. The cells were then counted with the haemocytometer. Afterwards, the cells were once again centrifuged at 500 g for 5 min and the supernatant was discarded. The pellet was dissolved in the lysis buffer (150 mM NaCl, 1 mM EDTA, 20 mM TRIS, 1% Triton x-100, pH=7.6) with addition of phosphatase inhibitor (PhosSTOP, 20x, Roche, Germany) and protease inhibitor (cOmplete, 20x, Roche, Germany) and kept on ice for 1 h. The whole cell lysate was then centrifuged at 1500 g for 20 min at 4°C. The protein concentration was determined by Bradford assay, as described before.. Hela whole cell lysate was prepared to contain 40, 20, 10, 5, 2.5, 1.25 µg of protein mixed with 5 x Laemmli buffer to be loaded on the gel.

The dilutions of cIAP1, cIAP2 and Hela were resolved on Nu-PAGE^{TM} 4-12% Bis-Tris Midi gel (Invitrogen, Thermo Fisher Scientific, Germany) at 200 V, 400 mA for 40 min as described before. The membranes were blocked as described before and primary antibodies were added to incubate overnight at 4°C. Proteins were detected by directly measuring fluorescence with an infrared imager (LI-COR Odyssey, LI-COR Biotechnology GmbH) and densitometry was performed on every signal (Figure 4).

The concentrations were calculated in two steps. Known concentrations of cIAP proteins were plotted against their densities (y= ax + b, where x was the ng of loaded protein and y its density).
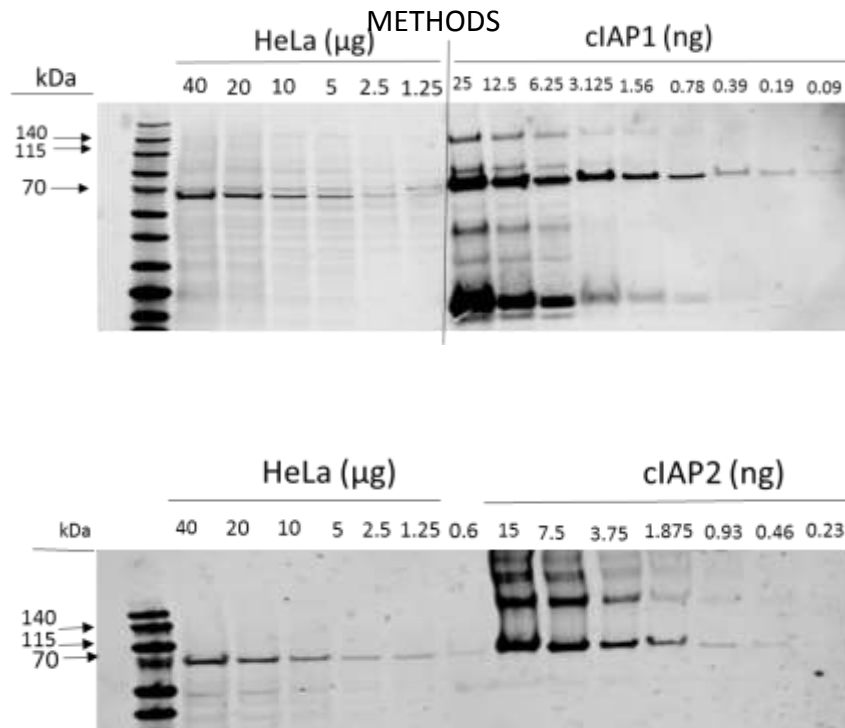
Figure 4. Determining the concentration of cIAP1 and cIAP2 in Hela cells. The concentration was calculated by comparing the western blot signal from Hela cells with the signal from the diluted recombinant proteins. All measurements were done in triplicates.

The density of Hela cells was then inserted instead of x in the equation. The concentration calculated was then divided by the number of Hela cells used to make a protein extract, for each band on the Western blot separately. The average of all bands was taken to finally calculate the concentration. The average concentration was then divided by the molecular weight of the respective protein and multiplied by the volume of 1 Hela cell (3.1 pL, (Rehm et al. 2006)) The concentration of cIAP1 was calculated to be 11.68 nM, and the concentration of cIAP2 39.85 nM, in Hela cells.

3.4 Production of IZI1551

The vector construct for IZI1551 (Flag/Fc (Q, G)-scTRAIL-pSecTag) was kindly provided by Prof. Dr. Roland Kontermann (Institute for Cell Biology and Immunology, Stuttgart, Germany). Production and purification was done according to the method developed by Hutt and colleagues (Hutt et al. 2017).

3.4.1 Transformation of plasmid DNA into bacteria and plasmid purification

An aliquot of DH5α bacterial culture was thawed on ice. In the meantime, 10 ng of plasmid DNA was diluted in 20 μL of H_2O and placed on ice. 40 μL of TCM buffer (10 mM Tris-HCl, pH=8, 10 mM $CaCl_2$ and 10 mM $MgCl_2$) and 100 μL of DH5α bacterial culture were added to the plasmid dilution. The mixture was incubated on ice for 30 min followed by 2 min heat-shock at 42°C and again 1 min on ice. 640 μL of prewarmed LB medium (10 % Tryptone, 10 % NaCl, 5 % yeast extract in ddH_2O, pH=7) was immediately added to the suspension followed by incubation of the mixture on a shaker (250 rpm) at 37°C for 1 h. 50 μL of the transformed bacterial suspension was spread on LB agar plates made with 25 μg/mL of Kanamycin and the plates were incubated at 37°C overnight. The next day one of the grown colonies was transferred into 1200 mL of LB medium containing 1% (w/v) glucose and 100 μg/mL Ampicillin and incubated overnight in an orbital shaker at 37 °C. Finally, plasmid DNA was prepared using NucleoBond® Xtra Midi kits (Midi-preparation from 150 mL overnight culture) according to the manufacturer's protocol. The DNA concentration was determined by measuring the absorbance at 260 nm using the NanoDrop™ ND-1000.

3.4.2 The cell culture of suspension HEK P2 cell line

Production of IZI1551 was done in the human embryonic kidney (HEK) P2 suspension cells with a DR5 knockout generated by Dr. Martin Siegemund (Institute of Cell Biology and Immunology, University of Stuttgart, Germany). HEK P2 cells were maintained in F17 Expression Style medium supplemented with 4 mM GlutaMAX, 0.1% Koliphor P188 and with the addition of 4 μg/mL Puromycin in Erlenmeyer flasks, continuously incubated on the orbital shaker at 37˚C and 5% CO_2. The cell number was monitored every second day by counting with CASY cell counter (Omni Life Sciences, Germany), making sure that the cell number does not exceed 2 x 10^6 cells/mL. One day before transfection, 1.2 x 10^6 cells were spun down at 500 g for 10 min and the supernatant aspired. The cell pellet was re-suspended in 360 mL of F17 Expression Style Medium supplemented with 4 mM GlutaMAX, 0.1% Koliphor P188, without antibiotics.

3.4.3 Transient transfection with polyethyleneimine (PEI)

Transfection was done when the cells were in their exponential growth phase ($1.5 - 2 \times 10^6$ cells/mL). Therefore, on the day of transfection, the cells were counted and visually inspected under the microscope if they looked healthy and if the viability was greater than 90%. 20 mL of F17 medium containing 400 µg of DNA was prepared and briefly vortexed. Also, another 20 mL of F17 medium was prepared, containing 1200 µL (1mg/mL) PEI and briefly vortexed. Both solutions were left to incubate for 5 min on RT. Next, two solutions were carefully mixed by adding the PEI mixture into the DNA mixture. The new 40 mL solution was left to incubate at RT for 20 min. Afterwards, the mixture was added to 360 mL of HEK P2 cells in their exponential growth phase.

3.4.4 Peptone feeding

24 h after transfection, 0.5% tryptone N1 (TN1) and 10 µM $ZnCl_2$ were added to the suspension cells. The cells were left to incubate for the next 96 h on the orbital shaker at 37°C and 5% CO_2. Afterwards, proteins were harvested from the supernatant of cultured cells and further purified.

3.4.5 Protein harvesting and purification by anti-FLAG chromatography

After 5 days, the suspension cells were harvested by centrifugation at 2000 x g for 30 min at 4°C. The supernatant was collected in a 1 L sterile bottle. In parallel, anti-FLAG M2 Affinity Gel (Sigma Aldrich, Germany) was equilibrated by washing three times with 100 mM glycine-HCl, pH=3.5 and another five washing rounds with PBS. To capture the target protein, the protein solution and affinity resin were incubated rolling at 4°C overnight. The affinity gel was collected by centrifugation at 1000 g for 10 min and subsequently transferred to a chromatography column. Washing was performed using PBS as a wash buffer. Wash and elution steps were analysed by qualitative Bradford assay as described before. Bound protein was eluted with PBS containing 100 µg/ml FLAG peptide. The elution progress was

continuously monitored to collect the complete protein-containing eluate, which was dialyzed against 5 L PBS overnight at 4°C. To recycle the affinity gel, equilibration was repeated, and the resin was stored in 50 % (v/v) glycerol in PBS containing 0.02% sodium azide at 4°C.

3.4.6 Preparative size-exclusion high-performance liquid chromatography (HPLC)

Purified protein was analysed by size exclusion HPLC. Protein eluates containing considerable amounts of aggregates, fractions with wrong oligomerization status, or cleavage products were further purified by size exclusion FPLC. The concentrated protein was applied to a Superdex 200 10/300 GL column using PBS as mobile phase and a flow rate of 0.5 ml/min. Protein was collected in 100 µl to 250 µl fractions. Fractions containing the desired protein configuration were pooled. Preparative size exclusion chromatography was performed by Doris Göttsch (Institute of Cell Biology and Immunology, University of Stuttgart, Germany) (Figure 5).
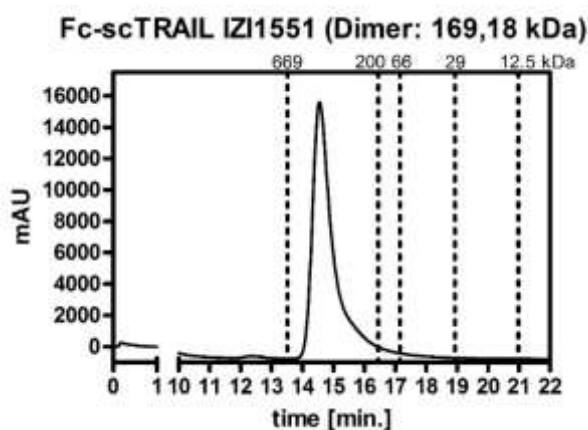
Figure 5. Preparative size-exclusion HPLC was used to investigate proteins under native conditions. Elution times of standard proteins and the corresponding molecular masses [kDa] are indicated.

3.4.7   SDS-PAGE and cell viability assay

SDS PAGE was performed to further confirm the purity of the protein. 5 µg of the protein was resolved on Bolt 4-12% Bis-Tris Plus Gel in reducing and non-reducing conditions. The gel was boiled in ddH$_2$O and incubated in Coomassie staining solution for 1 h at RT. Gel was visualised on photo scanner Epson Perfection V200 (Saiko Epson Corporation, Amsterdam, Netherlands). A band of approximately 170 kilo Dalton (kDa) was present under non-reducing conditions and one band of approximately 85 kDa was detected under reducing conditions (Figure 6).
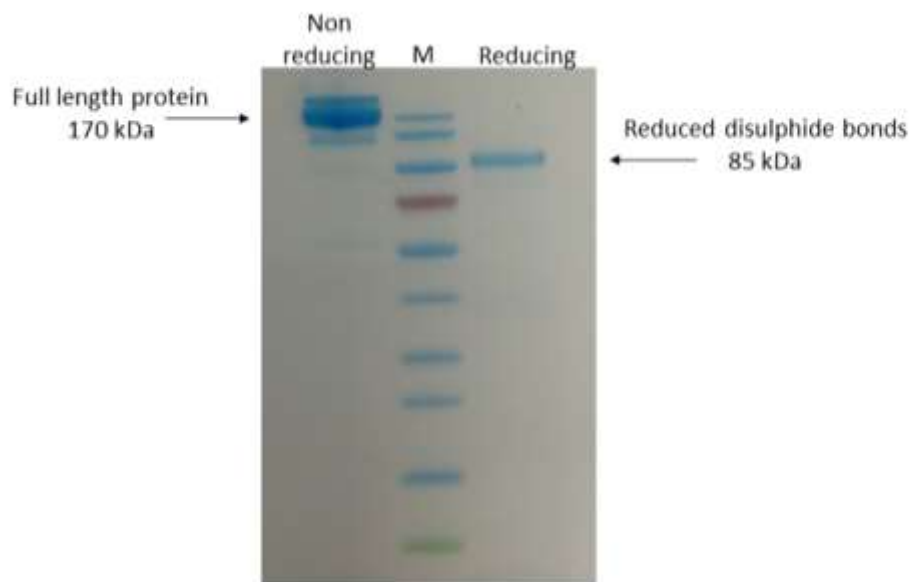
Figure 6. Examining the purification of produced protein with SDS PAGE. Protein was exposed to reducing and non-reducing conditions, resolved on a polyacrylamide gel and afterwards stained with Coomassie staining solution. Full length protein and reduced protein were detected, but not degradation products.

To test the efficacy, the concentration of the protein was calculated (as described before) and serial fold dilutions were made. 10 000 cells/well of melanoma cell line Mel Juso were seeded in a 96-well plate (F-bottom, transparent) and left to attach overnight at 37°C and 5% CO$_2$. On the next day, the cells were treated with serial dilutions of the protein and incubated for 24 h at 37°C and 5% CO$_2$. The viability of the cells was determined the next day by Crystal Violet staining. The treatment was removed, and the plate was washed under

a stream of tap water. 100 μL of 0.5% Crystal Violet solution was added to each well. After 1 h of incubation at RT, crystal violet staining was removed, and the cells were left to dry at RT overnight. 100 μL of methanol was added per well and the absorption was measured at 570 nm on a microplate reader (SPARK, Tecan, Meannedorf, Switzerland). The comparison was made with the IZI1551 TRAIL previously produced by Meike Hutt (Institute for Cell Biology and Immunology, Stuttgart, Germany). Reduced cell viability of the cell line Mel Juso upon the treatments with different production batches of IZI1551 is shown in Figure 7.
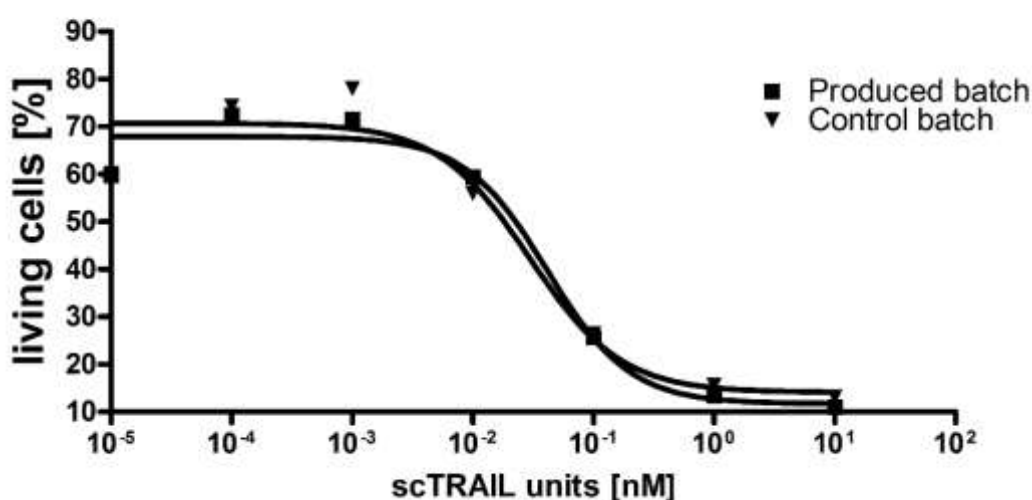
Figure 7. Loss of viability induced by IZI1551 TRAIL in the cell line Mel Juso. 10 000 cells per well was seeded in a 96-well plate. The cells were treated with indicated dilutions of IZI1551 for 24 h and afterwards stained with crystal violet. Absorption was measured at 570 nm.

3.5 Xenograft model in mice

This protocol was approved by Animal Welfare and Ethics Committee of the government of the State Baden Wuerttemberg, Germany and Department of Animal Physiology, University of Stuttgart. Animal care and all experiments were in accordance with federal and European guidelines.

3.5.1 Implanting the cell lines subcutaneously (s.c.)

Cell lines were expanded to a desired number of flasks. One day before the harvesting and injection, the cells were split in order to be in a log phase of the growth on the day of the harvest. For harvesting, the medium was aspirated, and the cells were washed twice with 5 mL 1 x PBS. Cells were detached by trypsinisation with 5 mL of 1 x trypsin for 10 min. 10 mL of the medium was added to inactivate the trypsin after 10 min. Cells were collected in the 50 mL Falcon tube and spun down at 300 g for 5 min. The cells were afterwards washed twice with 1 x PBS without Mg^{2+} and Ca^{2+} ions. Cells were finally spun down at 300 g for 5 min and diluted in an appropriate volume of 1 x PBS. For both pre-experiment and experiment, 5 x 10^6 cells in 100 µL PBS were injected subcutaneously. Mice were temporarily sedated with isoflurane before subcutaneous injection.

3.5.2 Determining the optimal concentration of Birinapant *in vivo*

5x10^6 MeWo and SkMel2 cells (in 100 µl PBS) were injected subcutaneously into the left and right flank of female NMRI nude mice. Tumour growth was monitored by measuring the length (a) and width (b) of the tumours with a digital calliper to calculate the tumour volume ($V = a \cdot b2/2$). Treatment started when tumours reached a size of approximately 100 cm³. Birinapant (diluted in 100 µl peanut oil) was injected intraperitoneally, whereas IZI1551 (in 100 µl PBS) was injected intravenously. A first experiment was performed to analyse the anti-tumour activity of Birinapant. Mice (8 weeks old, 7 per group) received 12 injections of either peanut oil or treatment (3 mg/kg, 10 mg/kg and 30 mg/kg). The injections were performed 3 times per week, during the period of 4 weeks, starting from the day 19 (12 injections all together). The blood was taken 1 h before and 3 h after the treatment to examine the changes in TNFα levels in the blood caused by the treatment.

3.5.3 Testing the efficacy of the combination treatment *in vivo*

The second experiment was performed to analyse the anti-tumour activity of single and combination treatment of Birinapant and IZI1551.

5×10^6 MeWo cells (in 100 µl PBS) were injected subcutaneously into the left and right flank of female NMRI nude mice. Tumour growth was monitored by measuring the length (a) and width (b) of the tumours with a digital calliper to calculate the tumour volume ($V = a \cdot b \cdot b/2$). Upon reaching a size of approximately 100 cm^3, treatment was started. Mice (8 weeks old, 5 per group) received 0.1 nmol of IZI1551 twice per week during the period of 4 weeks and 10 mg/kg of Birinapant three times per week.

3.5.4 Protein quantification in tumour tissue

Two mice were sacrificed upon the formation of the tumour of approximately 150 cm^3 to harvest the tumours and to quantify the baseline apoptotic proteins. Tumours were macerated in lysis buffer (100 µL per 0.1 g) and sonicated (6 pulses, Bandelin Sonoplus HD 200, BANDELIN electronic GmbH & Co. KG). The suspension was incubated on ice for 1 h and afterwards spun down at 1500 g for 20 min. The protein concentration was determined by Bradford assay, as described before.

3.5.5 Death receptor surface staining and quantification

After the tumours were harvested, one part of a tumour was used to make a single cell suspension using Tumour Dissociation Kit (Milteny Biotech, Germany) according to the protocol provided by the manufacturer. Death receptors were stained and analysed on the flow cytometer as described before. To gate only the MeWo cells among the several types of mouse cells in the tumour, a control was prepared by staining the human cells with anti-human HLA-ABC FITC conjugated antibody.

3.5.6 Predicting the responsiveness of untreated xenografts *in silico*

Quantified proteins (left tumour, right tumour) were positioned in the PC space and the responsiveness was calculated by using Linear Discriminant Analysis and Leave One Out Cross Validation, as described in the chapter Statistical methods and pattern recognition.

3.6 Statistical methods and pattern recognition: SYS ACT pipeline

The SYS ACT (Pipeline was first published by Passante and colleagues in 2013 (Passante et al. 2013). It was developed by Maximilian Würstle (Royal College of Surgeons In Ireland, Dublin, Ireland) and modified by Cristiano Guttá (Institute for Cell Biology and Immunology, Stuttgart, Germany) for the purpose of this study. MATLAB 2016b was used in this study.

3.6.1 Principal component analysis (PCA), Linear Discriminant Analysis (LDA) and Leave One Out Cross Validation (LOOCV)

PCA was used to reduce the dimensionality of the dataset with a minimum loss of variance of the data. This was done by transforming the original data into new parameters whose dimensions are called principal components. Each principal component is a linear combination of the original parameters, however the contribution of information that represents the original data varies between the principal components. The amount of information contained in the principal components is assessed by calculating the variance of the transformed dataset in relation to the original dataset. Principal components that describe the original data best are kept and the others are discarded in the consequent analysis. The Kaiser criterion is a decision guideline of which principal component contains the largest amount of information within the data (Kaiser 1960). Principal components with an eigenvalue larger than 1 should be considered, as they contain more information than a single original parameter. The MATLAB Function *pca* was used to perform this analysis. LDA is a widely used classification method that belongs to supervised machine learning algorithms, meaning it requires a training dataset that contains parameters and variables, and a classification. Based on a training dataset, LDA determines a linear function of those parameters that allow discriminating the training data into the given classes. Leave One Out Cross Validation (LOOCV) was used to calculate the predictive capacity of the model. The calculation was done on a reduced dataset. For each cell line its protein set was left out of the training dataset and used as test data. To perform LDA and LOOCV, the MATLAB function *classify* was used.

4 Results

4.1 Chapter 1: Birinapant sensitises melanoma cell lines to IZI1551-induced apoptosis that can be predicted by multivariate statistical modelling

16 melanoma cell lines were screened for their responsiveness to IZI1551, a novel hexavalent TRAIL receptor agonist, and Birinapant, a bivalent SMAC mimetic, to identify cell lines that exhibit synergistic or low responses after the combination treatment. As it was hypothesised that the expression level of proteins involved in apoptosis signalling influence the responsiveness of individual cell lines to treatment, multivariate statistical modelling was carried out to correlate protein amounts with susceptibility. Furthermore, this information was exploited to make predictions of the responsiveness to the drugs on a case-by-case basis. Analysis revealed that the expression pattern of 19 proteins involved in apoptosis could be used to predict the response in 13 out of 16 investigated cell lines, indicating that the measured protein panel allows for predicting response synergies on an individual basis.

4.1.1 Melanoma cell lines respond heterogeneously to single and combination treatment with IZI1551 and Birinapant

A panel of 16 melanoma cell lines was chosen to investigate the susceptibility to single and combination treatments of IZI1551 and Birinapant. The cell lines were taken from different stages of cancer progression, exhibiting diverse mutation status and therefore represent the heterogeneity of melanoma (Figure 8).

To investigate the cell lines for their susceptibility to the treatments, cells were seeded in a 96-well plate and treated in 3x5 dose-response matrices with IZI1551 (0, 1, 10 pM) and

Birinapant (0, 1, 10, 100, 1000 nM). After the cells were stimulated for 24 and 72 h, cell death was determined by propidium iodide uptake and flow cytometry (Figure 9).

The response of the tested cell lines to the combination treatment was heterogeneous, ranging from resistance and very low response (MeWo, WM3211, WM1791c and WM852) to pronounced synergies (WM1366, SkMel5, SkMel2, Malme 3M, Mel Juso, WM3060, WM35, WM115, SkMel 147, WM793, WM3248, and WM1346). Except for Malme 3M, all other cell lines responded only marginally to a single treatment with Birinapant (shown in Figure 10).
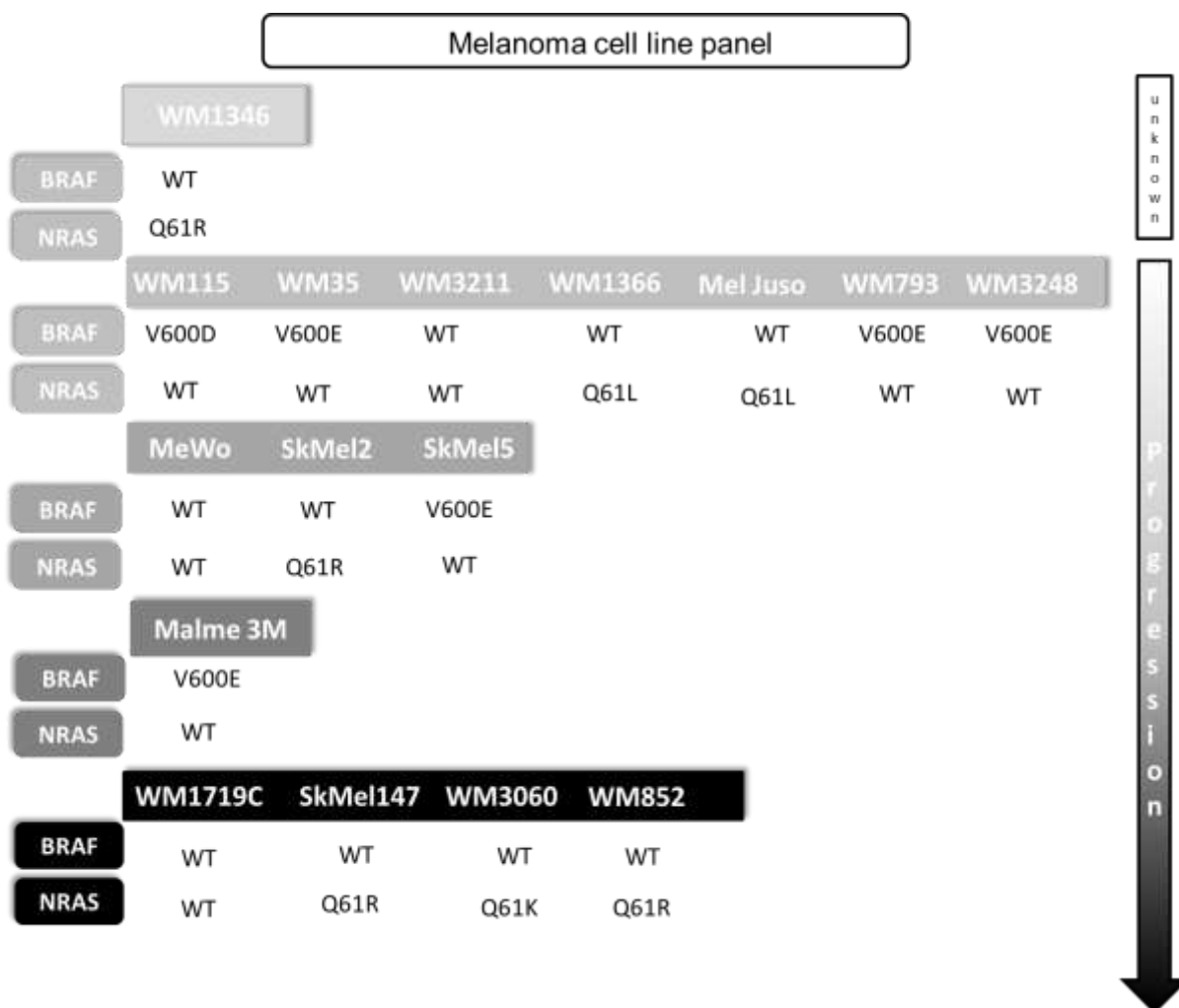
Figure 8. Melanoma cell line panel. The cell lines represent different stages of melanoma progression and exhibit diverse mutation status. The classification was done based on the information from Balch et al. 2009, American Type Culture Collection, Bioinformatics Resources Portal, and Catalogue of Somatic Mutations in Cancer

Synergy among different drugs suggests that the overall therapeutic benefit of the combination is greater than the sum of benefits caused by individual treatments. To identify a potential synergism between IZI1551 and Birinapant, the synergy coefficient was calculated by Webb's fractional product in all investigated cell lines (Figure 6). Combination treatments that scored between 0.1 and 0.9 were considered synergistic, whereas scores from 0.9 to 1 were considered slightly synergistic or additive. Scores above 1 were regarded antagonistic. Based on this classification, the panel was divided into synergistic cell lines comprising WM1366, WM35, SkMel2, SkMel5, WM3248, WM793, SkMel147, WM3060, WM115, Mel Juso, Malme 3M as well as WM1346 and low responding cell lines including MeWo, WM852, WM1791c, and WM3211.
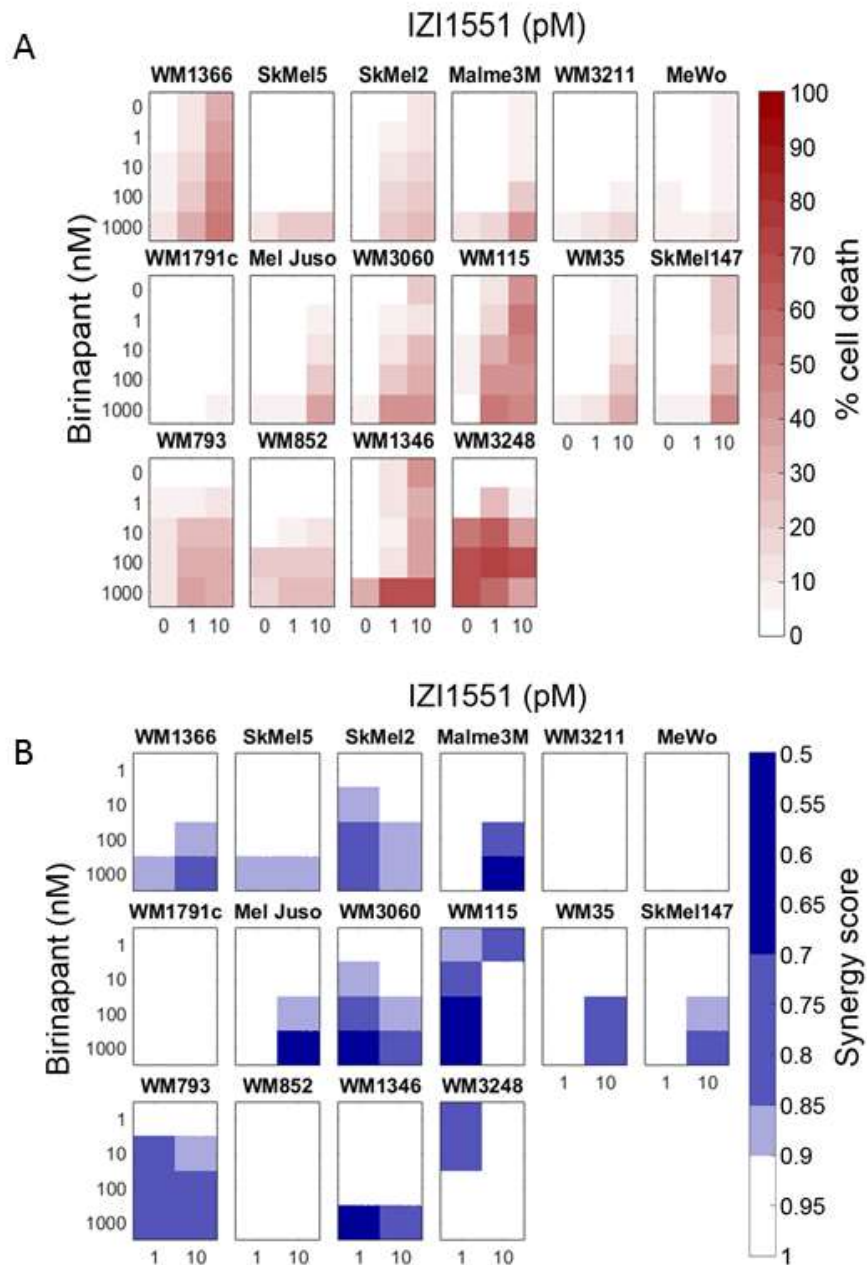
Figure 9. Melanoma cell lines exhibit heterogeneity in their response to single and combination treatment of IZI1551 and Birinapant. Cell lines were treated either with IZI1551 and Birinapant alone or in combination with the indicated concentrations for 72 h. Thereafter, cells were stained with propidium iodide (PI) and the percentage of dead cells (PI positive cells) was analysed by flow cytometry. All measurements were done in triplicates. Synergy scores were calculated using Webb's fractional product.

4.1.2 Melanoma cell lines treated with IZI1551 and Birinapant die by apoptosis

IZI1551 can trigger apoptotic cell death via clustering death receptors and activating the extrinsic apoptotic pathway. In order to verify that the investigated cell lines died by apoptosis after stimulation with IZI1551 and Birinapant, cells were additionally treated with QVD OPh to investigate whether the pan-caspase inhibitor was able to block cell death induced by the two drugs.

More precisely, six different cell lines, five cell lines of synergistic response and one of a low response, were seeded in 6-well plates and treated with 1000 pM IZI1551, 1000 nM Birinapant, their combination and their combination with the addition of 30 µM QVD OPh for 24, 48 and 72 h. The cell death could be completely blocked by adding the pan-caspase inhibitor QVD OPh, indicating that the cells die by apoptosis (Figure 10). For example, in cell line Mel Juso, combination treatment after 24 h yielded approximately 60% cell death, whereas combination treatment with the addition of QVD OPh yielded less than 5% of cell death. A similar result was observed for all synergistic cell lines.

To further verify that the cells were dying by apoptosis, the change in key apoptosis regulators upon the treatment was examined by western blotting. One resistant cell line (MeWo) and one sensitive cell line (Mel Juso) were stimulated with 1000 pM IZI1551, 1000 nM Birinpant, their combination and their combination with the addition of QVD OPh for 24 h. Thereafter, total cell lysates were investigated for cleavage of Procaspase 8, Procaspase 3, Bid and PARP by western blotting (Figure 11).

In the cell line Mel Juso, single stimulation with IZI1551 as well as combination treatment with IZI1551 and Birinapant for 24 h resulted in the depletion of Procaspase 8, Procaspase 3, Bid and PARP, verifying apoptotic cell death. Furthermore, cleavage of the investigated proteins after combination treatment could be prevented by adding the pan-caspase inhibitor QVD OPh which confirms apoptosis as a mode of cell death. In contrast, Birinapant single treatment did not affect the levels of Procaspase 8, Bid, Procaspase 3 and PARP when compared to the untreated control, meaning that Birinapant caused minimal cell death on its own in this cell line (Figure 11).

RESULTS

To investigate if apoptosis was activated in the resistant cell line, the same experiments were repeated with the cell line MeWo. Interestingly, the levels of Procaspase 8 were reduced by single stimulation with IZI1551 and combination treatment with IZI1551 and Birinapant, indicating that the apoptosis pathway was activated upon treatment. Furthermore, Bid was depleted upon stimulation with IZI1551 alone and in combination with Birinapant when compared to the control, indicating an activation of the mitochondrial apoptotic pathway. In contrast to Procaspase 8, the depletion of Procaspase 3 after the mentioned treatments was only marginal when compared to the untreated control, concurring with the finding that almost no PARP cleavage was observed. Interestingly, Procaspase 8 could not be completely restored to the levels of the untreated control by the addition of the pan-caspase inhibitor QVD OPh, whereas Bid and Procaspase 3 were fully restored (Figure 11).
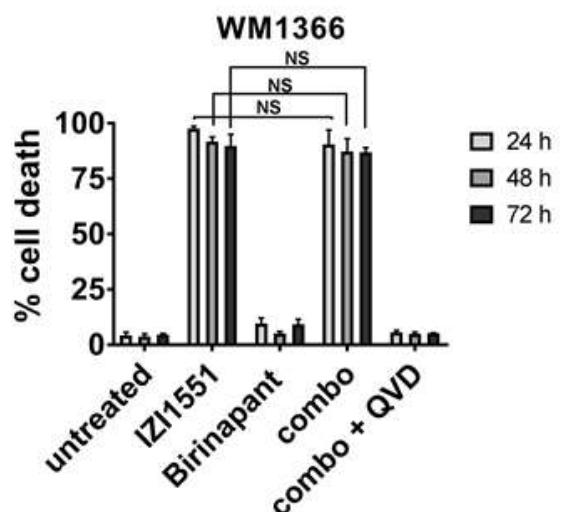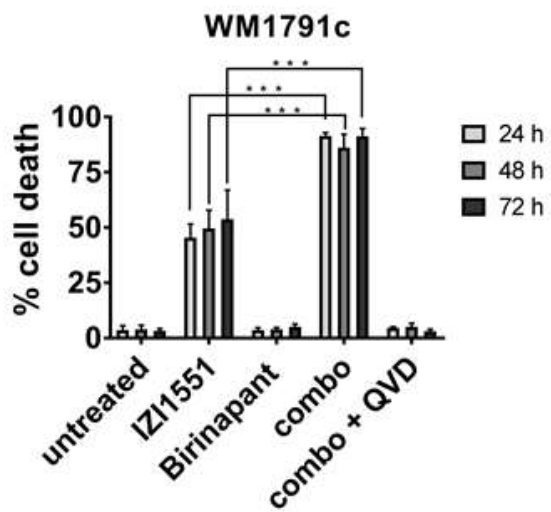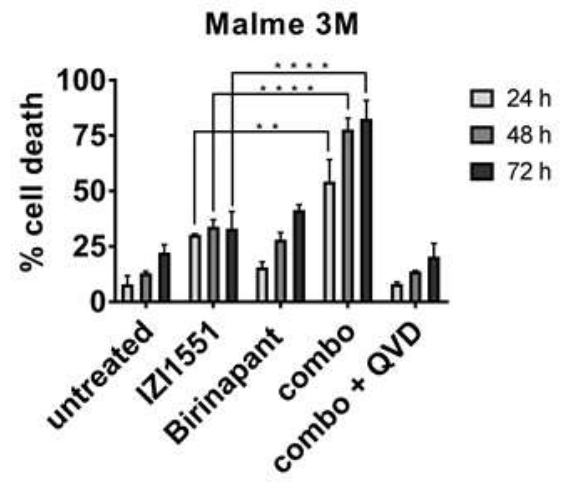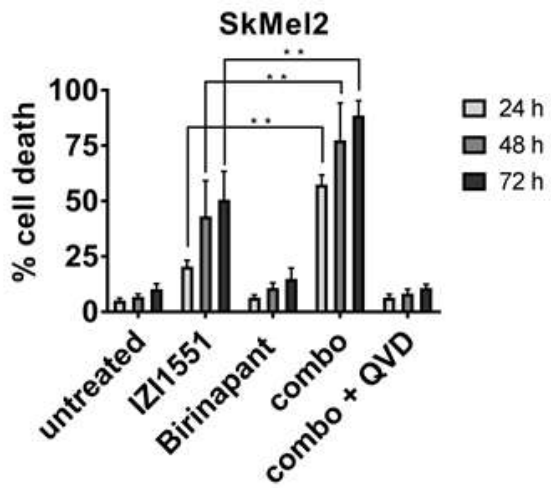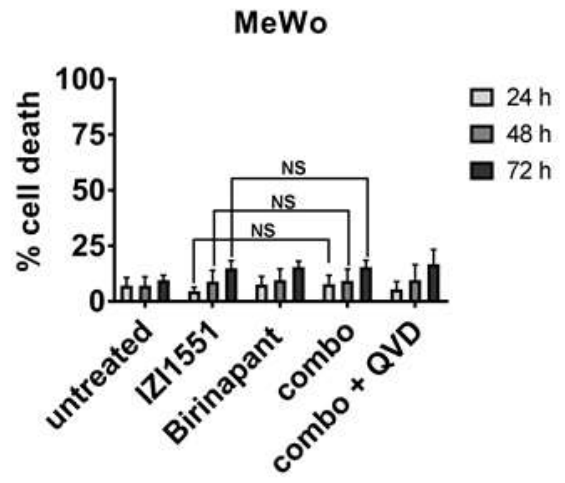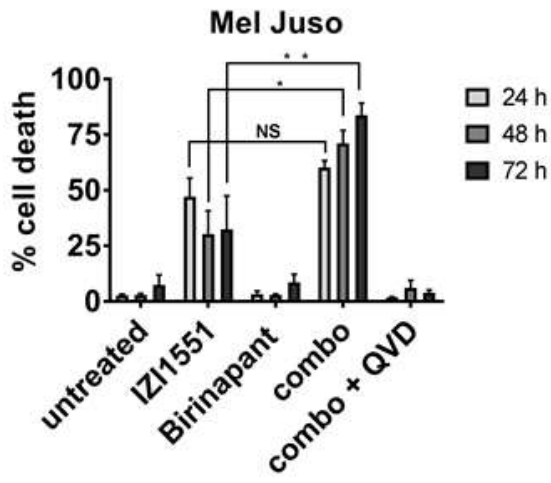
Figure 10. Melanoma cell lines die by apoptosis upon combination treatment with IZI1551 and Birinapant. Cell lines were treated with 1000 pM IZI1551 and 1000 nM Birinapant alone or in combination, with or without 50 µM QVD OPh respectively for 24, 48 and 72 h. Cells were stained with PI and Annexin V-APC. The percentage of dead cells (PI positive + Annexin V-APC positive cells) was determined by flow cytometry. Shown are mean values ± SD of three independent experiments. All measurements were done in triplicates. Statistical analysis was performed by two-way ANOVA followed by Dunett's multiple comparisons test; P= 0.12 (NS); 0.033 (*); 0.002 (**); 0.001 (***); 0.0001 (****); NS=not significant.
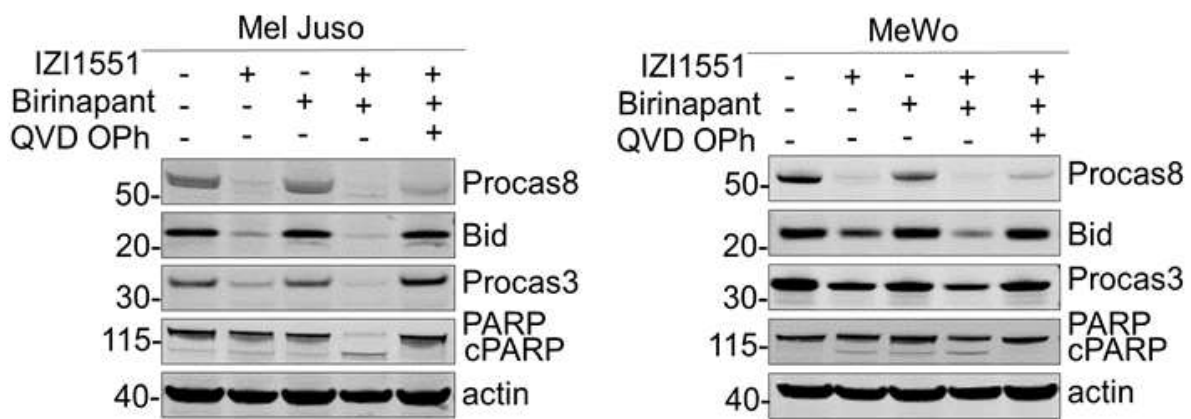
Figure 11. Treatment with IZI1551 induces cleavage of Procaspase 8 and Bid in both cell lines, but not cleavage of Procaspase 3 and PARP. Mel Juso and MeWo cells were treated for 24 h with 1000 pM IZI1551 and 1000 nM Birinapant alone or in combination, with or without the addition of 30 µM QVD OPh. Thereafter, whole cell lysates were analysed by western blotting using the indicated antibodies. Blots shown are representative of three independently performed experiments.

In order to conclude on the kinetics of cell death, Mel Juso and MeWo cells were treated with the combination treatment for 1, 2, 4, 8, 16 and 24 h and the levels of Procaspase 8, Bid, Procaspase 3 and PARP were again monitored by western blotting (Figure 12). In the sensitive cell line, Mel Juso, Procaspase 8, Bid and Procaspase 3 were fully cleaved after 4 to 8 h of the combination treatment, whereas processing of PARP could be seen 2 h after stimulation start. Simultaneous treatment with QVD OPh prevented the cleavage. Taken together, this result points to a fast and efficient activation and execution of apoptosis in synergistic melanoma cell lines by IZI1551/Birinpant combination treatment.
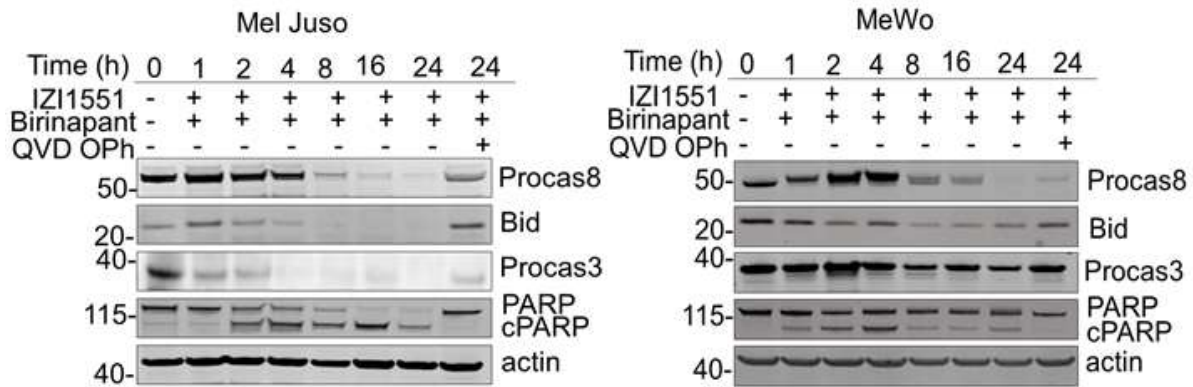
Figure 12. Combination treatment with IZI1551 and Birinapant induces cleavage of Procaspase 8 and Bid in both cell lines, but not cleavage of Procaspase 3 and PARP. Mel Juso and MeWo cells were treated with 1000 pM IZI1551 and 1000 nM Birinapant with or without 30 µM QVD OPh for the indicated time points. Thereafter, whole cell lysates were analysed by western blotting using the indicated antibodies. Blots shown are representative of three independently performed experiments.

Similar to what was observed in the synergistic cell line Mel Juso, cleavage of Procaspase 8 and Bid, also took place in the cell line MeWo. Procaspase 3 levels got slightly diminished between 4 and 8 hours of the stimulation. PARP cleavage was minimal, again consistent with approximately 10% of cell death measured by flow cytometry in the previous experiments. Processing of Procaspase 8 and Bid indicate that apoptosis was induced in this cell line, however, the only minimal cleavage observed for Procaspase 3 points to an inability in apoptosis execution.

4.1.3 Birinapant depletes cIAP1 and sensitises melanoma cell lines to IZI1551-induced apoptosis

Members of the IAP protein family such as cIAP1, cIAP2, and XIAP are often overexpressed in cancer. cIAP1 and cIAP2 modulate ubiquitin-dependent signalling via their E3-ligase activity, thereby regulating the activation of different NFκB transcription factors. Recruitment of IAPs to the receptor and their subsequent ubiquitination of RIPK1 results in pro-survival activation of the NFκB pathway. XIAP is the only IAP protein that can block

apoptosis upon different apoptotic stimuli by directly binding Caspase 3, -7 and -9. SMAC mimetics are drugs that bind and inactivate IAP proteins. By depleting IAPs, RIPK1 recruits FADD and Caspase 8 to form complex-IIA. Depending on the amount, RIPK3 is also recruited to complex-IIB contributing to cell death by necroptosis. Therefore, depleting IAPs represents a promising strategy in treating cancer.

In order to investigate the mechanism of synergy between IZI1551 and Birinapant, the effect of Birinapant on cIAP1, cIAP2, and XIAP protein level was examined in a resistant and a responsive cell line. The cell line Mel Juso was treated for 24 h with either IZI1551 alone, or in combination with Birinapant, with or without the addition of QVD OPh to investigate differences in the amounts of cIAP1, cIAP2, and XIAP (Figure 13).

In case Mel Juso cells were treated with Birinapant, the amounts of cIAP1 were strongly reduced. In contrast to that, cIAP2 levels were completely depleted only upon the combination treatment and partially degraded upon stimulation with IZI1551 alone. Furthermore, the levels of XIAP were reduced only after the combination treatment. Interestingly, the levels of cIAP2 and XIAP were restored after the addition of the pan-caspase inhibitor, indicating that their depletion was the result of cleavage by Caspase 3 rather than degradation caused by Birinapant.

In the low responding cell line, MeWo, cIAP1 was also completely depleted upon any kind of treatment including Birinapant. In contrast to that, the levels of cIAP2 and XIAP remained unchanged (Figure 13). Altogether, these findings indicate that Birinapant mainly targets cIAP1, whereas the observed depletion of cIAP2 and XIAP after combination treatment is the result of cleavage by Caspase 3 after stimulation with IZI1551.
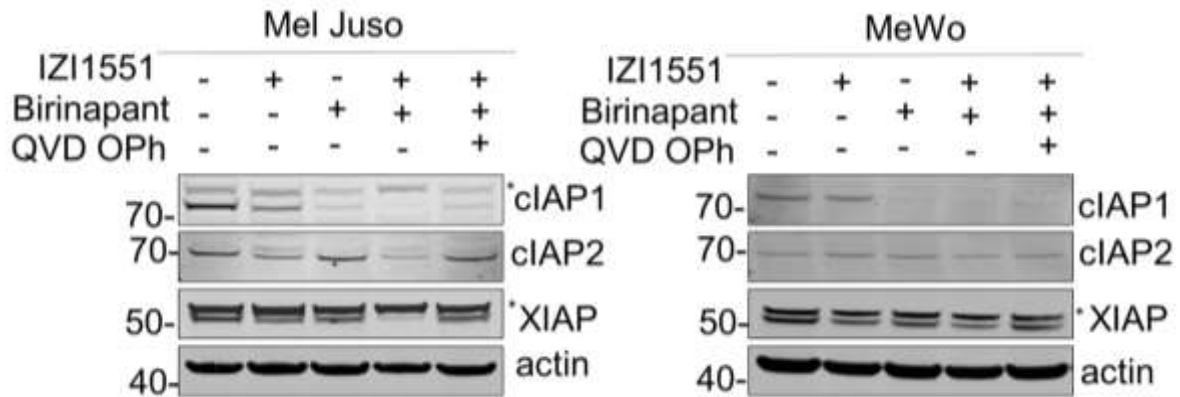
Figure 13. Treatment with Birinapant depletes cIAP1, but not cIAP2 and XIAP in melanoma cell lines. Mel Juso and MeWo cells were treated with 1000 pM IZI1551 and 1000 nM Birinapant with or without 30 µM QVD OPh for 24 h. Thereafter, whole cell lysates were analysed by western blotting using the indicated antibodies. The asterisk (*) indicates an unspecific band. Blots shown are representative of three independently performed experiments.

To determine the time-point at which cIAP1, cIAP2, and XIAP started to degrade after the combination treatment, cell lines Mel Juso and MeWo were treated with the combination treatment of IZI1551 and Birinapant for 1, 2, 4, 8, 16 and 24 h (Figure 14).

In both investigated cell lines, cIAP1 was depleted after 1 h of treatment. In the sensitive cell line, Mel Juso, the levels of cIAP2 dropped after 1 h stimulation and XIAP was depleted between 4 and 8 hours of the treatment, concurring with the activation of caspases and cleavage of PARP at that time point (Figure 9).

In contrast to that, cIAP2 levels did not change after stimulation with the two compounds in the resistant cell line, MeWo, whereas the levels of XIAP were slightly depleted after 16 to 24 hours of treatment. This result is in accordance with the observed low percentage of cell death occurring at those times.
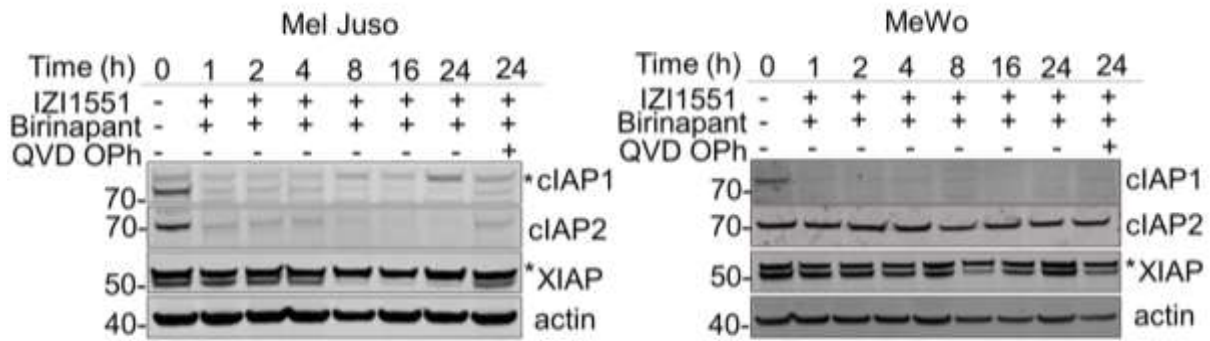
Figure 14. Treatment with Birinapant for 1 h is sufficient to degrade cIAP1 in the resistant and in the sensitive cell line. Mel Juso and MeWo cells were treated with 1000 pM IZI1551 and 1000 nM Birinapant with or without 30 µM QVD OPh for 24 h. Thereafter, whole cell lysates were analysed by western blotting using the indicated antibodies. Asterisk (*) indicates an unspecific band. Blots shown are representative of three independently performed experiments

4.1.4 Expression patterns of apoptosis proteins separate low-responding from synergistic cell lines

IZI1551 activates apoptosis in melanoma cell lines by binding to surface death receptors. Since apoptosis is involved in many processes necessary for normal functioning of the human organism, the process is tightly regulated by a number of pro- and anti-apoptotic proteins, as described in the introduction of this thesis. In short, IZI1551, a hexavalent TRAIL receptor agonist binds and clusters death receptors (DR4, DR5) on the surface of the cells. Trimerisation of the death receptors leads to the formation of the DISC, a complex consisting of the receptors, FADD, cFLIP and Procaspase 8. Recruitment of Procaspase 8 by binding to FADD via the DED domain takes place, recruiting further Procaspase 8 proteins. In addition, cFLIP can be employed thereby inhibiting the activation of Procaspase 8. Further, the protein Bid can be cleaved by Caspase 8 and initiate the formation of pores by Bax and Bak. MOMP is regulated by anti-apoptotic proteins of the Bcl-2 family such as Bcl-2, Bcl-xl, and Mcl-1 directly binding to Bax and/or Bak preventing pore formation. Afterwards, Cytochrome c is released from the mitochondrial intermembrane space and forms along with Apaf1 a heptameric complex that recruits Procaspase 9 and activates it. Procaspase activation can be negatively regulated by IAP proteins. XIAP binds and inactivates

executioner caspases, including Caspase 3 and Caspase 9. Two further proteins, cIAP1, and cIAP2 ubiquitinate RIP1 and thereby promote pro-survival signalling. During MOMP, SMAC is released from mitochondria and binds as a homodimer to XIAP resulting in the release of bound caspases.

Many of the proteins described above have been investigated as possible biomarkers for cancer susceptibility towards apoptosis-inducing drugs. However, until recently, no study could identify one single apoptosis protein as a diagnostic or prognostic biomarker. In order to find a correlation between the expression of a number of different proteins involved in apoptosis and the susceptibility of the investigated melanoma cell lines to IZI155 and Birinapant, the expression of 19 apoptosis proteins was investigated by quantitative western blotting or flow cytometrical analysis (Figure 15). Thereby, western blot analysis revealed that all investigated proteins were heterogeneously expressed in the panel of cell lines. This led to the conclusion that a classical approach of analysing only one protein as a biomarker for responsiveness did not yield an accurate result. Instead, to make a connection between the heterogeneity in responsiveness and heterogeneity of protein expression, a multivariate statistical approach was applied. The statistical pipeline SYS ACT (Systems simulations for the personalization and optimization of Anti-Cancer Treatments) was previously published by Passante and colleagues (Passante et al. 2013). It was developed by Maximilian Würstle (Royal College of Surgeons In Ireland, Dublin, Ireland) and modified by Cristiano Guttá in this study (Institute for Cell biology and Immunology, University of Stuttgart, Germany).

A data matrix consisting of 16 cell lines times 19 proteins was transformed into 16 uncorrelated principal components. Six of the principal components were considered when performing all further analysis, based on the calculations of their eigenvalues. First six principal components had an eigenvalue larger than 1 and retained approximately 80% of the data variance of the original dataset (Figure 16). The calculated weight coefficient table shows the different contribution that every protein had on the definition of each principal component (Figure 17).

The cell lines were positioned in a multi-dimensional space defined by the first six principal components according to the scores computed by the principal component analysis (PCA). The colour code, indicating whether the cell lines responded synergistically or with a low

response to the combination treatment, was added in the three-dimensional (3D) space to visually separate the two categories. Orange colour marked low response, and blue colour synergistically responding cell lines (Figure 18). To calculate the accuracy of separating the different categories of cell lines in the 3D PCA space, a Linear Discriminant Analysis (LDA) was applied. LDA is a mathematical function that separates the areas of a certain range of drug-specific treatment response. Cell lines located in the same response region had the same response class. With the LDA, 14 out of 16 cell lines (87.5%) were correctly assigned to their respective response categories. This result indicated a successful separation of the melanoma cell lines based on their protein amount.

A) Pro-apoptotic proteins
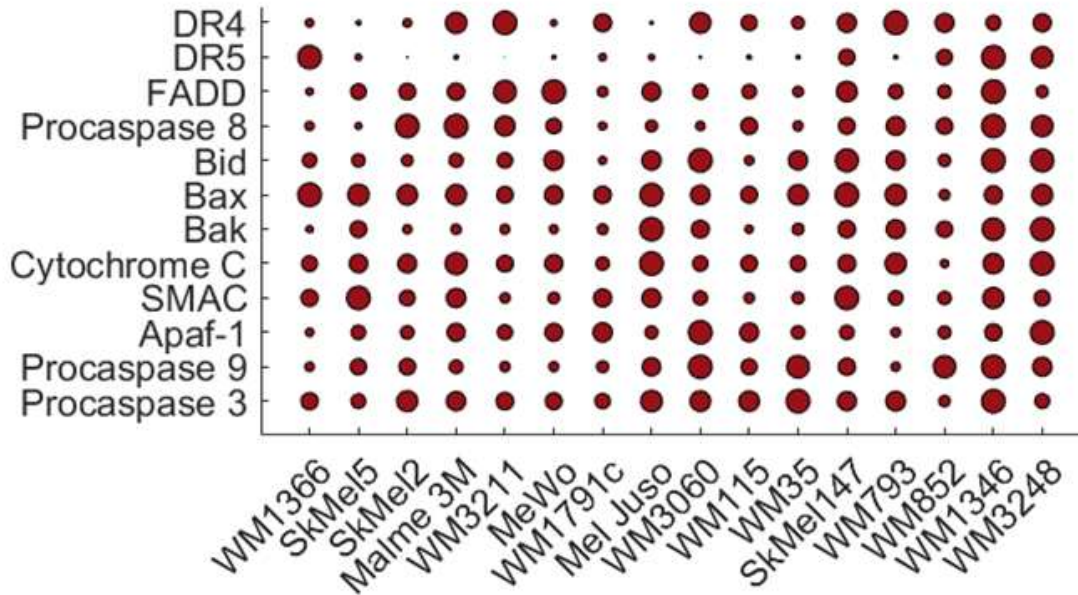
B) Anti-apoptotic proteins
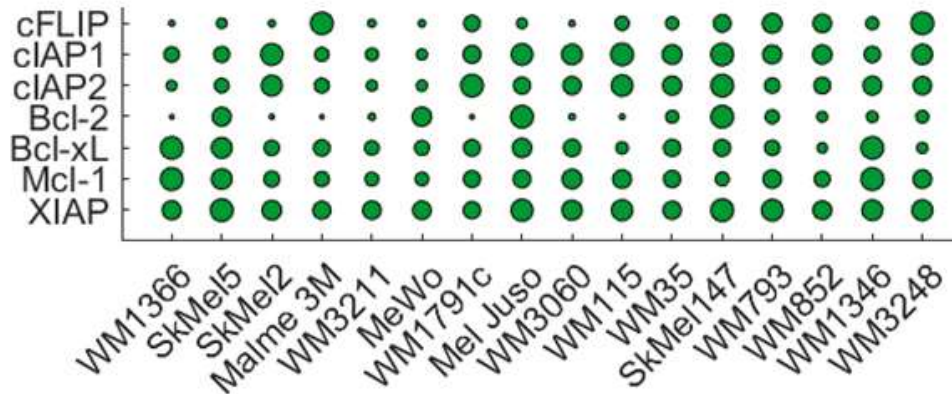
Figure 15. Pro- and anti-apoptotic proteins are heterogeneously expressed in the melanoma cell line panel. Expression of DR4 and DR5 was determined by staining untreated cells with respective primary and FITC-conjugated secondary antibodies. The stained cells were analysed with a flow cytometer. The expression of all further proteins was determined by quantitative western blotting. Circle sizes represent mean protein quantity determined from at least three independent experiments. Pro-apoptotic proteins (A) are depicted in red and anti-apoptotic proteins (B) in green colour.
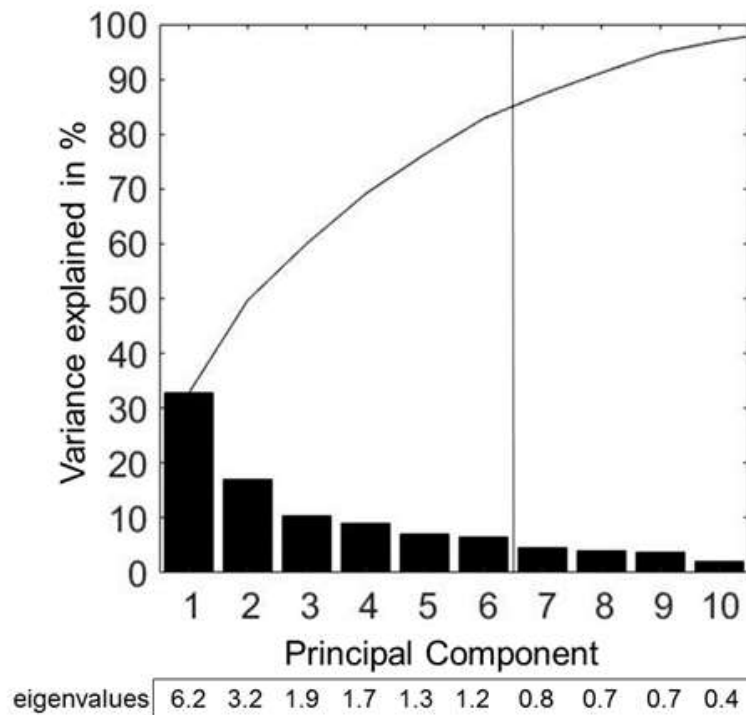
Figure 16. Percentage of the variance of the original dataset retained by each principal component. Principal components with an eigenvalue > 1 were considered for further analysis.

4.1.5 Cell line-specific pattern of apoptosis proteins allows for prediction of responsiveness on a case-by-case basis

To test whether the apoptosis protein pattern was sufficient to make predictions on a case-by-case basis, a leave-one-out cross-validation (LOOCV) with LDA defining the hyperspace regions of synergism and low response was performed. LOOCV is a common technique used for testing the predictive capacity of a model. In this thesis, a generated dataset of 15 cell lines was used to subsequently position the 16th cell line into the LDA segmented PCA space. The individually left out cell lines were then positioned into the PC space according to their

apoptosis protein pattern and their *in silico* responsiveness was calculated with LDA. In case the tested cell line was positioned into the correct response region, the prediction was considered successful or otherwise false (Figure 19).

LOOCV with LDA accurately predicted the responsiveness of 13 out of 16 cell lines (Figure 20). This demonstrated that the generated dataset of 19 proteins in 16 cell lines can serve as a basis for predicting the responsiveness of individual melanoma cell lines with high accuracy (81.25%). Furthermore, this confirmed the drawn hypothesis that a modelling approach has the potential to make a prediction if the treatment would be effective on a case-by-case basis.
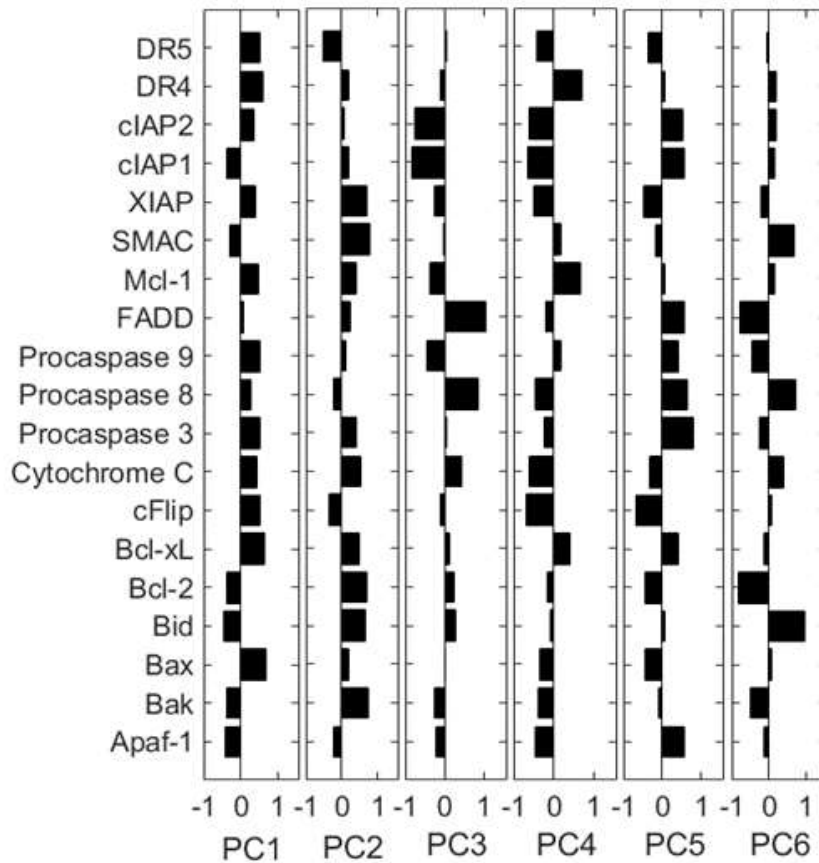
Figure 17. Weight coefficient table. Bars represent the effect of each protein on its respective principal component.
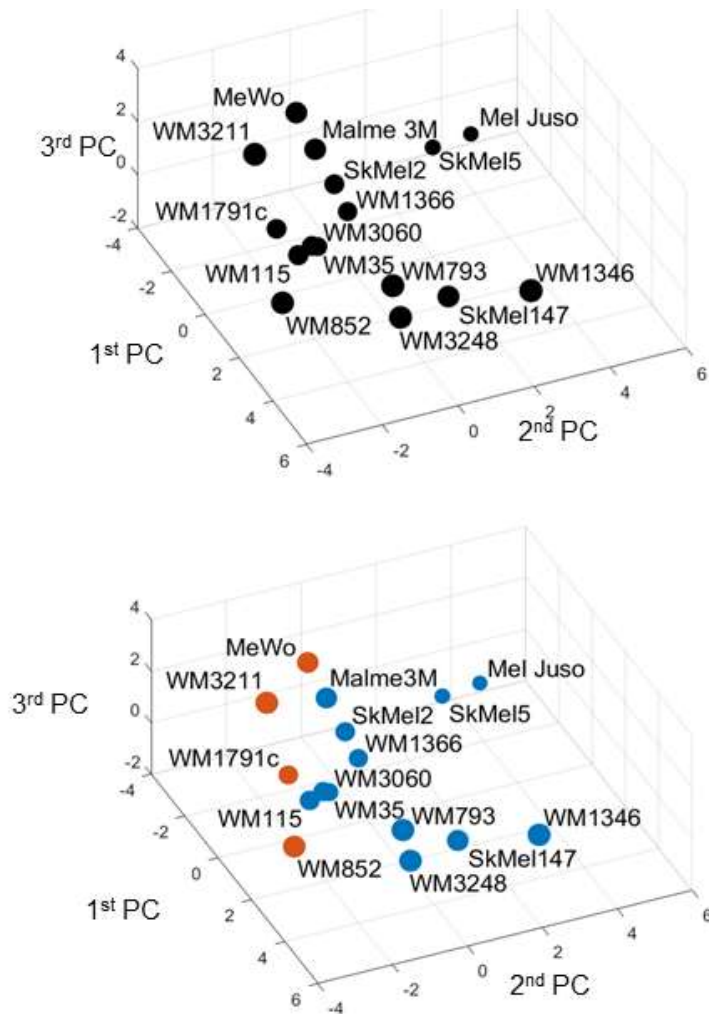
Separation of synergistic and low responsive cell lines (LDA)

Correctly classified #	Correctly classified in %
14	87.5

Figure 18. Synergistic responding cell lines occupy a subspace distinct from that of low responding cell lines. Cell lines were positioned in a multidimensional space defined by the first six principal components according to their apoptosis protein expression patterns. For visualization purposes, only the first three PCs are shown. The circle size decreases with distance from the observer to aid in 3D visualization. Colour coding indicates the responsiveness of the cell lines assessed in vitro. Orange = low response cell lines; blue = synergistically responding cell lines.
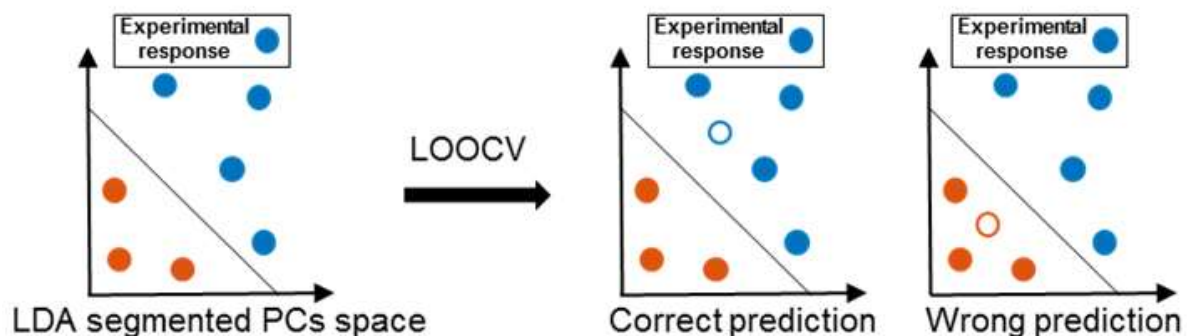
Figure 19. The principle of Leave One Out Cross Validation. Cell lines are positioned in the PCA space according to their protein profiles. Colour code is added according to the responsiveness of the cell lines in vitro (orange = low response cell lines; blue = synergistically responding cell lines). LDA function segregates two categories of cell lines in the PCA space. The cell line of unknown responsiveness (empty circle) is placed in the PCA space and the response colour code is added based on the protein pattern. LOOCV can result in either correctly predicted or wrongly predicted in silico responsiveness.
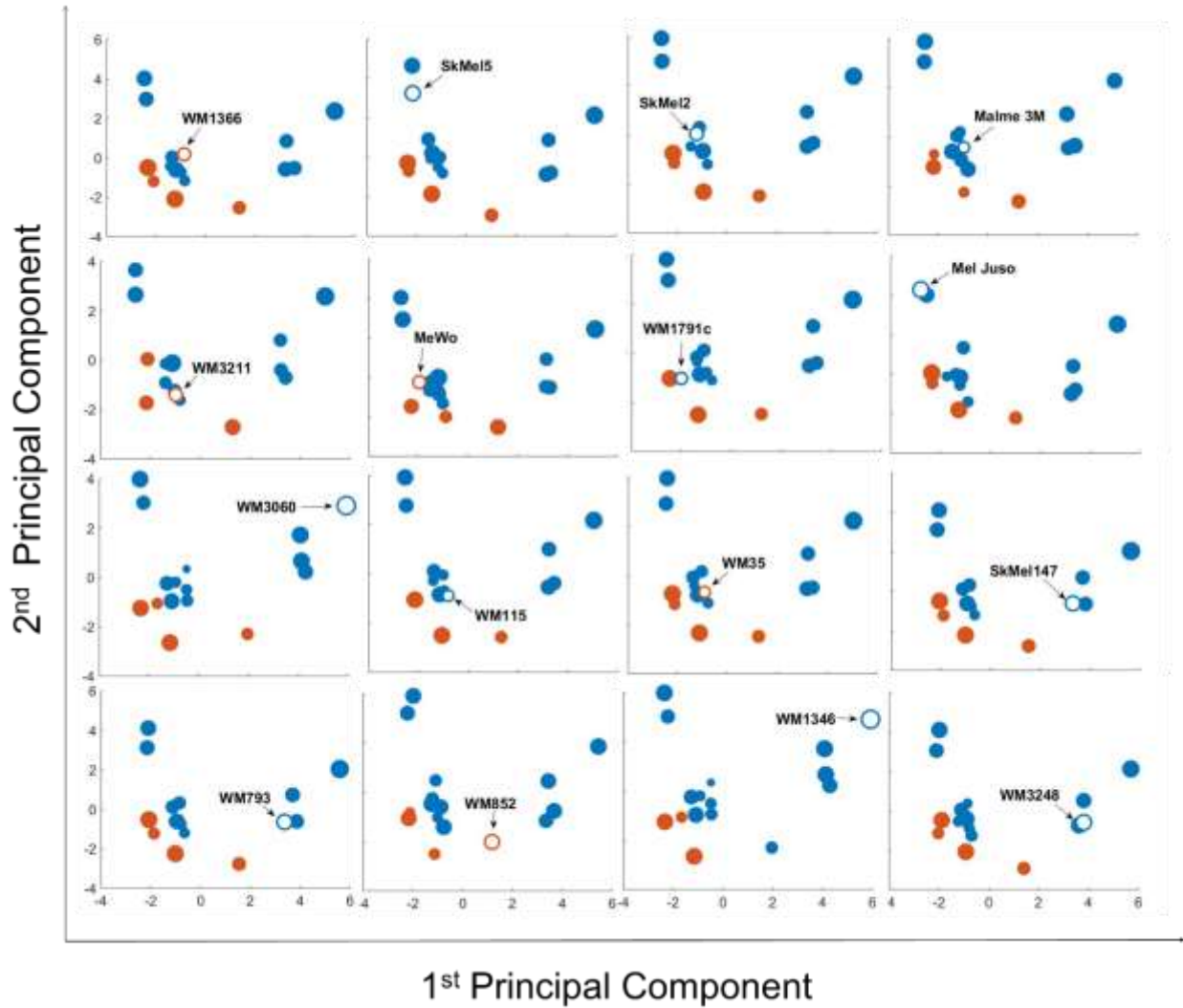
Prediction of synergistic and low responsive cell lines (LOOCV)

Correctly predicted #	Correctly predicted in %
13	81.25

Figure 20. 2D representation of Leave-One-Out-Cross Validation shown for the dataset of 15 cell lines. The responsiveness of the unknown cell line (empty circle) was calculated by LDA (blue for synergistic, orange for low responsive cell line). The circle size decreases with distance from the observer to aid in 3D visualization.

Chapter 2: Predicting the response of combination treatment in 3D cell culture and patient-derived metastatic melanoma cells

Numerous studies have shown that growing cells on a rigid plastic dish changes cell morphology and physiology (Duval et al. 2017; Edmondson et al. 2014). This may possibly yield misleading results in the translation of drug efficacy tests from cell culture to the *in vivo* situation. A three-dimensional (3D) cell culture more accurately represents the microenvironment of tissue, and thus the behaviour of 3D cells reflects the *in vivo* cellular responses in a more comparable way. On this account, 3D cell culture was employed in this study to test the efficacy of the combination treatment of IZI1551 and Birinapant, and secondary, to predict the responsiveness of individual 3D grown cell lines based on their protein expression using data-driven modelling.

Besides the differences in growing cells in 2D or 3D, over-subculturing can lead to dramatic changes in gene and protein expression between the model cell line and the original source material. Consequently, the model cell lines no longer retain the same properties than the primary material (Hughes et al. 2007). This could also yield misleading results in testing the efficacy of novel therapeutics. Therefore, in the second part of this study, patient-derived cell lines were tested for their responsiveness to the combination treatment which also helped to further validate the predictive capacity of the data-driven model.

4.1.6 Predicting the response to combination treatment with IZI1551 and Birinapant in 3D melanoma cell spheroids

4.1.6.1 3D melanoma spheroids exhibit a heterogeneous change in protein expression from 2D to 3D

To test whether the apoptosis protein pattern changes due to different growing conditions the basal levels of pro- and anti-apoptosis proteins were quantified in 3D spheroids of five melanoma cell lines. Cell lines responsive in 2D, WM1366, SkMel2, Malme 3M, Mel Juso,

and the low responding cell line in 2D, MeWo, were analysed for their apoptosis protein patterns in 3D. Quantification of the apoptosis proteins was assessed by western blotting and flow cytometry as described before (compare chapter 1). The protein analysis revealed that all investigated proteins were heterogeneously expressed in the analysed 3D melanoma cell lines (Figure 21). A heat map was generated to compare the difference in the expression of the proteins from 2D to 3D. This revealed a highly heterogeneous change from 2D to 3D and amongst cell lines. A number of pro- and anti-apoptosis proteins like Bid, Bcl-2, Procaspase 3, FADD, and Mcl-1 were considerably downregulated in all cell lines, whereas cFLIP appeared to be upregulated. Some proteins revealed a mixed change in the expression amounts between different cell lines. For example, the expression of DR4 was significantly upregulated in the 3D grown cell lines WM1366, SkMel2 and Mel Juso, while downregulated in the cell line MeWo. The expression of DR5 was downregulated in 3D grown WM1366, SkMel2 and Mel Juso and upregulated in MeWo.

In summary, the growth in 3D had complex consequences on cellular protein expression profiles and changes in both pro- and anti-apoptotic protein amounts did not allow to draw general conclusions on whether responsiveness of the cell lines would differ between 2D and 3D growth scenarios or not.
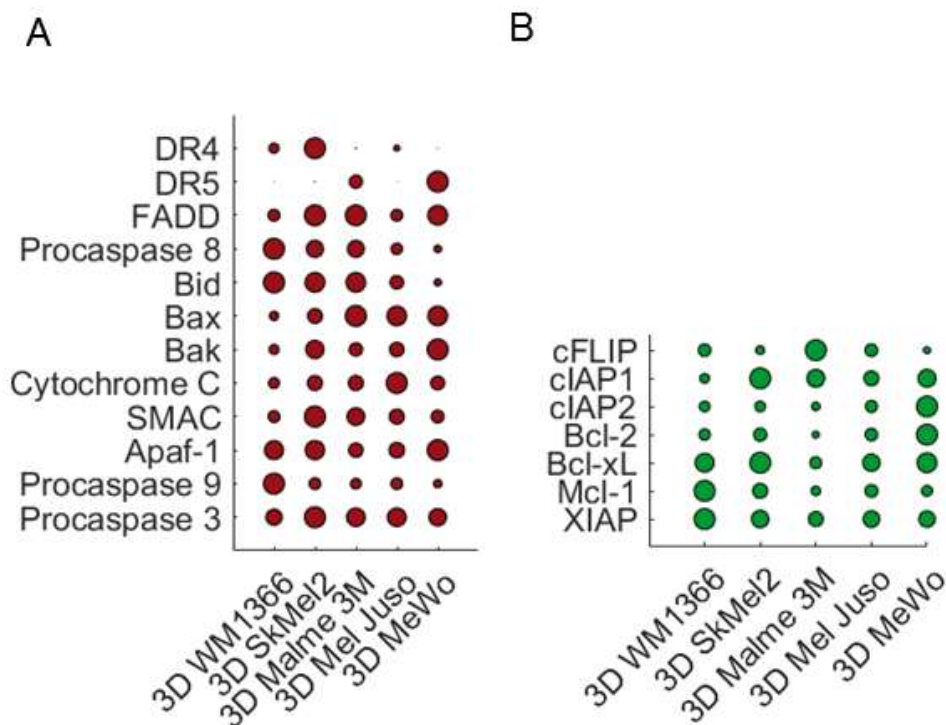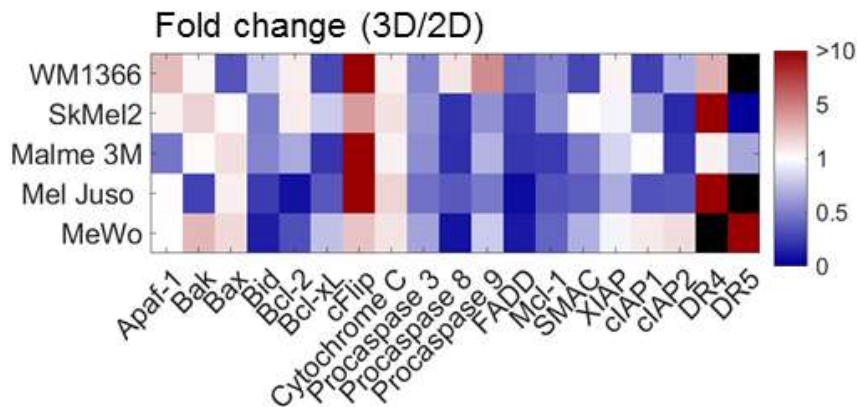
Figure 21. Pro- and anti-apoptosis proteins are heterogeneously expressed in the melanoma cell lines grown as 3D spheroids. Expression of DR4 and DR5 was determined by staining spheroid-derived single cell suspension with respective primary and FITC-conjugated secondary antibodies and subsequently analysed by flow cytometry. All other proteins were analysed by western blot on untreated whole cell lysate. (A) Circle sizes represent mean protein quantity determined from at least n=3 independent experiments. Red = pro-apoptotic, green = anti-apoptotic. (B) The heat map shows the fold change expression of proteins in 3D spheroids compared to 2D cell culture. Blue colour indicates a lower expression of proteins in 3D than in 2D, red colour indicates higher expression in 3D than in 2D. Black colour represents proteins that are not expressed either in 2D or 3D.

4.1.6.2 3D spheroids prominently changed their apoptosis protein profiles, but the *in silico* responsiveness remained the same as in 2D culture

The expression of apoptosis proteins in 3D melanoma spheroids has heterogeneously changed in comparison to 2D. This result reinforced the conclusion that the expression analysis of only one protein could not accurately reflect on the responsiveness of the cell line. Instead, the expression of all apoptosis regulators has to be considered when calculating responsiveness. For this, the responsiveness of each 3D cell lines was calculated using multivariate statistical modelling, based on its 3D apoptosis protein pattern.

Due to the protein expression differences between 2D and 3D cultured cells, new positions arose in the PCA space (Figure 22, marked by an empty circle). The cell lines WM1366, Mel Juso, Malme 3M, and SkMel2 grown in 3D, positioned themselves in the area of responding cell lines, as indicated by the blue color-coding by the LDA, which was the same in 2D

(compare Figure 18). The cell line MeWo grown in 3D was positioned in the orange-coded area of low responding cell lines, again like grown in 2D.

The repositioning of the cell lines can be explained on a simplified example of the Mel Juso cell line. Movement in the PCA space is influenced by the altered expression of the proteins in 3D compared to 2D and the effect individual proteins had on the positioning cell lines in the PCA space, so-called weight coefficients (shown in weight coefficient graph, compare Figure 17; Figure 22. Follow the arrows). For the cell line Mel Juso the 1st PC was positively influenced by cFLIP, DR4 and DR5, the 2nd and 3rd PC were negatively influenced by them. Grown in 3D the Mel Juso cells had a strong upregulation of the proteins cFLIP and DR4 and downregulation of DR5. This resulted in a movement towards the positive values of the 1st PC, towards the negative values of 2nd PC and a small movement towards the negative values of the 3rd PC. The movement in each PC is represented by the length and direction of the vector and the final position of the cell lines is the sum of movements of all three PCs.

In summary, cell lines grown as 3D spheroids prominently changed their apoptosis protein profiles, however, the responsiveness *in silico* remained the same as in 2D cell culture.

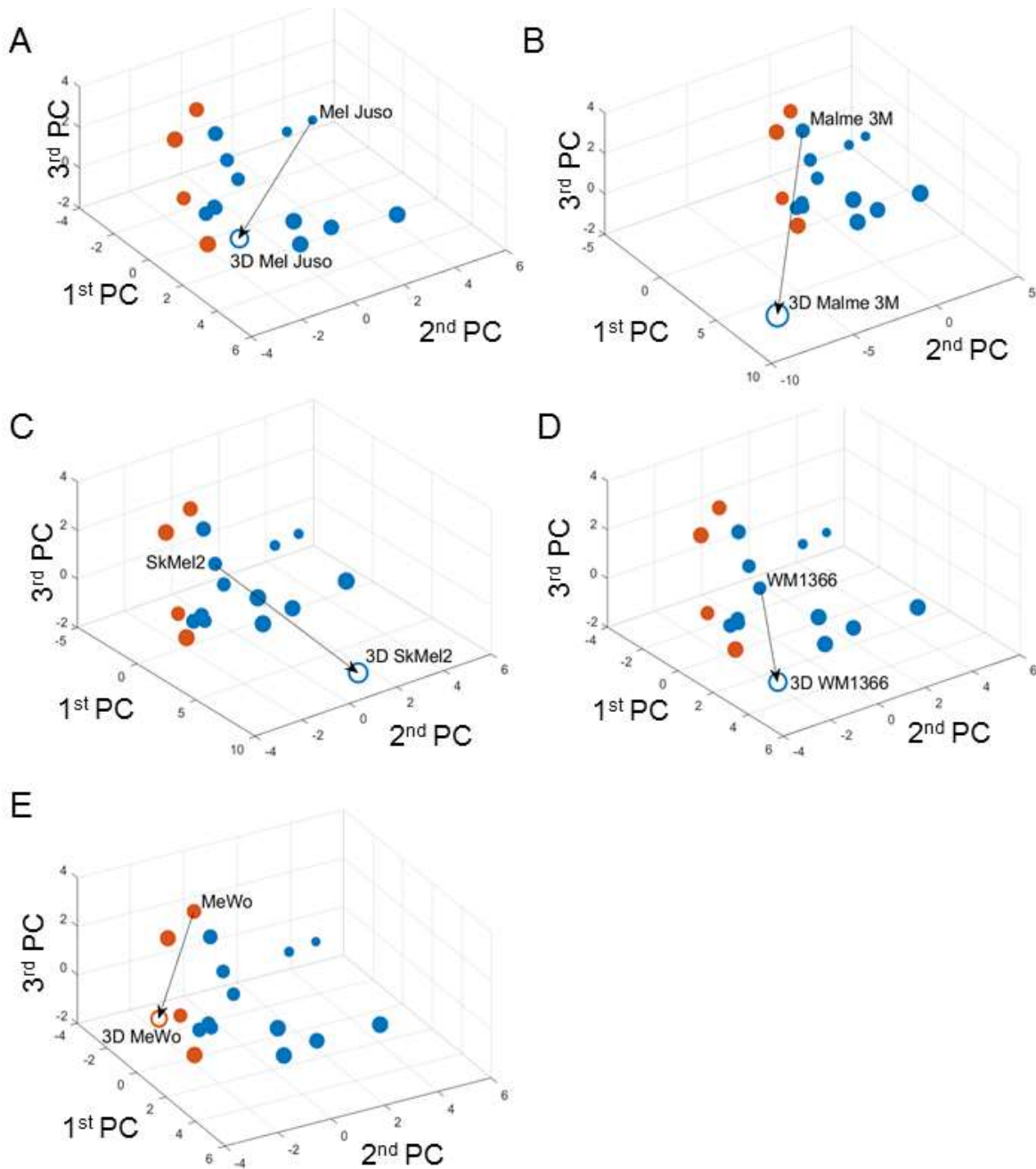**Figure 22.** *In silico* **prediction of synergistic responses to IZI1551 and Birinapant treatment in 3D cultures.** Cell lines grown in 3D were placed in the PCA space according to their apoptosis protein profile. *In silico* responsiveness was calculated by LDA (compare Fig. 18). Colour code indicates the responsiveness of the cell lines with the blue = synergistic response; orange = low response or resistance. An empty circle indicates the cell line grown in 3D. Arrow indicates the change of position in the PCA space caused by the change of the protein expression between 2D and 3D cultured cells. The circle size decreases with distance from the observer to aid the 3D visualization. Names of other melanoma cell lines were omitted for clarity. (A-D) cell lines Mel Juso (A), Malme 3M (B), SkMel2 (C) and WM1366 (D), synergistically responding in 2D, were predicted synergistic in 3D. (E) the cell line MeWo,

resistant in 2D, was predicted resistant in 3D. Thick arrows in (A) and (E) represent the vector movements influenced by the protein changes from 2D to 3D.

4.1.6.3 Calculated responsiveness predictions from 3D protein expression profiles can be verified *in vitro*

To verify the results of the predicted responsiveness, cell death was induced in 3D cultured cells. Therefore, the cells were treated by single or combination treatment with IZI1551 and Birinapant, with or without the addition of QVD OPh and subsequently analysed by flow cytometry.

Cell lines SkMel2 and MeWo grown in 3D exhibited low response to single treatment with IZI1551, while cell lines Malme 3M and Mel Juso showed a higher percentage of cell death. This was similar under 2D growth conditions after 24 h of stimulation. However, cell line WM1366 grown in 3D showed a low response, whereas this cell line grown in 2D was very sensitive to single treatment with IZI1551 (compare Figure 10). Furthermore, cell lines SkMel2 and Mel Juso grown in 3D slightly responded to single treatment with Birinapant. To compare, those cell lines had a very low response to Birinapant when grown in 2D. Interestingly, both 2D and 3D grown cell line Malme 3M were sensitive to single treatment with Birinapant (compare Figure 10; Figure 23A). To the combination treatment the cell lines WM1366, SkMel2, Malme 3M and Mel Juso, grown in 3D, exhibited a synergistic response, while cell line MeWo grown in 3D showed a low response (Figure 23A). This was comparable to the response of these cell lines when grown and treated in the 2D setting.

Cell lines SkMel2 and Mel Juso were also treated with pan-caspase inhibitor QVD OPh to confirm that cell lines grown in the 3D die by apoptosis. As shown in Figure 23B, QVD OPh partially rescued the 3D grown SkMel2 and Mel Juso from IZI1551 and Birinapant induced apoptosis. In contrast, apoptosis was completely blocked by QVD OPh in 2D grown cell lines (compare Figure 10).

These results confirmed the *in silico* prediction of responsiveness of 3D melanoma cell lines to the combination treatment of IZI1551 and Birinapant, despite the change in protein

expression. Interestingly, melanoma cell lines remained of the same responsiveness when grown as 3D spheroids like in 2D.
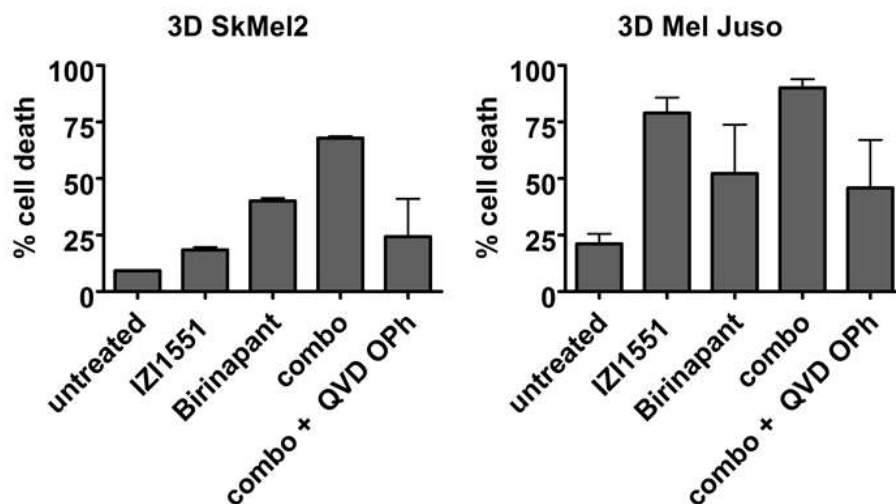
A
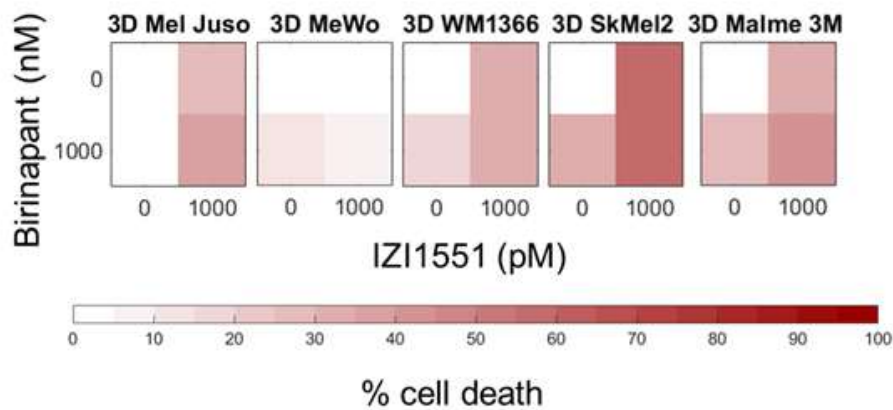
B

Figure 23. 3D melanoma spheroids die by apoptosis upon the combination treatment with IZI1551 and Birinapant. Indicated cell lines were grown as 3D spheroids and treated with 1000 pM IZI1551 and 1000 nM Birinapant or their combination for 24 h with or without the addition of 50 µM QVD OPh. Cell death measurement was performed by PI uptake by flow cytometry. Heat map represents mean of n=3 measurements.

Taken together, the response of five out of five cell lines (100 %) grown in 3D could be correctly predicted based on their basal apoptosis protein pattern and previously generated

melanoma cell lines datasets. In addition, responses of cell lines in 3D spheroid growing conditions could be predicted by multivariate modelling, confirming the hypothesis that the protein signature carries information on the responsiveness of the cell lines.

4.1.7 Predicting the response to combination treatment with IZI1551 and Birinapant in patient-derived metastatic melanoma cells

4.1.7.1 Patient-derived metastatic melanoma cells exhibit heterogeneity in apoptosis protein expression

In the second part of the study, patient-derived metastatic melanoma cells were used to exclude the possibility of cell line responsiveness to the drug combination being the result of molecular alterations due to over-subculturing. Therefore, the efficacy of the combination treatment and the predictive capacity of the model were tested on cells recently isolated from primary tissue. These patient-derived cancer cells M10, M20, M32, M34, and M45 were of metastatic origin and exhibited different BRAF and NRAS mutation status (see Chapter 2, 2.2 Prokaryotic and Eukaryotic cells). They were cultured as 2D cultures for all experiments.

4.1.7.2 Patient-derived melanoma cell lines exhibit heterogeneity in apoptosis protein expression

To validate the mathematical model by predicting the response of patient-derived cells *in silico*, pro- and anti-apoptotic proteins from untreated cells were quantified as described before (Figure 24, compare Figure 18). Apoptosis proteins were heterogeneously expressed in the patient-derived cells. When comparing the heterogeneity of patient-derived cells and melanoma cell lines, several general differences were noticeable. First, the expression of FADD, Apaf1 and Cytochrome C was almost the same among different patient-derived cells,

whereas melanoma cell lines exhibited a heterogeneous expression of these proteins. Second, the proteins cIAP2 and Bax were expressed in a larger amount in the panel of patient-derived cells. In contrast, the levels of cIAP1 and XIAP were similar in both panels. Third, both panels of cell lines exhibited heterogeneously expression of Bcl-2, DR4, DR5, Mcl-1, and Bcl-xL.

Based on these data it was not possible to conclude whether the differences protein expressions are due to the fact that one panel consists of freshly isolated cells and the other one from long-term cultures. In addition, it was not possible to conclude on the responsiveness of these cell lines based on their expression of individual proteins. Hence, in a next step, the responsiveness of patient-derived cell lines was tested *in silico* based on the expression of apoptosis proteins.
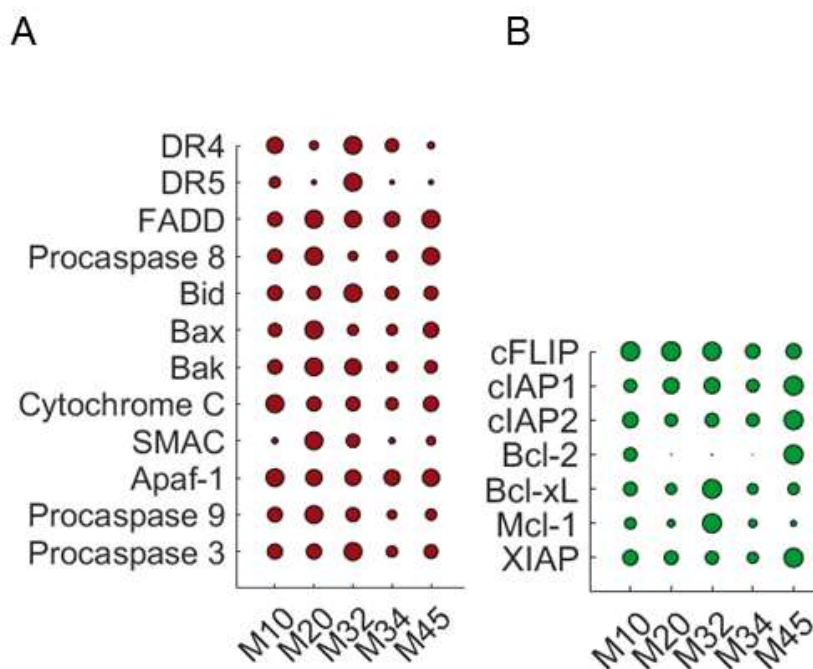

Figure 24. Pro- and anti-apoptotic proteins are heterogeneously expressed in patient-derived melanoma cells. Expression of DR4 and DR5 was determined by staining spheroid-derived single cell suspension with respective primary and FITC-conjugated secondary antibodies and subsequently analysed by flow cytometry. All other proteins were analysed by western blot on untreated whole cell lysate. Circle sizes represent mean protein quantity determined from at least n=3 independent experiments. Red = pro-apoptotic, green = anti-apoptotic

4.1.7.3 Responsiveness of patient-derived melanoma cells to IZI1551 and Birinapant can be predicted based on their apoptosis protein pattern

Patient-derived cells heterogeneously expressed apoptosis proteins. Because of that, the responsiveness of these patient-derived cells could not be predicted based on the expression of individual proteins, comparable to the 2D and 3D melanoma cell line panels. However, it was possible to determine the *in silico* responsiveness by placing the patient-derived cells in the PCA space.

Due to the difference in protein expression between the 2D melanoma cell line panel and patient-derived cells, new positions arose for the patient-derived cell lines in the PCA space (marked by the empty circle in Figure 25). Based on the basal protein levels cells M10, M20, M32, and M45 were predicted as synergistic and M34 as low responding (Figure 25). The positioning of the patient-derived cells followed the same principle as the movement of 3D melanoma spheroids in the PCA space: up- or downregulation of individual proteins based on the weight coefficients that define the influence of proteins in six different principal components. However, it was difficult to follow their positioning since there was no specific cell line to compare the patient-derived one with.

Still, a comparison could be made with the cell lines that lie closely to patient-derived ones in the PCA space. For example, patient-derived cell M10 positioned itself near the cell line WM1366. When comparing the protein profiles of two cell lines, it could be noticed that some proteins in M10 were downregulated (e.g. Bid, Bcl-xl, Procaspase 3, FADD, Mcl-1, SMAC, cIAP1, DR4) and some upregulated (e.g. Apaf1, Bak, Bax, Bcl-2, cFLIP, Cytochrome C, Procaspase 8, Procaspase 9, DR5, XIAP, and cIAP2) when compared to WM1366 (compare Figure 15). The expression profile of both cell lines differed in the expression of all the quantified proteins, however, both cell lines were marked as high responding *in silico*. Similar observations could be made for other patient-derived cells. This example strongly illustrates that the responsiveness of the cell line is strongly influenced by the quantity and interplay of all the apoptosis proteins.

4.1.7.4 Calculated responsiveness predictions from patient-derived melanoma cells protein expression profiles can be verified *in vitro*

To assess the responsiveness of the cells *in vitro* and therefore validate or reject the results of the *in silico* predictions, cell lines were treated in 2 x 5 dose-response matrix with IZI1551 (0, 1, 10, 100 and 1000 pM) and Birinapant (0 and 1000 nM). Afterwards, cell death was measured by propidium iodide uptake and flow cytometry. The *in vitro* response of patient-derived cells was heterogeneous. Cells M10, M20, and M32 responded to IZI1551 and Birinapant treatment, while M34 and M45 had a low response (Figure 26). The *in silico* responsiveness calculated by placing protein patterns in the PCA space indicated the cell lines M10, M20, M32, and M45 as responsive, whereas cell line M34 was predicted to be resistant. Therefore, the responsiveness of the cell lines M10, M20, M32, and M34 was correctly predicted *in silico* while the responsiveness of the cell line M45 was wrongly predicted. The accuracy of prediction of 80% (4/5 cell lines) in patient-derived cells further confirms the power of mathematical modelling in studying the efficacy of drugs and predicting the response on a case-by-case basis.

Both 3D-cultured cell lines and patient-derived cell lines showed a heterogeneous response to the combination treatment of IZI1551 and Birinapant. In addition, quantified apoptosis proteins exhibited large heterogeneity and a change of protein expression caused by the change of culturing conditions from 2D to 3D. Nevertheless, the responsiveness of 3D-cultured cell lines and patient-derived metastatic cells could be successfully predicted *in silico* with an accuracy of 100% (3D-cultured cell lines, n=5) and 80% (patient-derived cell lines, n=5), respectively.
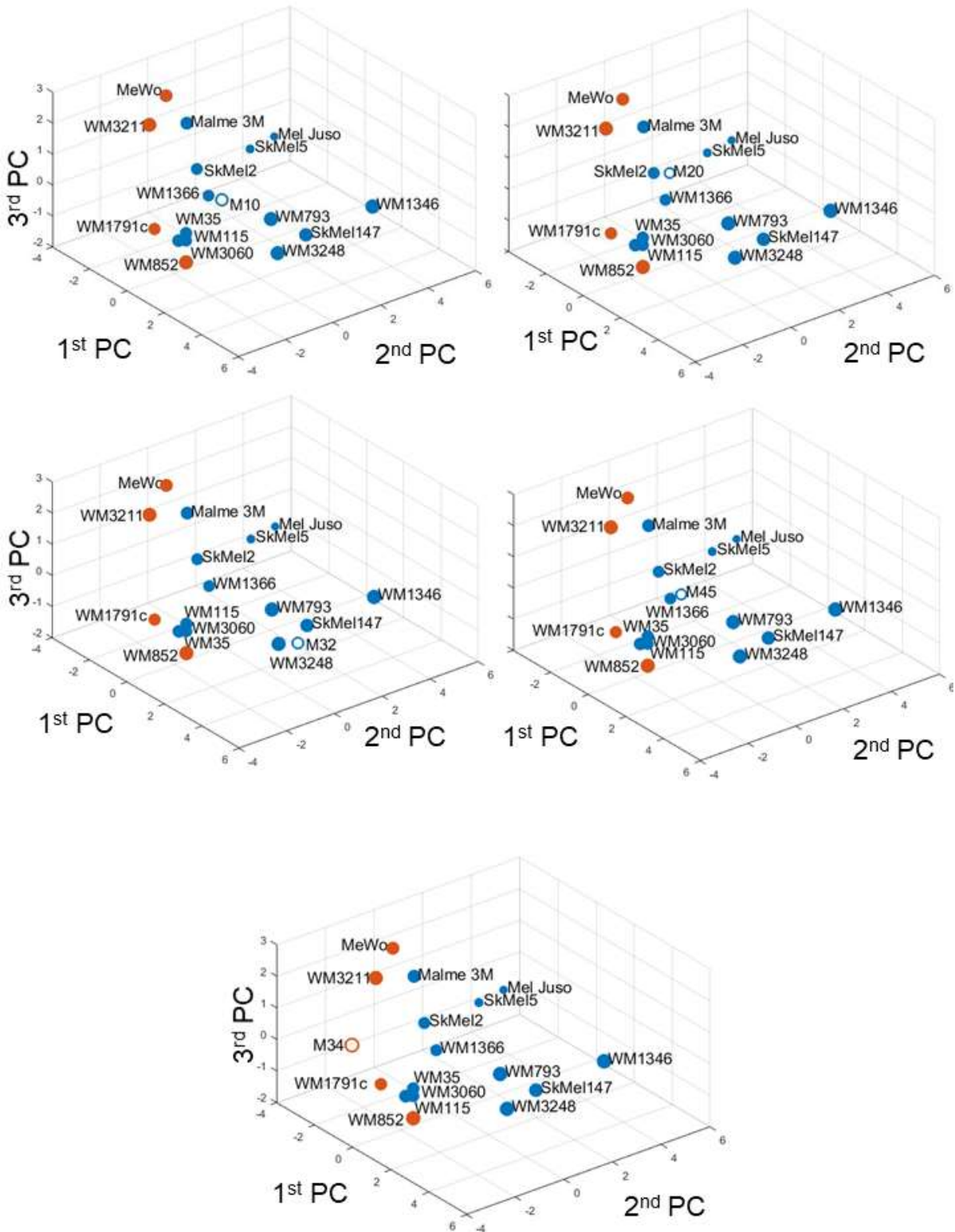
Figure 25. Positioning the patient-derived metastatic melanoma cells in the PCA space. Responsiveness of patient-derived cells was calculated by LDA after positioning the cell lines among the 16 melanoma cell lines. Colour code indicates the responsiveness of the cells (blue=synergistic response; orange=low response/resistant), whereas empty circles indicates the tested primary cancer cell. The circle size decreases with distance from the observer to aid in 3D visualization.
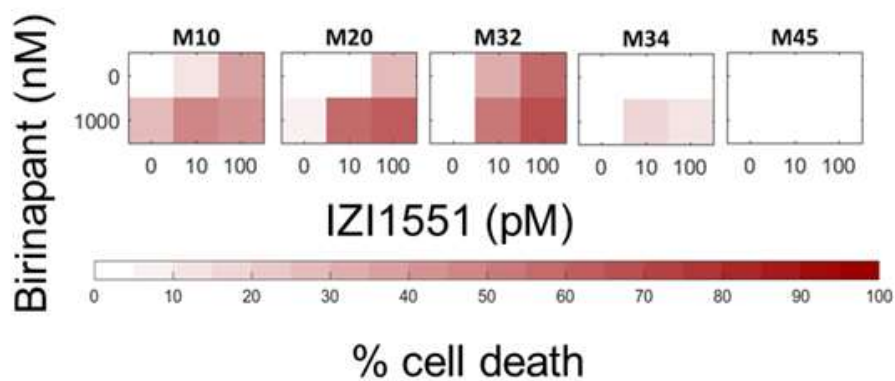

Figure 26. Patient-derived metastatic melanoma cells respond heterogeneously to the combination treatment with IZI1551 and Birinapant. Patient-derived cells were treated with IZI1551 and Birinapant either alone or in combination at indicated concentrations 24 h. Thereafter, cells were stained with propidium iodide (PI) and the percentage of dead cells (PI positive) was analysed by flow cytometry. Shown are mean values of three independent experiments. All measurements were done in triplicates. SDs were omitted for clarity.

4.2 Chapter 3: Testing the efficacy of IZI1551 and Birinapant *in vivo*

In this study so far, it was shown that the responsiveness of 2D and 3D cultivated melanoma cell lines as well as patient-derived melanoma cells to combination treatment with Birinapant and IZI1551 can be predicted with high accuracy, based on the expression pattern of apoptosis proteins. Therefore it was next investigated whether the melanoma cell lines grown as xenografts in nude mice respond to the combination treatment and whether the correct prediction of responsiveness can be made *in silico*. The experiments were approved by Animal Welfare and Ethics Committee of the government of the State Baden Wuerttemberg, Germany and Department of Animal Physiology, University of Stuttgart. Animal care and all experiments were in accordance with federal and European guidelines.

4.2.1 Single treatment with Birinapant does not induce cell death in MeWo xenograft model

To determine the suitable concentration of Birinapant *in vivo*, a pre-experiment was performed by testing 3 mg/kg, 10 mg/kg and 30 mg/kg (Figure 27). Thereby, it was shown that tumours in the control group as well as in the treatment groups exhibited steady growth. Although treatment with 3 mg/kg Birinapant did not slow down the tumour growth compared to the control group, treatment with 30 mg/kg seemed to reduce tumour volume. Nevertheless, observed differences in tumour growth between the four different groups were not significant.

To examine the on-target effect of Birinapant *in vivo*, tumours from all four groups were harvested after 28 days of treatment and the amounts of cIAP1, cIAP2 and XIAP were examined by western blotting**.** It was shown that different concentrations of Birinapant have successfully depleted the levels of cIAP1, but cIAP2 remained intact upon the treatments (Figure 28). The levels of XIAP were reduced when compared to the untreated control. As no differences in the tumour volume could be observed after treatment of the mice with different concentrations of Birinapant, and some animals that were treated with

30 mg/kg Birinapant had to be sacrificed due to weight loss, a concentration of 10 mg/kg Birinapant was chosen to be used in further experiments
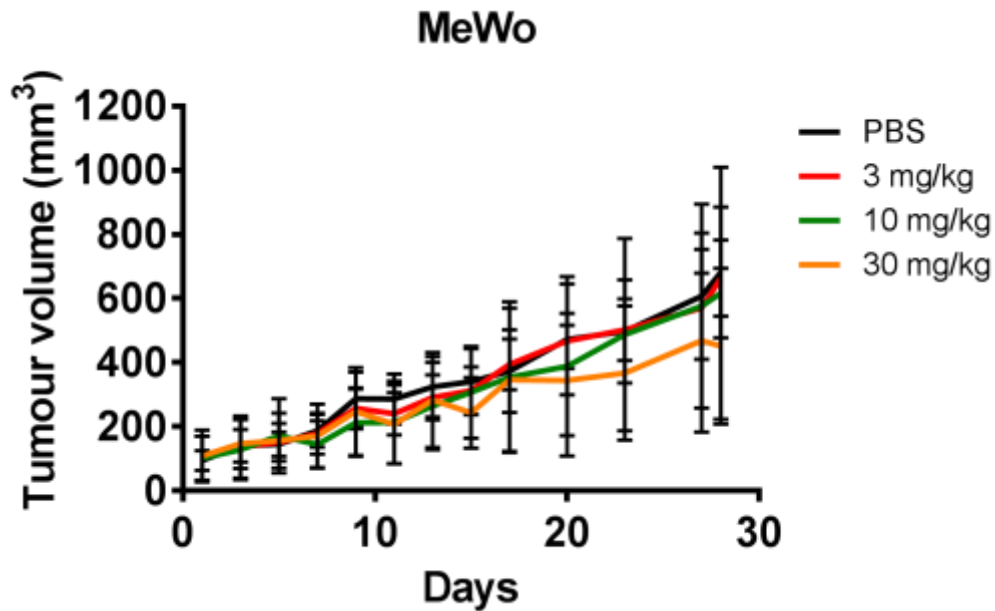

Figure 27. Cell death induction with Birinapant in MeWo xenograft model. Mice were treated with indicated concentration of Birinapant three times a week during a period of four weeks. The size of a tumour was monitored with digital callipers three times a week. Results are shown as average volume of the tumours in a group ± SD. There were 7 animals per treatment group, each animal bearing one or two subcutaneous tumours.
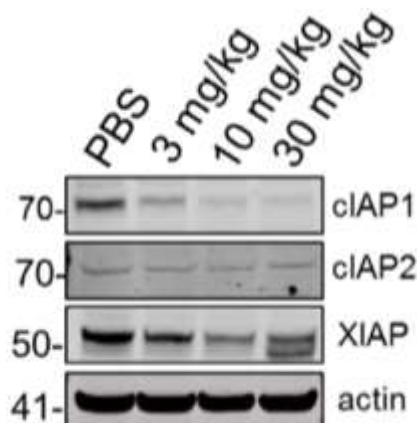

Figure 28. Birinapant depletes cIAP1 and XIAP, but not cIAP2 in MeWo xenograft model. Mice were treated wth indicated concentrations of Birinapant three times a week during a period of four weeks. One day after the last treatment, mice were sacrificed and one

tumour from each group was analysed for the expression of indicated proteins by western blotting. The experiment was performed once.

4.2.2 Validating the statistical model

Furthermore, the predictive capacity of SYS ACT was investigated in this setting. Mice were treated with single and combination treatment of IZI1551 and Birinapant for four weeks. Two mice bearing four tumours were sacrificed before the treatments begun in order to quantify the proteins from an untreated tumour and predict the *in silico* responsiveness to the combination treatment with IZI1551 and Birinapant. The responsiveness was measured by quantifying the basal levels of apoptosis proteins from untreated tumours and placing the tumour protein pattern in the PC space as described before. Investigations revealed that the change in protein expression from 2D culture to extracted tumours was heterogeneous (Figure 29). The expression of some proteins was found to be upregulated (Cytochrome C, DR4), while the expression of most proteins was found to be the same as in 2D or downregulated (cIAP1, cIAP2, Apaf1, Procaspase 9, Procaspase 3, XIAP, Mcl-1, FADD). Interestingly, the level of some of the proteins differed between two animals (Bid, Bcl-2, Bcl-xl, Procaspase 8), while the expression of DR5 and cFLIP differed between tumours harvested from the same animal. Four tumours, represented by four protein pattern sets, were placed in the previously constructed PCA space consisting of 16 melanoma cell lines. According to the LDA calculations, all four MeWo xenografts were predicted to be not responsive to the combination treatment *in silico* (Figure 30).
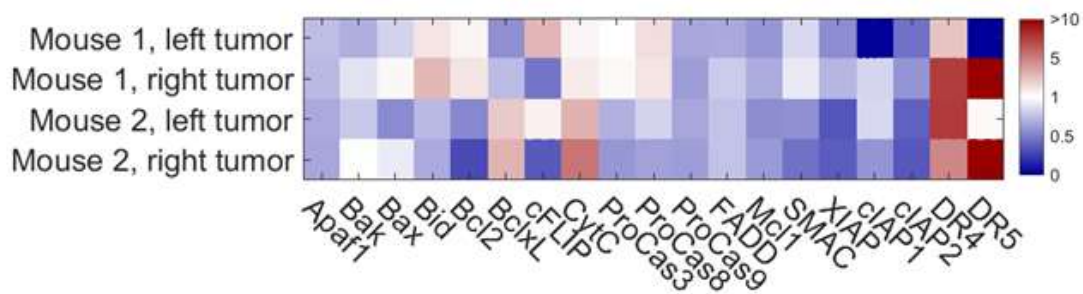
Figure 29. Expression of apoptosis proteins differed between MeWo cells grown in 2D or as tumours in a xenograft model. Two mice were sacrificed before the treatment was started. Tumours were harvested, and the expression of apoptosis proteins was determined by western blotting or flow cytometry (DR4/DR5). The heat map shows the fold change of expression of proteins between MeWo cells grown in 2D or as tumours in a xenograft model. Blue colour indicates a lower expression of proteins in MeWo xenograft model than in MeWo 2D, while red colour indicates higher expression in MeWo xenografts than in MeWo 2D.
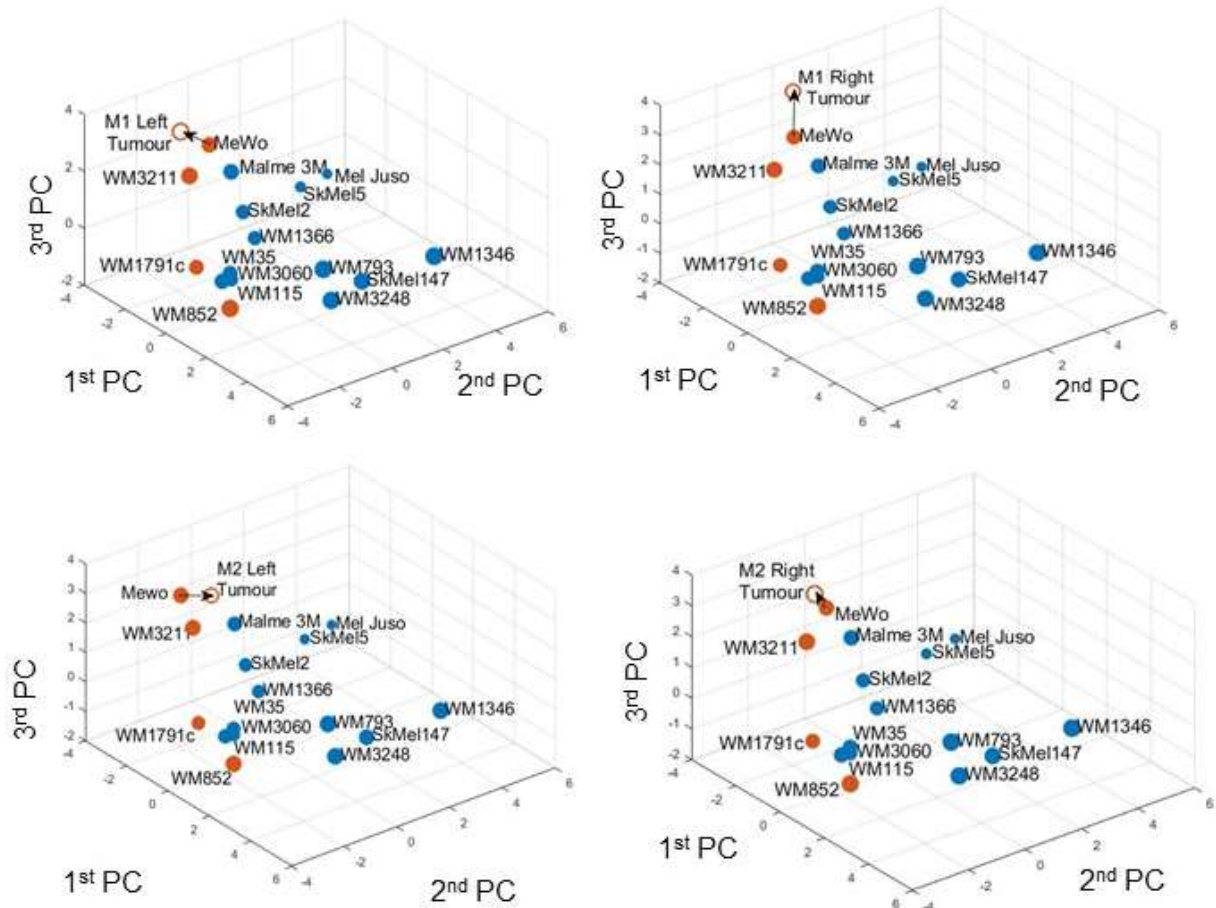

Figure 30. MeWo xenografts were predicted to be resistant to IZI1551 and Birinapant combination treatment. MeWo xenografts (empty circle) were placed in the PCA space according to their apoptosis protein profile. In silico responsiveness was calculated by LDA. Colour code indicates the responsiveness of the cell lines with blue = synergistic response and orange = low response or resistance. The arrow indicates the change of position in the

PCA space caused by the change of the protein expression between 2D and xenograft cell line.

4.2.3 Combination treatment with IZI1551 and Birinapant does not induce cell deah in MeWo xenograft

Mice were treated for four weeks with IZI1551, Birinapant, and their combination. There was no significant change of the tumour size upon single treatments or the combination treatment when compared to the untreated control. However, it was observed that tumours stimulated with IZI1551 were growing faster than the tumours in the other treatment groups (Figure 31). At the end of the treatment, the mice were sacrificed and the change of IAP proteins, as well as proteins of the apoptotic signalling cascade, was determined. As before, cIAP1 and XIAP levels were reduced in all treatment groups when compared to the untreated control, while the levels of cIAP2 remained unchanged (Figure 32). Furthermore, Procaspase 8 and Bid were depleted in the tumours that were treated with IZI1551, Birinapant, and combination treatment when compared to tumours from the control group. The cleavage of Procaspase 3 and were modest. In conclusion, MeWo cells grown as xenograft model remained resistant to the combination treatment with IZI1551 and Birinapant.
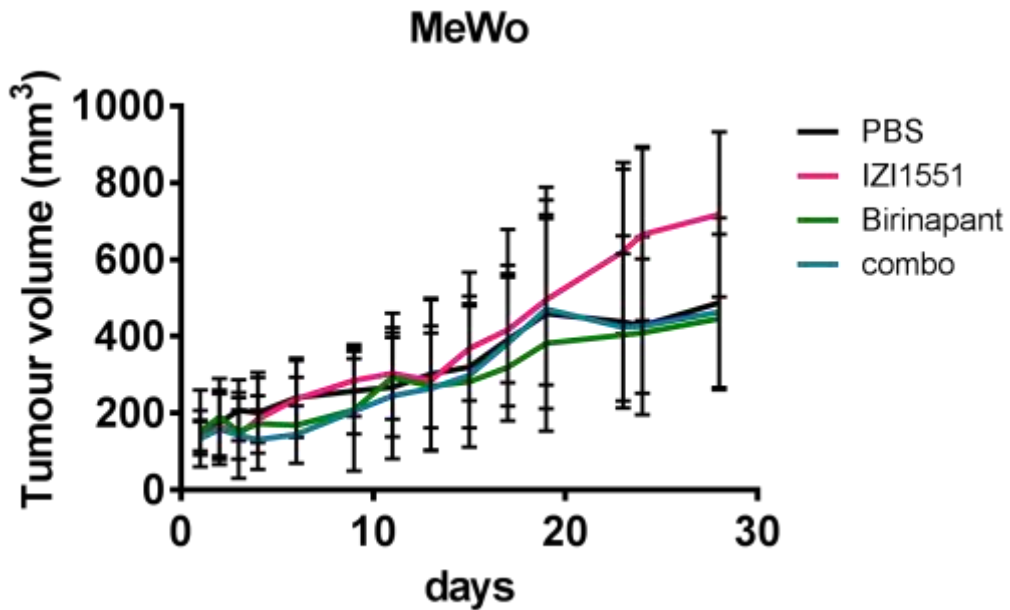
Figure 31. MeWo xenografts are resistant to combination treatment with IZI1551 and Birinapant. Mice were treated with the indicated concentration of IZI1551 and Birinapant and their combination for four weeks. The size of a tumour was monitored with digital callipers three times a week. Data represents the average tumour volume per group ± SD. There were 7 animals per treatment group, each animal bearing one or two subcutaneous tumours.
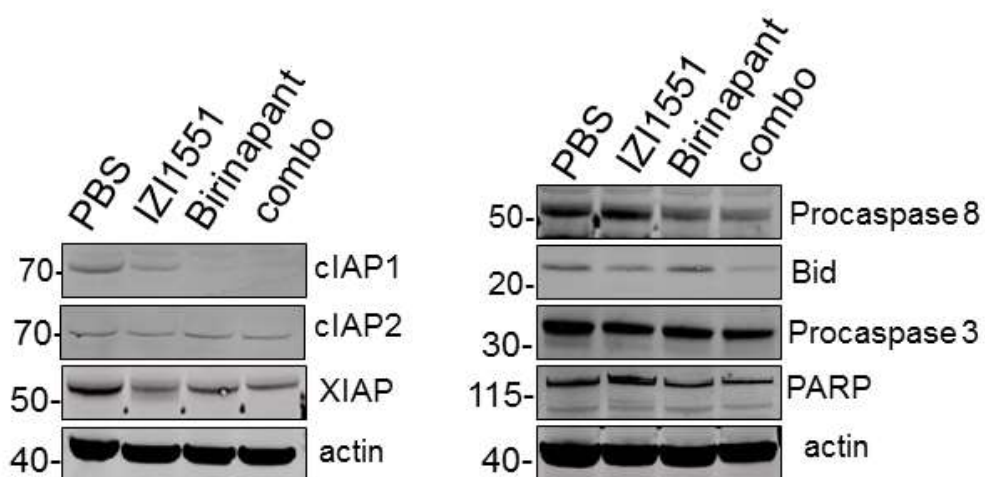

Figure 32. Apoptosis was not detected in MeWo xenograft model upon combination treatment with IZI1551 and Birinapant despite the depletion of cIAP1, Procaspase 8 and Bid. Mice were treated with 10 mg/kg Birinapant three times a week and 0.1 nmol IZI1551 and their combination twice a week during a period of four weeks. One day after the last treatment, mice were sacrificed and one tumour from each group was analysed for the expression of indicated proteins by western blotting. The experiment was performed once.

4.2.4 Experiments with SkMel2 xenograft model

Since the MeWo xenograft model was found to be resistant to single and combination treatment with IZI1551 and Birinapant, a second cell line, Mel Juso, was utilised to possibly demonstrate sensitivity to the combination treatment. However, this cell line did not form tumours in nude mice and the use of the cell line SkMel2 instead of Mel Juso was approved by the Ethics committee. Cell line SkMel2 was found to be sensitive to the combination treatment in Chapter I.

A second pre-experiment was therefore performed with the SkMel2 xenografts. After the tumours had formed, the treatments started when the average volume of tumours in each group was 100 mm^3. Mice were treated with 3 mg/kg, 10 mg/kg and 30 mg/kg Birinapant. Unfortunately, after 28 days of treatment, it was noticed that in all four groups the tumours did not increase their volume and therefore further experiments with this cell line were not performed (Figure 33).
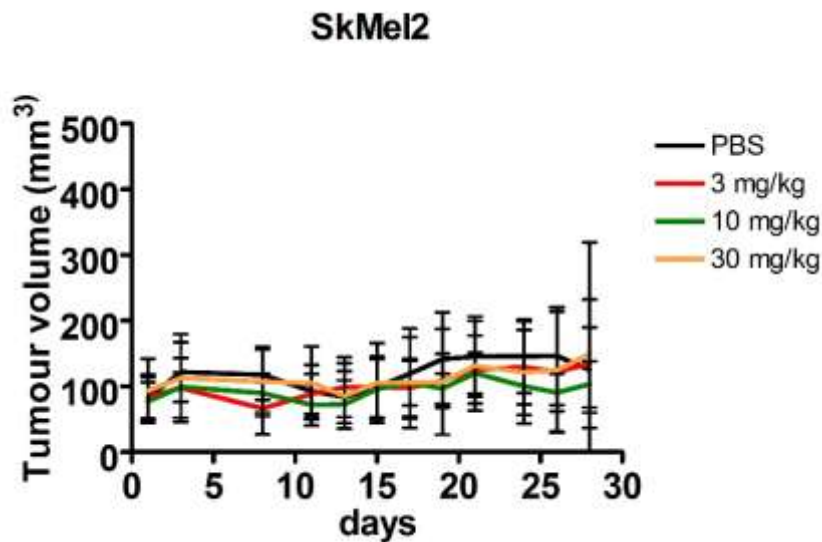

Figure 33. The volume of SkMel2 xenografts did not change during the four-week treatment with different concentrations of Birinapant. Mice were treated with indicated concentrations of Birinapant three times a week during a period of four weeks. The size of the tumours was monitored with digital callipers three times a week. Data represents the average volume of the tumours ± SD. There were 7 animals per treatment group, each animal bearing two subcutaneous tumours.

The experiments were stopped after the failure of two responsive cell lines to form viable tumours in mice. Further experiments with responsive cell lines were not persuaded. However, the results from the low responsive cell line MeWo suggest that the melanoma cell lines grown as xenografts retain their responsiveness to the treatment with IZI1551 and Birinapant as when grown in 2D. It was demonstrated that MeWo xenografts change their apoptosis protein expression compared to 2D grown cell line MeWo.

4.3 Chapter 4: Examining the efficacy of Dacarbazine and Birinapant in melanoma cell lines

Dacarbazine (DTIC), an FDA-approved chemotherapeutic for melanoma, was a first-line treatment for malignant melanoma since 1974 until the discovery of targeted therapy and immunotherapy despite low response rates and lack of evidence for improved overall survival. Nowadays, it remains in clinical use as a last-line treatment or as the treatment of loco-regionally spread advanced melanoma by technique called isolated limb perfusion. Additionally, up until 2018, it was a standard-of care treatment option in poorly funded health environments. The aim of this chapter was to assess the efficacy of DTIC and Birinapant (TL32711) as a combination treatment and to identify possible synergistic effects in inducing cell death in melanoma cell lines. The results of this chapter were published in the journal Oncology Research under the title "Examining the In Vitro Efficacy of the IAP Antagonist Birinapant as a Single Agent or in Combination with Dacarbazine to Induce Melanoma Cell Death" (Vetma et al. 2017).

4.3.1 Melanoma cell lines do not display synergistic cell death upon Dacarbazine and Birinapant combination treatment

To investigate the susceptibility to the combination treatments, cells were treated with Dacarbazine (0, 1, 10, 100, 1000 µg/mL) and Birinapant (0, 1, 10, 100, 1000 nM). After stimulation for 24 and 48 h, cell death was determined by propidium iodide uptake and flow cytometry. 24 h after the start of treatment, all cell lines remained highly resistant to single and combination treatments with Birinapant and Dacarbazine for concentration combinations of up to 100 nM and 100 µg/ml, respectively (Figure 34). Dacarbazine at 1 mg/ml resulted in less than 20% cell death, except for WM1366 and SkMel5 cells, where up to 50% cell death was detected. No synergy was detected for any of the cell lines or treatment conditions. After 48 h, all cell lines remained highly resistant for concentration combinations of up to 100 nM Birinapant and 100 µg/ml DTIC (Figure 35). A modest response to Birinapant
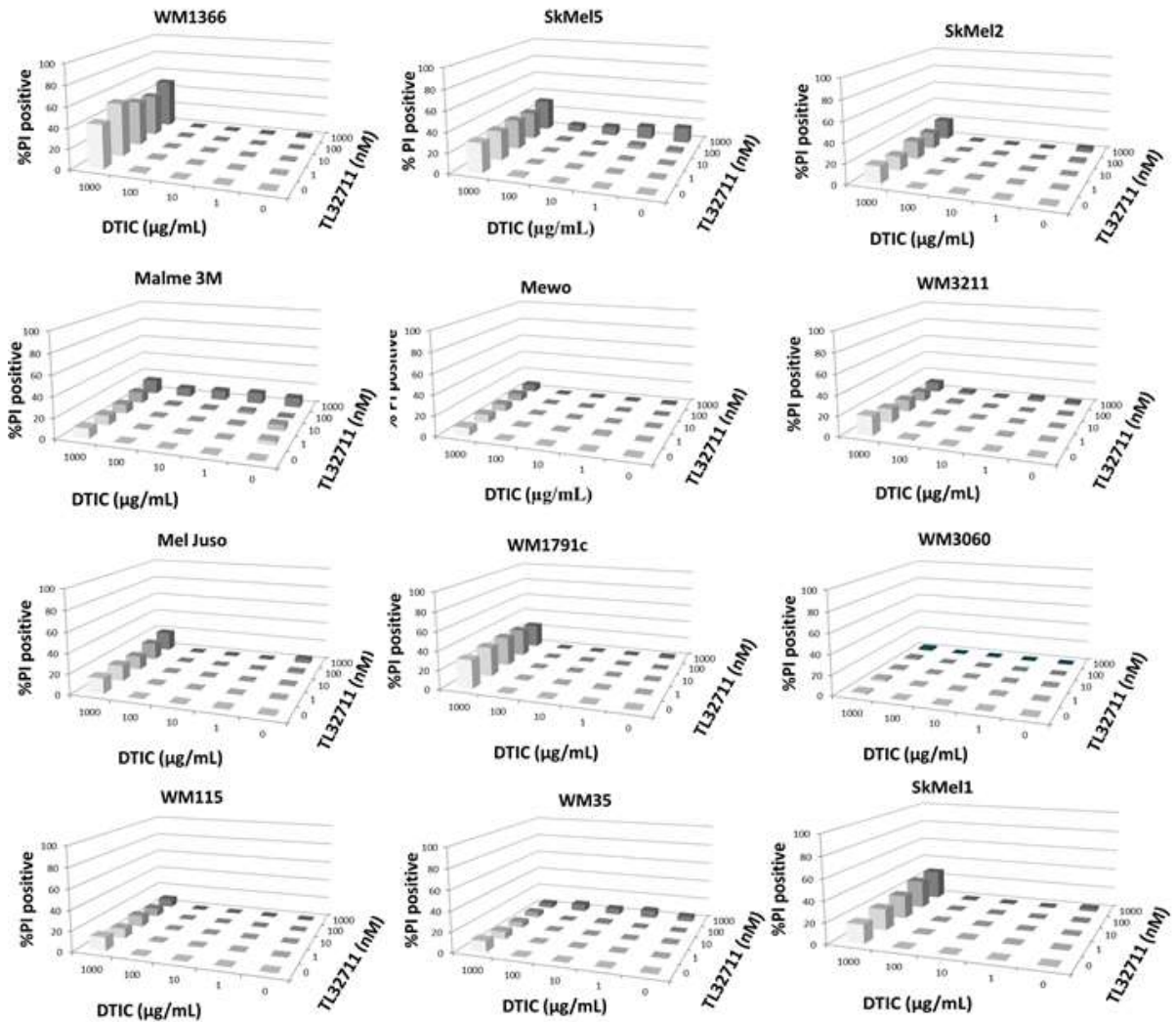
Figure 34. Responsiveness of the melanoma cell line panel 24 h after the combination treatment. Cell lines were treated either with Dacarbazine (1, 10, 100 and 1000 µg/mL) and Birinapant (1, 10, 100, 1000 nM) alone or in combination for 48 h. Thereafter, cells were stained with propidium iodide and the percentage of cell death (PI positive cells) was analysed by flow cytometry. Shown are mean values of three independent experiments. All measurements were done in triplicates. SD was omitted for clarity.
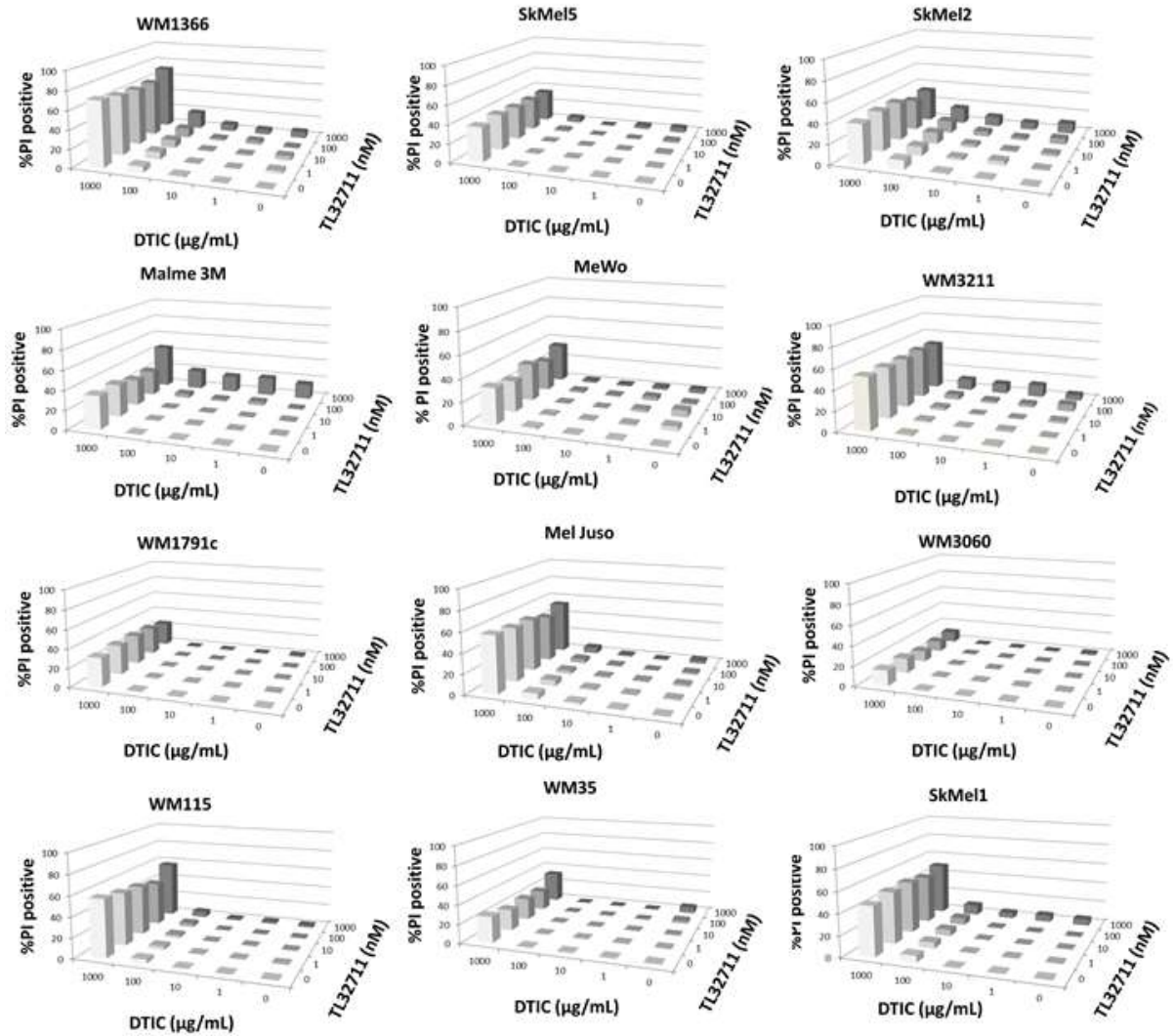
Figure 35. Responsiveness of the melanoma cell lines 48 h after combination treatment. Cell lines were treated either with Dacarbazine (1, 10, 100 and 1000 µg/mL) and Birinapant (1, 10, 100, 1000 nM) alone or in combination for 48 h. Thereafter, cells were stained with propidium iodide and the percentage of cell death (PI positive cells) was analysed by flow cytometry. Shown are mean values of three independent experiments. All measurements were done in triplicates. SD was omitted for clarity.

as a single agent and at the highest concentration was observed in Malme 3M cells (16% cell death).

Notable responses to Dacarbazine were observed at the concentration 1 mg/ml, and these responses were highly heterogeneous between cell lines. WM35 and WM3060 cells remained largely resistant with less than 20% cell death measured, whereas WM1366, WM3211, and SkMel1 cells exhibited 60% to 80% cell death. Combination index analysis by Webb's fractional product identified synergistic responses in Malme 3M cells with the concentrations 1 μM Birinapant and 1 mg/ml Dacarbazine (combination index CI = 0.658) and WM1366 cells with concentrations 1 μM Birinapant and 100 μg/ml Dacarbazine (combination index CI = 0.398).

The cell lines have been treated with clinically relevant concentration range of Dacarbazine (1-100 μg/mL), but the response of melanoma cell lines was poor throughout the panel. Additionally, Birinapant did not enhance the induction of cell death in melanoma cell lines treated with Dacarbazine. Only the highest concentration of the drug elicited noticeable cell death across the panel (1000 μg/mL). This concentration is achievable in the clinics only during the procedure of isolated limb perfusion, where the concentration of the drug achievable in the plasma of the patients during the treatment is 29 μg/mL. However, synergistic effects between the highest doses could not be measured. Therefore, Dacarbazine and Birinapant do not synergise in inducing cell death in malignant melanoma cell lines. However, it is possible that synergies between Dacarbazine and Birinapant manifest within the complexity of an *in vivo* environment, where additional sensitizing factors such as TNFα might be present. Such further experiments were not performed as a part of this research.

5 Discussion

Assessing the responsiveness of melanoma cell lines to combination treatment with DTIC and Birinapant

Inducing apoptosis is one of the most promising ways to eliminate cancer cells. It is highly specific and tightly regulated by more than 50 pro- and anti-apoptotic proteins (Wong 2011). Unfortunately, the expression of proteins of the apoptotic signalling cascade is often deregulated in cancer, conferring resistance of mutated cells to therapeutics. Among them are the proteins of the IAP family (Fernald and Kurokawa 2013). In line with these findings, combinations of IAP antagonists and chemotherapeutics have been reported to synergistically induce cell death in preclinical models of various cancers, including acute myeloid leukaemia, hepatocellular carcinoma and ovarian as well as bladder cancer (Amaravadi et al. 2015; Eytan et al. 2015; Benetatos et al. 2014)

Dacarbazine (DTIC), an FDA approved chemotherapeutic for melanoma, remains in frequent clinical use as second- or last-line treatment option or for the treatment of locoregionally spreading of advanced melanoma by isolated limb perfusion. Furthermore, DTIC remained the primary treatment option in poorly funded healthcare environments until very recently, despite low response rates and a lack of evidence for improved overall survival (Serrone et al. 2000). During systemic chemotherapy, DTIC serum concentrations can reach up to 29 µg/mL (Joukhadar et al. 2001). However, in this study melanoma cell lines were found to be resistant to the treatment with DTIC at that concentration. In line with this result, it was shown that cell lines responded heterogeneously to the very high concentrations of DTIC, achievable in the serum of the patients only during isolated limb perfusion or infusion (Han et al. 2011). The variability in DTIC-induced cell death between melanoma cell lines might be attributable to the heterogeneous expression patterns of apoptosis regulators. Unexpectedly, synergies or response potentiation upon the treatment with DTIC and Birinapant were not detected in this study despite having analysed 12 melanoma cell lines from different disease stages and with diverse mutational backgrounds. The fact that the combination of Birinapant and Dacarbazine failed to cause notable response synergies *in vitro* could either point toward a fundamental melanoma-inherent resistance mechanism

for this treatment regimen or, alternatively, indicate that stress responses to DNA-alkylating agents like DTIC in general cannot be enhanced by IAP antagonists.

Additionally, melanoma cell lines were found to be resistant or poorly responsive to the IAP antagonist Birinapant as a single agent. Interestingly, it was reported by Krepler and colleagues that only cell lines which produce TNFα were sensitive to single treatment with Birinapant (Krepler et al. 2013). Of note, only one cell line of this study, Malme 3M, was found to be sensitive to single treatment with Birinapant and further, this cell line secretes TNFα when untreated (Josip Skoko, unpublished data). These findings confirm a study by Krepler that likewise reported a high resistance of melanoma cells to Birinapant, despite clear evidence of on-target activity in these cells (Krepler et al. 2013). Besides not secreting TNFα, the resistance of melanoma cell lines could also be attributed to the lack of intrinsic ripoptosome formation upon cIAP depletion (Kocab and Duckett 2016; Fulda 2015). However, the latter conclusion conflicts with the finding of Wagner and colleagues that A172 glioma cells can respond synergistically to the combination of Temozolomide, a DNA-alkylating agent related to Dacarbazine, and BV6, a bivalent IAP antagonist with properties similar to Birinapant (Wagner et al. 2013). Furthermore, the possibility of synergies manifesting *in vivo* cannot be excluded. As mentioned before, IAP antagonists can sensitise cancer cell lines to extrinsic apoptosis induced by tumour necrosis factor receptor (TNFR)-1/-2 ligand TNFα) (Kocab and Duckett 2016; Fulda 2015). Indeed, Birinapant-induced sensitization to TNFα has previously been demonstrated for melanoma cells *in vitro*, and since TNFα is secreted into pro-inflammatory tumour microenvironments by invading macrophages, this may explain why 451Lu melanoma cells responded to Birinapant single treatment in an *in vivo* mouse xenograft model (Krepler et al. 2013). Whether synergies between Dacarbazine and Birinapant can manifest within the complexity of an *in vivo* environment, where additional sensitizing factors such as TNFα might be present, however, would require more comprehensive studies.

Testing the responsiveness of melanoma cell lines to combination treatment with IZI1551 and Birinapant

Since alkylating agents have not shown to be beneficial in the treatment of malignant melanoma, a different approach for inducing cell death was investigated in this study. More precisely, IZI1551, a novel TRAIL receptor agonist was investigated together with the

sensitizing agent Birinapant for its ability to induce apoptosis in different melanoma cell lines.

Several different TRAIL receptor agonists were already evaluated as anti-cancer agents in numerous *in vitro* experiments as well as in a few clinical trials. However, findings from *in vitro* studies did not translate into the clinics. Recently, multiple factors responsible for this inefficiency of TRAIL-based therapies were identified: TRAIL-receptor agonists with weak agonistic activity were selected to enter clinical trials, cancer cells are often resistant to TRAIL monotherapy and patients entering clinical trials were not selected based on validated biomarker that would indicate whether the patient would benefit from therapy (reviewed in Lemke et al. 2014).

To overcome the issue of weak agonistic activity, an improved TRAIL molecule, IZI1551, was designed at the University of Stuttgart. IZI1551 is a hexavalent TRAIL receptor agonist, consisting of two scTRAIL fragments crosslinked via the Fc part of an IgG antibody. It exhibited a significant increase in cell death induction and caspase activation when compared to rhTRAIL and antibodies directed against death receptors *in vitro* (Hutt et al. 2017). *In vivo* studies from the same publication also showed improved half-life and higher efficacy of hexavalent TRAIL when compared to other TRAIL formats. Taken together, these data strongly point out the superiority of IZI1551 over other TRAIL receptor agonists in treating cancer.

To further address the issue of cancer cells evading from TRAIL monotherapy by upregulating anti-apoptotic proteins, TRAIL-based treatment was combined with Birinapant. Birinapant acts as a sensitiser by binding and degrading cIAP1, enabling the formation of a RIPK1-FADD-Caspase 8 complex in the cytosol thereby lowering the threshold for death receptor-induced apoptosis (Benetatos et al. 2014). Pre-clinical studies already showed synergistic activity between Birinapant and several anti-tumour agents in various cancers (Allensworth et al. 2013b; Amaravadi et al. 2015). In these cases, Birinapant sensitised the malignant cells to treatment by rapid depletion of cIAP1, while at the same time sparing cIAP2 and XIAP (Amaravadi et al. 2015).

DISCUSSION

In line with these results, it was shown in this study that Birinapant sensitised different melanoma cell lines towards IZI1551-induced apoptosis. The synergy between IZI1551 and Birinapant was detected in 12 out of 16 2D-grown melanoma cell lines, 4 out of 5 3D-grown melanoma cell lines and 3 out of 5 patient-derived melanoma cell lines. In a study from Benetatos and colleagues, it was proposed that Birinapant depletes IAPs by binding with high affinity to the isolated BIR3 domain of cIAP1, cIAP2, and XIAP and rapidly degrades TRAF2-bound cIAP1 and cIAP2, therefore promoting caspase8-RIPK1 complex formation in response to death receptor stimulation (Benetatos et al. 2014). In the present study, it was shown that 1 µM Birinapant degraded cIAP1 within 1 h of combination treatment, whereas the levels of cIAP2 and XIAP were not affected. Of note, the concentrations of Birinapant used in this study were clinically relevant as they were comparable to the maximum concentration of the drug determined in the serum of patients receiving a dose ranging from 0.18 to 11.5 mg/m^2 (c$_{max}$ ranging from or 11 nM to 752 nM) (Amaravadi et al. 2015). Indeed, depletion of cIAP1 and subsequent sensitization of cancer cells to TRAIL-mediated apoptosis was confirmed to be a mechanism of synergy in many studies (Allensworth et al. 2013; Krepler et al. 2013; Benetatos et al. 2014; Werner et al. 2018). The levels of cIAP2 and XIAP were also noticed to be depleted upon apoptosis induction of the combination treatment between IZI1551 and Birinapant in this study. However, as stimulation with the pan-caspase inhibitor QVD OPh prevented cell death and restored the levels of cIAP2 and XIAP. Therefore, it is most likely that depletion of those proteins was due to cell death. Many mechanisms for Birinapant degrading cIAP1 but sparing cIAP2 and XIAP were already suggested in the literature. For example, it has been reported that cIAP2 is a substrate for cIAP1-mediated ubiquitination and that cIAP2 levels can be stabilized upon prolonged suppression of cIAP1 E3 ligase activity. Furthermore, the chemical composition of Birinapant dictates decreased affinity for BIR3 domains of cIAP2 and XIAP, making cIAP1 a preferable target (Condon et al. 2014). In a study by Lee and colleagues, cIAP2 depletion was found to be cell line specific and dependent on the expression of ubiquitin specific peptidase (USP11)-dependent deubiquitylation of cIAP2 (Lee et al. 2015). Taken together, the fact that Birinapant preferably degrades cIAPs and not XIAP, shown by this study and others, probably contributes to its tolerability in patients (Moulin et al. 2012; Amaravadi et al. 2015; Allensworth et al. 2013; Krepler et al. 2013). It was described in the study by Condon and colleagues that first generation IAP antagonists, like Compound A degraded cIAP1, cIAP2

and XIAP and were not tolerated well by patients (Condon et al. 2014). It was demonstrated by Moulin and colleagues that degradation of XIAP together with cIAP1 or cIAP2 led to mid-embryonic lethality in mice. Moreover, depletion of XIAP was found to be connected to increased motility and migration of cancer cells and perturbation of killer T-cell homeostasis (Dogan et al. 2008; Fulda 2015). Besides that, it was also shown to contribute to the X-linked lymphoproliferative syndrome (Mehrotra et al. 2010; Gradzka et al. 2018).

Testing the responsiveness of 3D and patient-derived melanoma cell line to the combination treatment

The process of drug discovery nowadays consists of screening potential therapeutics in 2D cell culture-based assays, followed by testing in animal models and subsequently clinical trials. However, only about 10% of the compounds tested progress successfully through this pipeline. Many of the compounds fail during clinical trials, due to the lack of clinical efficacy and/or unacceptable toxicity. One part of the failures can be attributed to the fact that *in vitro* data were generated with cancer cell lines grown in 2D, which does not resemble the situation of a 3D-grown tumour and can alter the responsiveness of the cells to the investigated drug (reviewed in Edmondson et al. 2014). Therefore, it is necessary to find a suitable method that would more faithfully represent the physiology of cancer and thus more accurately capture the responsiveness to the therapeutics. Multicellular tumour spheroids, also called 3D spheroids, have been utilized as a bridge between classical 2D cell culture and animal experiments with the aim to allow greater predictability of efficacy and toxicity in humans before drugs proceed to clinical trials (Fang and Eglen 2017).

In this study, beforehand 2D cultivated melanoma cell lines were grown in 3D and investigated for their responsiveness to the drug combination of IZI1551 and Birinapant. Although 12 out of 16 melanoma cell lines exhibited synergistic cell death upon the combination treatment, it was reported that growing cells as 3D spheroids can alter their response. In accordance with previous studies, this study also confirmed that melanoma cell lines exhibit the same responsiveness in 3D like they did in 2D (Krepler et al. 2013; Vörsmann et al. 2013; Wroblewski et al. 2013). IZI1551 and Birinapant acted synergistically in inducing cell death in the 3D grown melanoma cell lines Mel Juso, SkMel2, Malme 3M and WM1366, whereas MeWo, which was resistant to combination treatment when grown in 2D, remained unresponsive under 3D cultivation conditions. Vörsmann and colleagues

argued that all cells within a spheroid up to a size of 150-200 µm can sufficiently be supplied with nutrients and oxygen and that only spheroids of 500 µm can represent non-vascularized tumour tissue (Vörsmann et al. 2013). Barbone and colleagues investigated the distribution of soluble TRAIL in spheroids and found that it was equally distributed within a large mesothelioma spheroid of 500 µm 6 h after treatment (Barbone et al. 2008). Depending on the cell line, the size of the spheroids in this study ranged from 100 – 500 µm. The cell line MeWo, for example, exhibited very small and compact spheroids while other cell lines made very large and compact spheroids. However, 3D MeWo remained resistant and other cell lines remained responsive to the combination treatment. Even though drug penetration studies were not conducted with IZI1551, it is safe to state that IZI1551 successfully penetrated melanoma cell line spheroids of different sizes. This can be further corroborated with compelling evidence from Hutt and colleagues that IZI1551 successfully induces cell death in colorectal cancer xenograft models (Hutt et al. 2017). The size of the xenografted tumour could reach up to 1200 mm^3 with obvious effects of IZI1551 on the reduction of the tumour size, hence the cell death of the tumour. This result suggests that the drugs can effectively enter the spheroids.

Four of five 3D melanoma cell lines exhibited synergistic cell death to the combination treatment. Although the methods to examine the cleavage of caspases and PARP were not utilized, cell death was confirmed to be partially apoptosis by addition of the pan-caspase inhibitor QVD OPh. This indicated that one part of the spheroid consisted of cells that most likely died by necrosis. Due to the growth of the spheroid from 250 cells to a mature spheroid of 100 to 500 µm in diameter, different zones of growth emerged: an outer layer of proliferative cells, an inner layer of quiescent cells and a most inner layer of necrotic cells (Nath and Devi 2016). Necrotic part of the spheroid was speculated to excrete TNFα that could sensitise spheroids resistant to the combination treatment through stimulation of NFκB pathway. Simultaneous treatment with IAP antagonists and TNFα was shown to induce apoptosis in cancer cell lines (Fulda 2014). Although cell lines SkMel2 and Mel Juso showed a higher percentage of cell death in 3D upon the treatment, cell line MeWo could not be sensitised to IZI1551 even when grown as 3D spheroid. Thereby, melanoma cell lines grown as 3D spheroids responded to the combination treatment in the same way as when grown in 2D. In addition, expression of apoptosis proteins changed in 3D when compared to

2D, as discussed later in the chapter. To conclude, 3D melanoma cell lines died by apoptosis when treated with a combination treatment of IZI1551 and Birinapant and despite the change in expression of apoptosis proteins, remained of the same response as when grown in 2D.

Many studies suggested that a difference in gene and protein expression can result in changed drug responsiveness of patient-derived cell lines compared to commonly used cell lines (Luebker, Zhang, and Koepsell 2017; Garman et al. 2017). Therefore, a set of five patient-derived metastatic melanoma cells isolates was employed to test the efficacy of the combination treatment. Although the expression of the proteins between melanoma cell lines and patient-derived metastatic cells was different, patient-derived cell lines were also found to be heterogeneously responding to the combination treatment of IZI1551 and Birinapant.

Testing the combination treatment in melanoma cell lines grown as xenografts

Finally, two cell lines from the initial melanoma cell line panel, one synergistically responding (Mel Juso) and the other one exhibiting a low response to the combination treatmetnt (MeWo), were chosen to test their responsiveness to the combination treatment when grown as xenografts in mice. However, as one cell line Mel Juso did not form tumours in nude mice, the cell line SkMel2 was employed instead.

MeWo xenografts have found to be resistant to different doses of Birinapant. Nevertheless, cIAP1 was depleted upon treatment with Birinapant, while cIAP2 was intact in collected tumour samples. Interestingly, the levels of XIAP were slightly diminished in the treatment groups when compared to the group stimulated with PBS, probably due to ongoing apoptosis in a portion of cells within the tumours, indicated by detected cleavage of Procaspase 8. In this study, the cell line MeWo produced TNFα neither under 2D nor 3D cultivation, pointing out the possible reason for resistance to single treatment with Birinapant. Additionally, MeWo was resistant to combination treatment under all cultivating conditions despite the depletion of cIAP1 and cleavage of Procaspase 8 and Bid. The inability of the cell line to execute apoptosis even though cleavage of Procaspase 8 and Bid was detected upon the combination treatment, is suggesting that the cell line might not be able

to execute apoptosis via the mitochondrial pathway. This points out that the cell line MeWo might be a type II cell line requiring the activation of intrinsic mitochondrial pathway for the execution of apoptosis (Özören and El-Deiry 2002). Indeed, when the levels of anti-apoptotic proteins were quantified, it was noticed that compared to other cell lines in the panel, MeWo cells contained higher amounts of the Bcl-2 protein. Also, although the growth of MeWo-derived tumours did not differ significantly in mice treated with PBS, Birinapant or IZI1551, xenografts stimulated with IZI1551 in general seemed to grow slightly faster. Taken together these results suggest that the event of minority MOMP is induced in MeWo cells upon treatment with IZI1551 and Birinapant. As suggested by Ichim and colleagues, stimulation of cells that contain high levels of Bcl-2 proteins can cause "minority MOMP", meaning that cells exhibit the permeabilization of the mitochondrial membrane but do not die (Ichim et al. 2015; Kalkavan and Green 2018). Instead, repeated administration of a sublethal dose of therapeutics induces DNA damage and activation of caspase-activated DNases (CAD) that result in mutations, thereby promoting tumourigenesis and proliferation. Whether minority MOMP is indeed induced in the MeWo cell line by administration of TRAIL could be further investigated by conditioning the cell lines to sublethal doses of IZI1551 over a longer period *in vitro* and examining the proliferation rate via a scratch test or colony forming assay.

The cell line Mel Juso was the second cell line chosen to be grown as a xenograft in mice. Although it was reported in many studies that these cells can form a tumour in nude mice, this was not the case in the present study (Massoumi et al. 2009; Nyholm et al. 2014; Mirkina et al. 2014). Mel Juso tumours did not form although five million proliferative cells were injected. It is conceivable that the cells did not survive injection or that they were destroyed by immune cells. Furthermore, nude mice lack T-cell immunity but still exhibit NK (natural killer) cell activity which can impair engraftment of tumours (Szadvari, Krizanova, and Babula 2016). In contrast to Mel Juso, the cell line MeWo was shown by Shojaei and colleagues to lack the NKG2D ligand on the surface which allows for NK cell recognition, indicating the possible reason why this cell line escaped the surveillance of NK cells in nude mice and the engraftment was successful (Shojaei et al. 2009). Furthermore, the cell line Mel Juso was also described to express the major histocompatibility complex class I-related chain A (MICA), a protein homologous to NKG2D proteins, which is also targeted by NK cells

(Yadav et al. 2009). In future studies, this could possibly be addressed by screening the cell lines for expression of major surface immune antigens or to use immunodeficient severe combined immunodeficiency (SCID) mice which are severely deficient in functional B and T lymphocytes.

Due to the mentioned difficulties, an alteration of the initial study was made using the cell line SkMel2 instead of Mel Juso cells, which also synergistically responds to the combination treatment both in 2D and 3D culture. Indeed, the SkMel2 xenografts successfully formed in mice and the treatment was applied when the average size of the tumours in the group of mice was 100 mm^3, according to the protocol. However, the tumours did not grow more than 150 mm^3 in average over the period of 60 days neither in the control group nor in the treatment groups, although the cells were proliferative before harvesting, media was exchanged and Matrigel was used for growth support. Due to the described problems, the experiments with this cell line were not continued. Therefore, a conclusion whether melanoma cell lines are sensitive to the combination treatment *in vivo* could not be made. Further investigations should be done to assess if other cell lines that are sensitive in 2D would remain sensitive also when grown as xenografts.

Predicting the responsiveness of different melanoma entities to IZI1551-induced apoptosis by using multivariate statistics

As shown in the literature as well as in this study, some tumour types are resistant to TRAIL even when it is applied together with sensitisers such as Birinapant. As treatment with drugs is expensive and exhausting for the patients, it is necessary to determine which patients would benefit from selected treatment regimens. Several potential biomarkers for predicting the outcome of stimulation with apoptosis-inducing agents were proposed in melanoma, however, none were validated or translated into clinics. For example, deregulation of expression of the proteins of the Bcl-2 family (Bcl-2, Mcl-1, Bcl-xl, Bax, Bak) was shown to be one of the main resistance mechanisms in many cancers, including melanoma. High expression of Bcl-2 was demonstrated to correlate with a malignant phenotype and higher metastatic potential in several studies, while other studies indicated that Bcl-2 expression decreases during melanoma progression and does not correlate with resistance to chemotherapeutics at later stages (reviewed in Anvekar et al. 2011). There are several reasons why Bcl-2 from this example could not be used as a prognostic marker in

melanoma. Those different studies showed a conflicting role of Bcl-2 in melanoma, probably due to the complexity and non-linearity of apoptosis signaling, but also due to possible chance correlation. This again demonstrated that analyzing the expression of a single protein as a biomarker is not enough to make predictions about responsiveness. In contrast, analyzing candidate biomarkers in a context of signalling network by using multivariate identification methods could yield a more accurate result in identifying biomarkers, as suggested in a study by Manfredi and colleague (Manfredi and Robotti 2013). Additionally, the expression of Bcl-2 has not been validated in a large and independent study aimed at discovering biomarkers. A defined process of biomarker discovery includes biomarker assay development and analytical validation, validation of clinical utility and clinical implementation (Goosens et al. 2015). This problem is also obvious on a larger scale, as approximately 3000 papers per year propose biomarkers for cancer therapy, but only a dozen of them are used in the clinic. These findings point out to some extent why single proteins, like an expression of solely Bcl-2 protein, failed to be prognostic markers for the treatment of melanoma.

In this study, the baseline expression of 19 proteins involved in TRAIL signalling was analysed in 16 melanoma cell lines with the aim to connect the heterogeneity of protein expression to the heterogeneity of response to treatment with IZI1551 and Birinapant by using the previously published SYS ACT pipeline (Passante et al. 2013). The result was further validated by testing the *in silico* responsiveness of 3D-grown melanoma cell lines, patient-derived and cell lines grown as xenografts. This approach was rather successful as the responsiveness to the combination treatment of 13 out of 16 cell lines could be correctly predicted and it verified the hypothesis that apoptosis susceptibility depends on the quantitative interplay of multiple proteins. Further on, the result is in line with the hypothesis that a single optimal treatment strategy cannot be suggested for every melanoma patient due to the heterogeneity of apoptosis protein expression (Passante et al. 2013; Weyhenmeyer et al. 2016; Rožanc et al. 2018). These studies also showed that analyzing the baseline expression of proteins involved in the execution of cell death could correctly predict the responsiveness of the cell lines to different drugs. Further on, the change of expression of apoptotic proteins from 2D to 3D growth conditions was determined in this study in order to predict the responsiveness of the melanoma spheroids

based on their changes in protein expression. Thereby, it was shown that cultivation as spheroids changed the expression of apoptosis proteins in investigated cell lines. In some cell lines, cFLIP and DR4 were upregulated in 3D in comparison to 2D while Bcl-2 and IAP protein family were downregulated. Individually, these changes point out to different responsiveness outcomes towards apoptosis-inducing therapeutics. However, using data-driven modelling, considering the overall change in basal protein expression, revealed that although the expression of apoptosis proteins changed from 2D to 3D cell culture, the responsiveness to the combination treatment of IZI1551 and Birinapant was not altered. Five out of five melanoma cell lines cultivated in 3D were correctly predicted for their responsiveness to the combination treatment using data-driven modelling.

Furthermore, the difference in the expression of apoptosis proteins between melanoma cell lines and patient-derived cell lines were investigated in this study. Thereby, it was shown that expression of apoptosis proteins also differed between melanoma cell lines and patient-derived cell lines. However, predictions could still be made by using data-driven modelling. The accuracy of prediction (80%) indicates that the cell lines used to generate a training dataset highly conserved the tumour characteristics such as heterogeneity and malignant phenotype and genotype. Although most likely, gene and protein expression in melanoma cell lines changed when compared to an original tumour they were derived from, cells still reflect the characteristics of melanoma.

Additionally, the *in silico* responsiveness was tested in melanoma cell lines grown as xenografts in mice. In line with the previously described findings, the expression of apoptosis proteins also differed between cell lines cultivated in 2D and the same cell lines grown as xenografts. Furthermore, the protein expression pattern did not only differ between xenografts grown in different mice, but also in tumours harvested from the same animal. This could be attributed to clonal heterogeneity of the cell line since different cells initiated tumour formation, as well as the effect of the microenvironment on the tumour (Grzywa, Paskal, and Włodarski 2017; Shannan et al. 2016). Nevertheless, the resistance of all four MeWo xenografts was correctly predicted by placing the protein pattern of each tumour in the PCA space, which was confirmed at the end of the treatment period. This result additionally confirmed the quality of the generated 2D dataset as a basis for predicting the responsiveness of differently grown melanoma cell lines.

DISCUSSION

To sum it up, in this study, the systems biology approach has proved to be highly successful in predicting the responsiveness of melanoma cell lines grown in 2D, 3D and as xenografts as well as the sensitivity of patient-derived cells to combination treatment with IZI1551 and Birinapant. As pointed out in previous studies, the high level of prediction accuracy is probably the result of covering all critical TRAIL signalling regulators in determining the responsiveness, rather than analyzing expression of a single protein (Passante et al. 2013; Weyhenmeyer et al. 2016; Lindner et al. 2017; Rožanc et al. 2018; Lucantoni et al. 2018). The results also confirmed the quality of the generated 2D dataset in terms of reflecting the heterogeneity of melanoma, exhibiting different mutation status, responsiveness or origin of the cell lines and thus covering the broad-range of possible variables.

However, validation of these models for clinical application is challenging due to the need for a large-scale quantitative protein data. Often, fresh frozen tissue required for immunoblotting is rarely collected or available at all. Patient-derived cells are difficult to establish, the culturing conditions can be very specific, and they do not last long. Also, as it was argued in a study by Xi and Riker, gene expression can significantly differ from freshly frozen patient-tissue and cell lines derived from it (Xi et al. 2008). To overcome this, it was suggested by Pauli and colleagues to establish tumour organoids from biopsies (Pauli et al. 2017). However, this method was technically and clinically challenging and time from biopsy to the identification of the drug can be very long. Ideally, the model should be tested on tumour material freshly isolated from the patients. Fast and reliable high-throughput methods for quantifying protein amounts are necessary for parametrization of systems-models. Reverse protein phase arrays (RPPA), a method commonly used to quantify large amounts of different proteins, require pre-validated antibodies due to their dot-blot nature (O'Mahony et al. 2013). Commonly used immunohistochemistry in clinical diagnostics is of limited dynamic range, but some highly accurate quantitative methods are currently being developed (Van Eycke et al. 2016). By improving the method for fast and accurate quantification of required proteins, along with proper patient-derived material, this method could be further optimized as a valuable decision-making tool in the clinic.

Taken together, the results of this study indicate that melanoma cell lines can be used as a basis for predicting the synergistic effect of IZI1551 and Birinapant in inducing cell death in 3D and patient-derived cell cultures. This study, therefore, represents a proof-of-concept in

developing stratifying markers for malignant melanoma in response to a novel, clinically relevant combination treatment of the hexavalent TRAIL IZI1551 and Birinapant.

6 Summary and conclusion

In this study, it was demonstrated that the combination of IZI1551, a hexavalent TRAIL-receptor agonist, and Birinapant, a bivalent SMAC mimetic, can induce synergistic cell death in melanoma cell and patient-derived melanoma cell lines grown as 2D or 3D cell culture. In accordance with the current literature, Birinapant was found to exhibit fast and efficient on-target activity in eliminating cIAP1. Depletion of cIAP1 could possibly lead to formation of cell death inducing ripoptosome signalling complexes in the cytosol in addition to the apoptosis signalling triggered by IZI1551. Heterogeneous cell death upon the combination treatment was speculated to be connected to the heterogeneous expression of proteins involved in death signalling triggered by the combination treatment. As the type of cell death was concluded to be apoptosis, quantified basal levels of apoptosis proteins were connected to the responsiveness of melanoma cell lines by using data-driven statistical modelling. Previous studies tried to link the expression of single apoptosis proteins as biomarkers for responsiveness in melanoma, but however, validation of single proteins as possible biomarkers has failed. Therefore, the systems level approach of identifying biomarkers was utilized in this study. The responsiveness of 13 out of 16 cell lines could be correctly predicted using the computational modelling and consequently, this dataset also served as a basis for predicting the responsiveness of other melanoma entities to the combination treatment. Therefore, the response to IZI1551 and Birinapant was correctly predicted in 3D melanoma cell lines (100%), patient-derived cell lines (80%) and mice xenografts (100%). Taken together, these results pointed out the importance of taking into account all the signalling regulators when concluding on responsiveness instead of analysing the expression of single proteins. Also, this study points out to the possible benefit of a similar hexavalent TRAIL ABBV-621 currently being examined in the phase I clinical trials as a treatment for malignant melanoma and offers a proof-of-concept approach as a stratifying tool in personalized medicine and also for utilizing systems biology approach in biomarker discovery in highly heterogeneous cancers such as melanoma.

7 Bibliography

Albeck, John G., John M. Burke, Bree B. Aldridge, Mingsheng Zhang, Douglas A. Lauffenburger, and Peter K. Sorger. 2008. "Quantitative Analysis of Pathways Controlling Extrinsic Apoptosis in Single Cells." *Molecular Cell* 30 (1): 11–25.

Albertini, Mark R. 2018. "The Age of Enlightenment in Melanoma Immunotherapy." *Journal for ImmunoTherapy of Cancer* 6 (1): 80.

Allensworth, Jennifer L., Scott J. Sauer, H. Kim Lyerly, Michael a. Morse, and Gayathri R. Devi. 2013. "Smac Mimetic Birinapant Induces Apoptosis and Enhances TRAIL Potency in Inflammatory Breast Cancer Cells in an IAP-Dependent and TNF-α-Independent Mechanism." *Breast Cancer Research and Treatment* 137 (2): 359–71.

Almagro, M C de, and D. Vucic. 2012. "The Inhibitor of Apoptosis (IAP) Proteins Are Critical Regulators of Signaling Pathways and Targets for Anti-Cancer Therapy." *Experimental Oncology* 34 (3): 200–211.

Amaravadi, R. K., R. J. Schilder, L. P. Martin, M. Levin, M. A. Graham, D. E. Weng, and A. A. Adjei. 2015. "A Phase I Study of the SMAC-Mimetic Birinapant in Adults with Refractory Solid Tumors or Lymphoma." *Molecular Cancer Therapeutics* 14 (11): 2569–75.

Anvekar, Rina A., James J. Asciolla, Derek J. Missert, and Jerry E. Chipuk. 2011. "Born to Be Alive: A Role for the BCL-2 Family in Melanoma Tumor Cell Survival, Apoptosis, and Treatment." *Frontiers in Oncology* 1 (34).

Archier, E., S. Devaux, E. Castela, A. Gallini, F. Aubin, M. Le Maître, S. Aractingi, et al. 2012. "Carcinogenic Risks of Psoralen UV-A Therapy and Narrowband UV-B Therapy in Chronic Plaque Psoriasis: A Systematic Literature Review." *Journal of the European Academy of Dermatology and Venereology* 26 (SUPPL. 3): 22–31.

Ashkenazi, Avi. 2002. "Targeting Death and Decoy Receptors of the Tumour-Necrosis Factor Superfamily." *Nature Reviews Cancer* 2 (6): 420–30.

Balch, Charles M., Jeffrey E. Gershenwald, Seng Jaw Soong, John F. Thompson, Michael B. Atkins, David R. Byrd, Antonio C. Buzaid, et al. 2009. "Final Version of 2009 AJCC Melanoma Staging and Classification." *Journal of Clinical Oncology* 27 (36): 6199–6206.

BIBLIOGRAPHY

Barbone, Dario, Tsung Ming Yang, Jeffrey R. Morgan, Giovanni Gaudino, and V. Courtney Broaddus. 2008. "Mammalian Target of Rapamycin Contributes to the Acquired Apoptotic Resistance of Human Mesothelioma Multicellular Spheroids." *Journal of Biological Chemistry* 283 (19): 13021–30.

Beer, Lucian, Maximilian Hochmair, and Helmut Prosch. 2018. "Pitfalls in the Radiological Response Assessment of Immunotherapy." *Memo - Magazine of European Medical Oncology* 11 (2): 138–43.

Benetatos, C. A., Y. Mitsuuchi, J. M. Burns, E. M. Neiman, S. M. Condon, G. Yu, M. E. Seipel, et al. 2014. "Birinapant (TL32711), a Bivalent SMAC Mimetic, Targets TRAF2-Associated CIAPs, Abrogates TNF-Induced NF- B Activation, and Is Active in Patient-Derived Xenograft Models." *Molecular Cancer Therapeutics* 13 (4): 867–79.

Bentele, M., I. Lavrik, M. Ulrich, S. Stößer, D. W. Heermann, H. Kalthoff, P. H. Krammer, and R. Eils. 2004. "Mathematical Modeling Reveals Threshold Mechanism in CD95-Induced Apoptosis." *Journal of Cell Biology* 166 (6): 839–51.

Bertolotto, Corine. 2013. "Melanoma: From Melanocyte to Genetic Alterations and Clinical Options." *Scientifica* 2013: 1–22.

Bräuer, G. 2014. "Magnetron Sputtering." In *Comprehensive Materials Processing*, 4:57–73. Elsevier.

Calzone, Laurence, Laurent Tournier, Simon Fourquet, Denis Thieffry, Boris Zhivotovsky, Emmanuel Barillot, and Andrei Zinovyev. 2010. "Mathematical Modelling of Cell-Fate Decision in Response to Death Receptor Engagement." *PLoS Computational Biology* 6 (3): e1000702.

Campioni, Mara, Daniele Santini, Giuseppe Tonini, Raffaele Murace, Emanuele Dragonetti, Enrico P. Spugnini, and Alfonso Baldi. 2005. "Role of Apaf-1, a Key Regulator of Apoptosis, in Melanoma Progression and Chemoresistance." *Experimental Dermatology* 14 (11): 811–18.

Carswell, E. A., L. J. Old, R. L. Kassel, S. Green, N. Fiore, and B. Williamson. 1975. "An Endotoxin-Induced Serum Factor That Causes Necrosis of Tumors." *Proceedings of the National Academy of Sciences* 72 (9): 3666–70.

BIBLIOGRAPHY

Carter, Bing Z., Po Yee Mak, Duncan H. Mak, Yuexi Shi, Yihua Qiu, James M. Bogenberger, Hong Mu, et al. 2014. "Synergistic Targeting of AML Stem/Progenitor Cells with IAP Antagonist Birinapant and Demethylating Agents." *Journal of the National Cancer Institute* 106 (2): 1–12.

Charbel, Halim, and Firas H. Al-Kawas. 2011. "Cholangiocarcinoma: Epidemiology, Risk Factors, Pathogenesis, and Diagnosis." *Current Gastroenterology Reports* 13 (2): 182–87.

Charles, Emilie M, and Markus Rehm. 2014. "Key Regulators of Apoptosis Execution as Biomarker Candidates in Melanoma." *Molecular and Cellular Oncology* 1 (3): 37–41.

Cildir, Gökhan, Kee Chung Low, and Vinay Tergaonkar. 2016. "Noncanonical NF-KB Signaling in Health and Disease." *Trends in Molecular Medicine* 22 (5): 414–29.

Coley, William B. 1891. "Contribution to the Knowledge of Sarcoma." *Annals of Surgery* 14 (3): 199–220.

Condon, Stephen M., Yasuhiro Mitsuuchi, Yijun Deng, Matthew G. Laporte, Susan R. Rippin, Thomas Haimowitz, Matthew D. Alexander, et al. 2014. "Birinapant, a Smac-Mimetic with Improved Tolerability for the Treatment of Solid Tumors and Hematological Malignancies." *Journal of Medicinal Chemistry* 57 (9): 3666–77.

Coricovac, Dorina, Cristina Dehelean, Elena Alina Moaca, Iulia Pinzaru, Tiberiu Bratu, Dan Navolan, and Ovidiu Boruga. 2018. "Cutaneous Melanoma—a Long Road from Experimental Models to Clinical Outcome: A Review." *International Journal of Molecular Sciences* 19 (6).

Cory, Suzanne, and Jerry M. Adams. 2002. "The BCL2 Family: Regulators of the Cellular Life-or-Death Switch." *Nature Reviews Cancer* 2 (9): 647–56.

Crawford, Nyree, Manuela Salvucci, Christian T. Hellwig, Frank A. Lincoln, Ruth E. Mooney, Carla L. O'Connor, Jochen Hm Prehn, Daniel B. Longley, and Markus Rehm. 2018. "Simulating and Predicting Cellular and in Vivo Responses of Colon Cancer to Combined Treatment with Chemotherapy and IAP Antagonist Birinapant/TL32711." *Cell Death and Differentiation* 25 (11): 1952–66.

Crook, Norman E, Rollie J Clem, and Lois K Miller. 1993. "An Apoptosis-Inhibiting Baculovirus Gene with a Zinc Finger-like Motif." *Journal of Virology* 67 (4): 2168–74.

D'Mello, Stacey A.N., Graeme J. Finlay, Bruce C. Baguley, and Marjan E. Askarian-Amiri. 2016. "Signaling Pathways in Melanogenesis." *International Journal of Molecular Sciences* 17 (7).

Darding, Maurice, and Pascal Meier. 2012. "IAPs: Guardians of RIPK1." *Cell Death and Differentiation* 19 (1): 58–66.

Dewson, Grant, and Ruth M. Kluck. 2009. "Mechanisms by Which Bak and Bax Permeabilise Mitochondria during Apoptosis." *Journal of Cell Science* 122 (16): 2801–8.

Dickens, Laura S., Robert S. Boyd, Rebekah Jukes-Jones, Michelle A. Hughes, Gemma L. Robinson, Louise Fairall, John W.R. Schwabe, Kelvin Cain, and Marion MacFarlane. 2012. "A Death Effector Domain Chain DISC Model Reveals a Crucial Role for Caspase-8 Chain Assembly in Mediating Apoptotic Cell Death." *Molecular Cell* 47 (2): 291–305.

Dogan, Taner, Gregory S. Harms, Mirko Hekman, Christiaan Karreman, Tripat Kaur Oberoi, Emad S. Alnemri, Ulf R. Rapp, and Krishnaraj Rajalingam. 2008. "X-Linked and Cellular IAPs Modulate the Stability of C-RAF Kinase and Cell Motility." *Nature Cell Biology* 10 (12): 1447–55.

Domingues, Beatriz, Jose Lopes, Paula Soares, and Helena Populo. 2018. "Melanoma Treatment in Review." *ImmunoTargets and Therapy* 7: 35–49.

Duval, Kayla, Hannah Grover, Li-Hsin Han, Yongchao Mou, Adrian F. Pegoraro, Jeffery Fredberg, and Zi Chen. 2017. "Modeling Physiological Events in 2D vs. 3D Cell Culture." *Physiology* 32 (4): 266–77.

Echevarría-Vargas, Ileabett M, and Jessie Villanueva. 2017. "Combating NRAS Mutant Melanoma: From Bench to Bedside." *Melanoma Management* 4 (4): 183–86.

Edmondson, Rasheena, Jessica Jenkins Broglie, Audrey F Adcock, and Liju Yang. 2014. "Three-Dimensional Cell Culture Systems and Their Applications in Drug Discovery and Cell-Based Biosensors." *Assay and Drug Development Technologies* 12 (4): 207–18.

Eycke, Yves Remi Van, Justine Allard, Melanie Derock, Isabelle Salmon, Olivier Debeir, and

Christine Decaestecker. 2016. "Image Normalization for Quantitative Immunohistochemistry in Digital Pathology." In *Proceedings - International Symposium on Biomedical Imaging*, 795–98.

Eytan, Danielle F., Grace E. Snow, Sophie Carlson, Adeeb Derakhshan, Anthony Saleh, Stephen Schiltz, Hui Cheng, et al. 2016. "SMAC Mimetic Birinapant plus Radiation Eradicates Human Head and Neck Cancers with Genomic Amplifications of Cell Death Genes FADD and BIRC2." *Cancer Research* 76 (18): 5442–54.

Eytan, Danielle F., Grace E. Snow, Sophie G. Carlson, Stephen Schiltz, Zhong Chen, and Carter Van Waes. 2015. "Combination Effects of SMAC Mimetic Birinapant with TNFα, TRAIL, and Docetaxel in Preclinical Models of HNSCC." *Laryngoscope* 125 (3): E118–24.

Fang, Ye, and Richard M. Eglen. 2017. "Three-Dimensional Cell Cultures in Drug Discovery and Development." *SLAS Discovery* 22 (5): 456–72.

Fernald, Kaleigh, and Manabu Kurokawa. 2013. "Evading Apoptosis in Cancer." *Trends in Cell Biology* 23 (12): 620–33.

Fricker, Nicolai, Joel Beaudouin, Petra Richter, Roland Eils, Peter H. Krammer, and Inna N. Lavrik. 2010. "Model-Based Dissection of CD95 Signaling Dynamics Reveals Both a pro- and Antiapoptotic Role of c-FLIPL." *Journal of Cell Biology* 190 (3): 377–89.

Fulda, Simone. 2010. "Evasion of Apoptosis as a Cellular Stress Response in Cancer." *International Journal of Cell Biology* 2010: 1–6.

Fulda, Simone. 2013. "The Dark Side of TRAIL Signaling." *Cell Death & Differentiation* 20: 845–46.

Fulda, Simone. 2014. "Targeting Inhibitor of Apoptosis Proteins for Cancer Therapy: A Double-Edge Sword?" *Journal of Clinical Oncology* 32 (28): 3190–91.

Fulda, Simone. 2015. "Promises and Challenges of Smac Mimetics as Cancer Therapeutics." *Clinical Cancer Research* 21 (22): 5030–36.

Fussenegger, Martin, James E. Bailey, and Jeffrey Varner. 2000. "A Mathematical Model of Caspase Function in Apoptosis." *Nature Biotechnology* 18 (7): 768–74.

Galluzzi, Lorenzo, Ilio Vitale, Stuart A. Aaronson, John M. Abrams, Dieter Adam, Patrizia

Agostinis, Emad S. Alnemri, et al. 2018. "Molecular Mechanisms of Cell Death: Recommendations of the Nomenclature Committee on Cell Death 2018." *Cell Death & Differentiation* 25 (3): 486–541.

Garman, Bradley, Ioannis N. Anastopoulos, Clemens Krepler, Patricia Brafford, Katrin Sproesser, Yuchao Jiang, Bradley Wubbenhorst, et al. 2017. "Genetic and Genomic Characterization of 462 Melanoma Patient-Derived Xenografts, Tumor Biopsies, and Cell Lines." *Cell Reports* 21 (7): 1936–52.

Gieffers, C., M. Kluge, C. Merz, J. Sykora, M. Thiemann, R. Schaal, C. Fischer, et al. 2013. "APG350 Induces Superior Clustering of TRAIL Receptors and Shows Therapeutic Antitumor Efficacy Independent of Cross-Linking via Fc Receptors." *Molecular Cancer Therapeutics* 12 (12): 2735–47.

Gilchrest, Barbara A., Mark S. Eller, Alan C. Geller, and Mina Yaar. 2002. "The Pathogenesis of Melanoma Induced by Ultraviolet Radiation." *New England Journal of Medicine* 340 (17): 1341–48.

Goosens N., S. Nakagawa, Sun X., and Hoshida Y. 2015. "Cancer Biomarker Discovery and Validation." *Translational Cancer Research* 4 (3): 256–69.

Gradzka, Sylwia, Oliver S. Thomas, Oliver Kretz, Aladin Haimovici, Lazaros Vasilikos, Wendy Wei-Lynn Wong, Georg Häcker, and Ian E. Gentle. 2018. "Inhibitor of Apoptosis Proteins Are Required for Effective Fusion of Autophagosomes with Lysosomes." *Cell Death & Disease* 9 (5): 529.

Grzywa, Tomasz M., Wiktor Paskal, and Paweł K. Włodarski. 2017. "Intratumor and Intertumor Heterogeneity in Melanoma." *Translational Oncology* 10 (6): 956–75.

Gyrd-Hansen, Mads, and Pascal Meier. 2010. "IAPs: From Caspase Inhibitors to Modulators of NF-KB, Inflammation and Cancer." *Nature Reviews Cancer* 10 (8): 561–74.

Han, Dale, Georgia M Beasley, Douglas S Tyler, and Jonathan S Zager. 2011. "Minimally Invasive Intra-Arterial Regional Therapy for Metastatic Melanoma: Isolated Limb Infusion and Percutaneous Hepatic Perfusion." *Expert Opinion on Drug Metabolism & Toxicology* 7 (11): 1383–94.

BIBLIOGRAPHY

Hantusch, Annika, Markus Rehm, and Thomas Brunner. 2018. "Counting on Death –
Quantitative Aspects of Bcl-2 Family Regulation." *The FEBS Journal* 285 (22): 4124–38.

Henry, Conor M., and Seamus J. Martin. 2017. "Caspase-8 Acts in a Non-Enzymatic Role as a
Scaffold for Assembly of a Pro-Inflammatory 'FADDosome' Complex upon TRAIL
Stimulation." *Molecular Cell* 65 (4): 715-729.e5.

Heppt, Markus V., Timo Siepmann, Jutta Engel, Gabriele Schubert-Fritschle, Renate Eckel,
Laura Mirlach, Thomas Kirchner, et al. 2017. "Prognostic Significance of BRAF and NRAS
Mutations in Melanoma: A German Study from Routine Care." *BMC Cancer* 17 (1): 536.

Hodis, Eran, Ian R. Watson, Gregory V. Kryukov, Stefan T. Arold, Marcin Imielinski, Jean
Philippe Theurillat, Elizabeth Nickerson, et al. 2012. "A Landscape of Driver Mutations
in Melanoma." *Cell* 150 (2): 251–63.

Hogan, Sabrina A., Mitchell P. Levesque, and Phil F. Cheng. 2018. "Melanoma
Immunotherapy: Next-Generation Biomarkers." *Frontiers in Oncology* 8: 178.

Holcik, Martin, Chiaoli Yeh, Robert G. Korneluk, and Terry Chow. 2000. "Translational
Upregulation of X-Linked Inhibitor of Apoptosis (XIAP) Increases Resistance to Radiation
Induced Cell Death." *Oncogene* 19 (36): 4174–77.

Hollander, Martha W. den, Jourik A. Gietema, Steven de Jong, Annemiek M.E. Walenkamp,
Anna K.L. Reyners, Corina N.A.M. Oldenhuis, and Elisabeth G.E. De Vries. 2013.
"Translating TRAIL-Receptor Targeting Agents to the Clinic." *Cancer Letters* 332 (2):
194–201.

Horssen, R. van. 2006. "TNF- in Cancer Treatment: Molecular Insights, Antitumor Effects,
and Clinical Utility." *The Oncologist* 11 (4): 397–408.

Hughes, Peyton, Damian Marshall, Yvonne Reid, Helen Parkes, and Cohava Gelber. 2007.
"The Costs of Using Unauthenticated, over-Passaged Cell Lines: How Much More Data
Do We Need?" *BioTechniques* 43 (5): 575–86.

Hughes, Ian R. Powley, Rebekah Jukes-Jones, Sebastian Horn, Maria Feoktistova, Louise
Fairall, John W.R. Schwabe, Martin Leverkus, Kelvin Cain, and Marion MacFarlane.
2016. "Co-Operative and Hierarchical Binding of c-FLIP and Caspase-8: A Unified Model

Defines How c-FLIP Isoforms Differentially Control Cell Fate." *Molecular Cell* 61 (6): 834–49.

Hunter, Allison M., Eric C. LaCasse, and Robert G. Korneluk. 2007. "The Inhibitors of Apoptosis (IAPs) as Cancer Targets." *Apoptosis* 12 (9): 1543–68.

Hutt, Meike. 2017. "Multivalent Antibody-ScTRAIL Fusion Proteins for Tumor Therapy – Impact of Format and Targeting." PhD thesis. Institute for Cell Biology and Immunology, Univeristy of Stuttgart.

Hutt, Meike, Lisa Marquardt, Oliver Seifert, Martin Siegemund, Ines Müller, Dagmar Kulms, Klaus Pfizenmaier, and Roland E. Kontermann. 2017. "Superior Properties of Fc-Comprising ScTRAIL Fusion Proteins." *Molecular Cancer Therapeutics* 16 (12): 2792–2802.

Ichim, Gabriel, Jonathan Lopez, Shafiq U. Ahmed, Nathiya Muthalagu, Evangelos Giampazolias, M. Eugenia Delgado, Martina Haller, et al. 2015. "Limited Mitochondrial Permeabilization Causes DNA Damage and Genomic Instability in the Absence of Cell Death." *Molecular Cell* 57 (5): 860–72.

Iyer, Arun K., Greish Khaled, Jun Fang, and Hiroshi Maeda. 2006. "Exploiting the Enhanced Permeability and Retention Effect for Tumor Targeting." *Drug Discovery Today* 11 (17–18): 812–18.

Janes, Kevin A., and Michael B. Yaffe. 2006. "Data-Driven Modelling of Signal-Transduction Networks." *Nature Reviews Molecular Cell Biology* 7 (11): 820–28.

Janzen, D. M., E. Tiourin, J. A. Salehi, D. Y. Paik, J. Lu, M. Pellegrini, and S. Memarzadeh. 2015. "An Apoptosis-Enhancing Drug Overcomes Platinum Resistance in a Tumour-Initiating Subpopulation of Ovarian Cancer." *Nature Communications* 6 (1): 7956.

Johnson, Lincoln V., and Patricia G. Calarco. 1980. "Mammalian Preimplantation Development: The Cell Surface." *The Anatomical Record* 196 (2): 201–19.

Joukhadar, Christian, Nikolas Klein, Robert M. Mader, Claudia Schrolnberger, Blanka Rizovski, Elisabeth Heere-Ress, Hubert Pehamberger, Nadja Strauchmann, Burkhard Jansen, and Markus Mller. 2001. "Penetration of Dacarbazine and Its Active Metabolite

5-Aminoimidazole-4-Carboxamide into Cutaneous Metastases of Human Malignant Melanoma." *Cancer* 92 (8): 2190–96.

Kaiser, Henry F. 1960. "The Application of Electronic Computers to Factor Analysis." *Educational and Psychological Measurement* 20 (1): 141–51.

Kalkavan, Halime, and Douglas R. Green. 2018. "MOMP, Cell Suicide as a BCL-2 Family Business." *Cell Death and Differentiation* 25 (1): 46–55.

Kocab, Andrew J., and Colin S. Duckett. 2016. "Inhibitor of Apoptosis Proteins as Intracellular Signaling Intermediates." *FEBS Journal* 283 (2): 221–31.

Krepler, Clemens, Srinivas K Chunduru, Molly B Halloran, Xu He, Min Xiao, Adina Vultur, Jessie Villanueva, et al. 2013. "The Novel SMAC Mimetic Birinapant Exhibits Potent Activity against Human Melanoma Cells." *Clinical Cancer Research* 19 (7): 1784–94.

Kütting, Birgitta, and Hans Drexler. 2010. "UV-Induced Skin Cancer at Workplace and Evidence-Based Prevention." *International Archives of Occupational and Environmental Health* 83 (8): 843–54.

Lafont, Elodie, Chahrazade Kantari-Mimoun, Peter Draber, Diego De Miguel, Torsten Hartwig, Matthias Reichert, Sebastian Kupka, et al. 2017. "The Linear Ubiquitin Chain Assembly Complex Regulates TRAIL-induced Gene Activation and Cell Death." *The EMBO Journal* 36 (9): 1147–66.

Laussmann, Maike A., Egle Passante, Christian T. Hellwig, Bartłomiej Tomiczek, Lorna Flanagan, Jochen H. M. Prehn, Heinrich J. Huber, and Markus Rehm. 2012. "Proteasome Inhibition Can Impair Caspase-8 Activation upon Submaximal Stimulation of Apoptotic Tumor Necrosis Factor-Related Apoptosis Inducing Ligand (TRAIL) Signaling." *Journal of Biological Chemistry* 287 (18): 14402–11.

Lavrik, Inna N., Alexander Golks, Dagmar Riess, Martin Bentele, Roland Eils, and Peter H. Krammer. 2007. "Analysis of CD95 Threshold Signaling." *Journal of Biological Chemistry* 282 (18): 13664–71.

Lawlor, Kate E., Rebecca Feltham, Monica Yabal, Stephanie A. Conos, Kaiwen W. Chen, Stephanie Ziehe, Carina Graß, et al. 2017. "XIAP Loss Triggers RIPK3- and Caspase-8-

Driven IL-1β Activation and Cell Death as a Consequence of TLR-MyD88-Induced CIAP1-TRAF2 Degradation." *Cell Reports* 20 (3): 668–82.

Lee, E. W., D. Seong, J. Seo, M. Jeong, H. K. Lee, and J. Song. 2015. "USP11-Dependent Selective CIAP2 Deubiquitylation and Stabilization Determine Sensitivity to Smac Mimetics." *Cell Death and Differentiation* 22 (9): 1463–76.

Lee, Noor Ul-Ain-Tariq, Alberto Fusi, Samantha Bowyer, and Paul Lorigan. 2014. "The Role of Chemotherapy in the Modern Management of Melanoma." *Melanoma Management* 1 (2): 173–84.

Lemke, J., S von Karstedt, J. Zinngrebe, and H. Walczak. 2014. "Getting TRAIL Back on Track for Cancer Therapy." *Cell Death & Differentiation* 21 (9): 1350–64.

Leonardi, Giulia C., Luca Falzone, Rossella Salemi, Antonino Zanghì, Demetrios A. Spandidos, James A. Mccubrey, Saverio Candido, and Massimo Libra. 2018. "Cutaneous Melanoma: From Pathogenesis to Therapy (Review)." *International Journal of Oncology* 52 (4): 1071–80.

Lindner, Andreas U., Caoimhín G. Concannon, Gerhardt J. Boukes, Mary D. Cannon, Fabien Llambi, Deborah Ryan, Karen Boland, et al. 2013. "Systems Analysis of BCL2 Protein Family Interactions Establishes a Model to Predict Responses to Chemotherapy." *Cancer Research* 73 (2): 519–28.

Lindner, Andreas U., Manuela Salvucci, Clare Morgan, Naser Monsefi, Alexa J. Resler, Mattia Cremona, Sarah Curry, et al. 2017. "BCL-2 System Analysis Identifies High-Risk Colorectal Cancer Patients." *Gut* 66 (12): 2141–48.

Lucantoni, Federico, Andreas U. Lindner, Norma O'Donovan, Heiko Düssmann, and Jochen H. M. Prehn. 2018. "Systems Modeling Accurately Predicts Responses to Genotoxic Agents and Their Synergism with BCL-2 Inhibitors in Triple Negative Breast Cancer Cells." *Cell Death & Disease* 9 (2): 42.

Luebker, Stephen A, Weiwei Zhang, and Scott A Koepsell. 2017. "Comparing the Genomes of Cutaneous Melanoma Tumors to Commercially Available Cell Lines." *Oncotarget* 8 (70).

Majkut, J., M. Sgobba, C. Holohan, N. Crawford, A. E. Logan, E. Kerr, C. A. Higgins, et al. 2014.

"Differential Affinity of FLIP and Procaspase 8 for FADD's DED Binding Surfaces Regulates DISC Assembly." *Nature Communications* 5 (1): 3350.

Manfredi, Marcello, and Elisa Robotti. 2013. "Biomarkers Discovery through Multivariate Statistical Methods: A Review of Recently Developed Methods and Applications in Proteomics." *Journal of Proteomics & Bioinformatics* s3 (003).

Massoumi, Ramin, Silke Kuphal, Claus Hellerbrand, Bodo Haas, Peter Wild, Thilo Spruss, Alexander Pfeifer, Reinhard Fässler, and Anja K Bosserhoff. 2009. "Down-Regulation of CYLD Expression by Snail Promotes Tumor Progression in Malignant Melanoma." *The Journal of Experimental Medicine* 206 (1): 221–32.

Mazarakis, Nicholas D., A. David Edwards, and Huseyin Mehmet. 1997. "Apoptosis in Neural Development and Disease." *Archives of Disease in Childhood - Fetal and Neonatal Edition* 77 (3): F165–70.

McManus, Dan C., Charles A. Lefebvre, Gabriele Cherton-Horvat, Martine St-Jean, Ekambar R. Kandimalla, Sudhir Agrawal, Stephen J. Morris, Jon P. Durkin, and Eric C. LaCasse. 2004. "Loss of XIAP Protein Expression by RNAi and Antisense Approaches Sensitizes Cancer Cells to Functionally Diverse Chemotherapeutics." *Oncogene* 23 (49): 8105–17.

Mehnert, Janice M., and Harriet M. Kluger. 2012. "Driver Mutations in Melanoma: Lessons Learned from Bench-to-Bedside Studies." *Current Oncology Reports* 14 (5): 449–57.

Mehrbod, Parvaneh, Sudharsana R. Ande, Javad Alizadeh, Shahrzad Rahimizadeh, Aryana Shariati, Hadis Malek, Mohammad Hashemi, et al. 2019. "The Roles of Apoptosis, Autophagy and Unfolded Protein Response in Arbovirus, Influenza Virus, and HIV Infections." *Virulence* 10 (1): 376–413.

Mehrotra, Swarna, Lucia R Languino, Christopher M Raskett, Arthur M Mercurio, Takehiko Dohi, and Dario C Altieri. 2010. "IAP Regulation of Metastasis." *Cancer Cell* 17 (1): 53–64.

Merino, D., N. Lalaoui, A. Morizot, P. Schneider, E. Solary, and O. Micheau. 2006. "Differential Inhibition of TRAIL-Mediated DR5-DISC Formation by Decoy Receptors 1 and 2." *Molecular and Cellular Biology* 26 (19): 7046–55.

BIBLIOGRAPHY

Miguel, D. De, J. Lemke, A. Anel, H. Walczak, and L. Martinez-Lostao. 2016. "Onto Better TRAILs for Cancer Treatment." *Cell Death and Differentiation* 23 (5): 733–47.

Mirkina, Irina, Emir Hadzijusufovic, Clemens Krepler, Mario Mikula, Diana Mechtcheriakova, Sabine Strommer, Alexander Stella, et al. 2014. "Phenotyping of Human Melanoma Cells Reveals a Unique Composition of Receptor Targets and a Subpopulation Co-Expressing ErbB4, EPO-R and NGF-R." Edited by Andrzej T. Slominski. *PLoS ONE* 9 (1): e84417.

Mitsuuchi, Y, CA Benetatos, Y Deng, T Haimowitz, SC Beck, MR Arnone, GS Kapoor, et al. 2017. "Bivalent IAP Antagonists, but Not Monovalent IAP Antagonists, Inhibit TNF-Mediated NF-KB Signaling by Degrading TRAF2-Associated CIAP1 in Cancer Cells." *Cell Death Discovery* 3 (1): 16046.

Moreno-Ramirez, D., L. de la Cruz-Merino, L. Ferrandiz, R. Villegas-Portero, and A. Nieto-Garcia. 2010. "Isolated Limb Perfusion for Malignant Melanoma: Systematic Review on Effectiveness and Safety." *The Oncologist* 15 (4): 416–27.

Morgan-Lappe, Susan E. 2017. "Abstract DDT01-03: ABBV-621: A Best-in-Class TRAIL-Receptor Agonist Fusion Protein That Enhances Optimal Clustering for the Treatment of Solid and Hematologic Tumors." In *Cancer Research*, DDT01-03-DDT01-03.

Moulin, Maryline, Holly Anderton, Anne K. Voss, Tim Thomas, Wendy Wei Lynn Wong, Aleksandra Bankovacki, Rebecca Feltham, et al. 2012. "IAPs Limit Activation of RIP Kinases by TNF Receptor 1 during Development." *EMBO Journal* 31 (7): 1679–91.

Mühlenbeck, Frank, Pascal Schneider, Jean Luc Bodmer, Ralph Schwenzer, Angelika Hauser, Gisela Schubert, Peter Scheurich, Dieter Moosmayer, Jürg Tschopp, and Harald Wajant. 2000. "The Tumor Necrosis Factor-Related Apoptosis-Inducing Ligand Receptors TRAIL-R1 and TRAIL-R2 Have Distinct Cross-Linking Requirements for Initiation of Apoptosis and Are Non-Redundant in JNK Activation." *Journal of Biological Chemistry* 275 (41): 32208–13.

Nagata, Shigekazu. 2018. "Apoptosis and Clearance of Apoptotic Cells." *Annual Review of Immunology* 36 (1): 489–517.

Nath, Sritama, and Gayathri R. Devi. 2016. "Three-Dimensional Culture Systems in Cancer

Research: Focus on Tumor Spheroid Model." *Pharmacology & Therapeutics* 163: 94–108.

Neumann, Simon, Jan Hasenauer, Nadine Pollak, and Peter Scheurich. 2014. "Dominant Negative Effects of Tumor Necrosis Factor (Tnf)-Related Apoptosis-Inducing Ligand (TRAIL) Receptor 4 on TRAIL Receptor 1 Signaling by Formation of Heteromeric Complexes." *Journal of Biological Chemistry* 289 (23): 16576–87.

Nyholm, Anne Marie, Catharina M Lerche, Valentina Manfé, Edyta Biskup, Peter Johansen, Niels Morling, Birthe Mørk Thomsen, Martin Glud, and Robert Gniadecki. 2014. "MiR-125b Induces Cellular Senescence in Malignant Melanoma." *BMC Dermatology* 14 (1): 8.

O'Donoghue, Cristina, Matthew C. Perez, John E. Mullinax, Danielle Hardman, Sean Sileno, Syeda Mahrukh Hussnain Naqvi, Youngchul Kim, Ricardo J. Gonzalez, and Jonathan S. Zager. 2017. "Isolated Limb Infusion: A Single-Center Experience with Over 200 Infusions." *Annals of Surgical Oncology* 24 (13): 3842–49.

O'Mahony, Fiach C., Jyoti Nanda, Alexander Laird, Peter Mullen, Helen Caldwell, Ian M. Overton, Lel Eory, et al. 2013. "The Use of Reverse Phase Protein Arrays (RPPA) to Explore Protein Expression Variation within Individual Renal Cell Cancers." *Journal of Visualized Experiments*, no. 71: pii:50221.

Obexer, Petra, and Michael J. Ausserlechner. 2014. "X-Linked Inhibitor of Apoptosis Protein - A Critical Death Resistance Regulator and Therapeutic Target for Personalized Cancer Therapy." *Frontiers in Oncology* 4: 197.

Özören, Nesrin, and Wafik S. El-Deiry. 2002. "Defining Characteristics of Types I and II Apoptotic Cells in Response to TRAIL." *Neoplasia* 4 (6): 551–57.

Pan, Guohua, Karen O'Rourke, Arul M. Chinnaiyan, Reiner Gentz, Reinhard Ebner, Jian Ni, and Vishva M. Dixit. 1997. "The Receptor for the Cytotoxic Ligand TRAIL." *Science* 276 (5309): 111–13.

Passante, Egle, Maximilian L. Würstle, Christian T Hellwig, Martin Leverkus, and Markus Rehm. 2013. "Systems Analysis of Apoptosis Protein Expression Allows the Case-Specific Prediction of Cell Death Responsiveness of Melanoma Cells." *Cell Death and*

Differentiation 20 (11): 1521–31.

Pauli, Chantal, Benjamin D. Hopkins, Davide Prandi, Reid Shaw, Tarcisio Fedrizzi, Andrea Sboner, Verena Sailer, et al. 2017. "Personalized in Vitro and in Vivo Cancer Models to Guide Precision Medicine." *Cancer Discovery* 7 (5): 462–77.

Pyzik, Michal, Timo Rath, Wayne I. Lencer, Kristi Baker, and Richard S. Blumberg. 2015. "FcRn: The Architect Behind the Immune and Nonimmune Functions of IgG and Albumin." *The Journal of Immunology* 194 (10): 4595–4603.

Raisova, Monika, Amir M. Hossini, Jürgen Eberle, Christian Riebeling, Thomas Wieder, Isrid Sturm, Peter T. Daniel, Constantin E. Orfanos, and Christoph C. Geilen. 2001. "The Bax/Bcl-2 Ratio Determines the Susceptibility of Human Melanoma Cells to CD95/Fas-Mediated Apoptosis." *Journal of Investigative Dermatology* 117 (2): 333–40.

Rana, Brinda K., David Hewett-Emmett, Li Jin, Benny H.J. Chang, Naymkhishing Sambuughin, Marie Lin, Scott Watkins, et al. 1999. "High Polymorphism at the Human Melanocortin 1 Receptor Locus." *Genetics* 151 (4): 1547–57.

Rehm, Markus, Heinrich J Huber, Heiko Dussmann, and Jochen H M Prehn. 2006. "Systems Analysis of Effector Caspase Activation and Its Control by X-Linked Inhibitor of Apoptosis Protein." *The EMBO Journal* 25 (18): 4338–49.

Reid, Penny, and Ingunn Holen. 2009. "Pathophysiological Roles of Osteoprotegerin (OPG)." *European Journal of Cell Biology* 88 (1): 1–17.

Roshal, M., Y. Zhu, and V. Planelles. 2001. "Apoptosis in AIDS." *Apoptosis* 6 (1–2): 103–16.

Roskoski, Robert. 2018. "Targeting Oncogenic Raf Protein-Serine/Threonine Kinases in Human Cancers." *Pharmacological Research* 135: 239–58.

Rožanc, Jan, Theodore Sakellaropoulos, Asier Antoranz, and Cristiano Guttà. 2018. "Phosphoprotein Patterns Predict Trametinib Responsiveness and Optimal Trametinib Sensitization Strategies in Melanoma." *Cell Death & Differentiation* 26: 1365–1378.

Schleich, Kolja, J. H. Buchbinder, S. Pietkiewicz, T. Kähne, U. Warnken, S. Öztürk, M. Schnölzer, M. Naumann, P. H. Krammer, and I. N. Lavrik. 2016. "Molecular Architecture of the DED Chains at the DISC: Regulation of Procaspase-8 Activation by Short DED

Proteins c-FLIP and Procaspase-8 Prodomain." *Cell Death and Differentiation* 23 (4): 681–94.

Schleich, Kolja, and Inna N. Lavrik. 2013. "Mathematical Modeling of Apoptosis." *Cell Communication and Signaling* 11 (1): 44.

Schneider, B., S. Münkel, A. Krippner-Heidenreich, I. Grunwald, W. S. Wels, H. Wajant, K. Pfizenmaier, and J. Gerspach. 2010. "Potent Antitumoral Activity of TRAIL through Generation of Tumor-Targeted Single-Chain Fusion Proteins." *Cell Death and Disease* 1 (8).

Schreuer, Max, Yanina Jansen, Simon Planken, Ines Chevolet, Teofila Seremet, Vibeke Kruse, and Bart Neyns. 2017. "Combination of Dabrafenib plus Trametinib for BRAF and MEK Inhibitor Pretreated Patients with Advanced BRAFV600-Mutant Melanoma: An Open-Label, Single Arm, Dual-Centre, Phase 2 Clinical Trial." *The Lancet Oncology* 18 (4): 464–72.

Scott, Fiona L., Jean Bernard Denault, Stefan J. Riedl, Hwain Shin, Martin Renatus, and Guy S. Salvesen. 2005. "XIAP Inhibits Caspase-3 and -7 Using Two Binding Sites: Evolutionary Conserved Mechanism of IAPs." *EMBO Journal* 24 (3): 645–55.

Seifert, O., A. Plappert, S. Fellermeier, M. Siegemund, K. Pfizenmaier, and R. E. Kontermann. 2014. "Tetravalent Antibody-ScTRAIL Fusion Proteins with Improved Properties." *Molecular Cancer Therapeutics* 13 (1): 101–11.

Serrone, L, M Zeuli, F M Sega, and F Cognetti. 2000. "Dacarbazine-Based Chemotherapy for Metastatic Melanoma: Thirty-Year Experience Overview." *Journal of Experimental & Clinical Cancer Research : CR* 19 (1): 21–34.

Shannan, Batool, Michela Perego, Rajasekharan Somasundaram, and Meenhard Herlyn. 2016. "Heterogeneity in Melanoma." In *Cancer Treatment and Research*, 167:1–15.

Shaw, Tanya J., Eric C. Lacasse, Jon P. Durkin, and Barbara C. Vanderhyden. 2008. "Downregulation of XIAP Expression in Ovarian Cancer Cells Induces Cell Death in Vitro and in Vivo." *International Journal of Cancer* 122 (6): 1430–34.

Shojaei, Hamed, Hans Heinrich Oberg, Matthias Juricke, Lothar Marischen, Monika Kunz,

Christoph Mundhenke, Frank Gieseler, Dieter Kabelitz, and Daniela Wesch. 2009. "Toll-like Receptors 3 and 7 Agonists Enhance Tumor Cell Lysis by Human Γσ T Cells." *Cancer Research* 69 (22): 8710–17.

Silke, John, and Pascal Meier. 2013. "Inhibitorofapoptosis(IAP)Proteins-Modulators of Cell Death and Inflammation." *Cold Spring Harbor Perspectives in Biology* 5 (2).

Soares, Daniele de Almeida, Claes von Hofsten, and Eloisa Tudella. 2012. "Development of Exploratory Behavior in Late Preterm Infants." *Infant Behavior and Development* 35 (4): 912–15.

Spencer, Sabrina L., and Peter K. Sorger. 2011. "Measuring and Modeling Apoptosis in Single Cells." *Cell* 144 (6): 926–39.

Srinivasula, Srinivasa M., Ramesh Hegde, Ayman Saleh, Pinaki Datta, Eric Shiozaki, Jijie Chai, Ryung Ah Lee, et al. 2001. "A Conserved XIAP-Interaction Motif in Caspase-9 and Smac/DIABLO Regulates Caspase Activity and Apoptosis." *Nature* 410 (6824): 112–16.

Sun, Haiying, Jianfeng Lu, Liu Liu, Chao Yie Yang, and Shaomeng Wang. 2014. "Potent and Selective Small-Molecule Inhibitors of CIAP1/2 Proteins Reveal That the Binding of Smac Mimetics to XIAP BIR3 Is Not Required for Their Effective Induction of Cell Death in Tumor Cells." *ACS Chemical Biology* 9 (4): 994–1002.

Sun, Shao-Cong. 2011. "Non-Canonical NF-KB Signaling Pathway." *Cell Research* 21 (1): 71–85.

Sun, Shao-Cong. 2017. "The Non-Canonical NF-KB Pathway in Immunity and Inflammation." *Nature Reviews Immunology* 17 (9): 545–58.

Szadvari, I., O. Krizanova, and P. Babula. 2016. "Athymic Nude Mice as an Experimental Model for Cancer Treatment." *Physiological Research* 65 (Supplementum 4): S441–53.

Thayaparasingham, B., A. Kunz, and D. Kulms. 2009. "Sensitization of Melanoma Cells to TRAIL by UVB-Induced and NF-KB-Mediated Downregulation of XIAP." *Oncogene* 28 (3): 345–62.

Tian, Fang, and Sam W. Lee. 2010. "X-Linked Inhibitor of Apoptosis Protein as a Therapeutic Target in Metastatic Melanoma." *Journal of Investigative Dermatology* 130 (9): 2169–

72.

Trisciuoglio, Daniela, Maria Grazia Tupone, Marianna Desideri, Marta Di Martile, Chiara Gabellini, Simonetta Buglioni, Matteo Pallocca, Gabriele Alessandrini, Simona D'Aguanno, and Donatella Del Bufalo. 2017. "BCL-XL Overexpression Promotes Tumor Progression-Associated Properties." *Cell Death & Disease* 8 (12): 3216.

Tsuchiya, Yuichi, Osamu Nakabayashi, and Hiroyasu Nakano. 2015. "FLIP the Switch: Regulation of Apoptosis and Necroptosis by CFLIP." *International Journal of Molecular Sciences* 16 (12): 30321–41.

Tuthill, M. H., A. Montinaro, J. Zinngrebe, K. Prieske, P. Draber, S. Prieske, T. Newsom-Davis, S. Von Karstedt, J. Graves, and H. Walczak. 2014. "TRAIL-R2-Specific Antibodies and Recombinant TRAIL Can Synergise to Kill Cancer Cells." *Oncogene* 34 (16): 2138–44.

Tutuka, Candani S. A., Miles C. Andrews, John M. Mariadason, Paul Ioannidis, Christopher Hudson, Jonathan Cebon, and Andreas Behren. 2017. "PLX8394, a New Generation BRAF Inhibitor, Selectively Inhibits BRAF in Colonic Adenocarcinoma Cells and Prevents Paradoxical MAPK Pathway Activation." *Molecular Cancer* 16 (1): 112.

Venturini, Marina, Paola Pasquali, Azael Freites-Martinez, Arianna Zanca, Piergiacomo Calzavara Pinton, and Salvador González. 2017. "Monitoring of Noninvasive Treatment of Basal Cell Carcinoma." In *Reflectance Confocal Microscopy of Cutaneous Tumors, Second Edition*, 496–512.

Verma, Vivek, Tanja Sprave, Waqar Haque, Charles B. Simone, Joe Y. Chang, James W. Welsh, and Charles R. Thomas. 2018. "A Systematic Review of the Cost and Cost-Effectiveness Studies of Immune Checkpoint Inhibitors." *Journal for ImmunoTherapy of Cancer* 6 (1): 128.

Vetma, Vesna, Jan Rožanc, Emilie M Charles, Christian T Hellwig, Leonidas G Alexopoulos, and Markus Rehm. 2017. "Examining the In Vitro Efficacy of the IAP Antagonist Birinapant as a Single Agent or in Combination With Dacarbazine to Induce Melanoma Cell Death." *Oncology Research Featuring Preclinical and Clinical Cancer Therapeutics* 25 (9): 1489–94.

Vörsmann, H, F Groeber, H Walles, S Busch, S Beissert, H Walczak, and D Kulms. 2013.

"Development of a Human Three-Dimensional Organotypic Skin-Melanoma Spheroid Model for in Vitro Drug Testing." *Cell Death and Disease* 4 (7): e719.

Wagner, L., V. Marschall, S. Karl, S. Cristofanon, K. Zobel, K. Deshayes, D. Vucic, K. M. Debatin, and S. Fulda. 2013. "Smac Mimetic Sensitizes Glioblastoma Cells to Temozolomide-Induced Apoptosis in a RIP1- and NF-KB-Dependent Manner." *Oncogene* 32 (8): 988–97.

Wajant, H. 2015. "Principles of Antibody-Mediated TNF Receptor Activation." *Cell Death and Differentiation* 22 (11): 1727–41.

Walczak, Henning, Robert E. Miller, Kiley Ariail, Brian Gliniak, Thomas S. Griffith, Marek Kubin, Wilson Chin, et al. 1999. "Tumoricidal Activity of Tumor Necrosis Factor-Related Apoptosis-Inducing Ligand in Vivo." *Nature Medicine* 5 (2): 157–63.

Waterhouse, Nigel J., Joshua C. Goldstein, Oliver Von Ahsen, Martin Schuler, Donald D. Newmeyer, and Douglas R. Green. 2001. "Cytochrome c Maintains Mitochondrial Transmembrane Potential and ATP Generation after Outer Mitochondrial Membrane Permeabilization during the Apoptotic Process." *Journal of Cell Biology* 153 (2): 319–28.

Werner, Thomas A., Inga Nolten, Levent Dizdar, Jasmin C. Riemer, Sina C. Schütte, Pablo E. Verde, Katharina Raba, Matthias Schott, Wolfram T. Knoefel, and Andreas Krieg. 2018. "IAPs Cause Resistance to TRAIL-Dependent Apoptosis in Follicular Thyroid Cancer." *Endocrine-Related Cancer* 25 (3): 295–308.

Weyhenmeyer, Birgit C., Janis Noonan, Maximilian L. Würstle, Frank A. Lincoln, Grainne Johnston, Markus Rehm, and Brona M. Murphy. 2016. "Predicting the Cell Death Responsiveness and Sensitization of Glioma Cells to TRAIL and Temozolomide." *Oncotarget* 7 (38): 61295–311.

Wong, Rebecca S.Y. 2011. "Apoptosis in Cancer: From Pathogenesis to Treatment." *Journal of Experimental and Clinical Cancer Research* 30 (1): 87.

Wroblewski, David, Branka Mijatov, Nethia Mohana-Kumaran, Fritz Lai, Stuart J. Gallagher, Nikolas K. Haass, Xu Dong Zhang, and Peter Hersey. 2013. "The BH3-Mimetic ABT-737 Sensitizes Human Melanoma Cells to Apoptosis Induced by Selective BRAF Inhibitors but Does Not Reverse Acquired Resistance." *Carcinogenesis* 34 (2): 237–47.

BIBLIOGRAPHY

Xi, Yaguang, Adam Riker, Lalita Shevde-Samant, Rajeev Samant, Christopher Morris, Elaine Gavin, Oystein Fodstad, and Jingfang Ju. 2008. "Global Comparative Gene Expression Analysis of Melanoma Patient Samples, Derived Cell Lines and Corresponding Tumor Xenografts." *Cancer Genomics and Proteomics* 5 (1): 1–35.

Yadav, Deepak, Jennifer Ngolab, Rod Seung-Hwan Lim, Siddharth Krishnamurthy, and Jack D Bui. 2009. "Cutting Edge: Down-Regulation of MHC Class I-Related Chain A on Tumor Cells by IFN-γ-Induced MicroRNA." *The Journal of Immunology* 182 (1): 39–43.

https://www.expasy.org/

https://cancer.sanger.ac.uk/cosmic

https://www.atcc.org/

List of Figures

List of Tables

Acknowledgments

I would like to thank all of you for being a part of my PhD journey, in one way or another.

First, I'd like to thank Markus for giving me the opportunity to do this project within the Melplex consortium. You were a great supervisor and I have learned a lot from you. Thanks for your guidance and patience. Also, thanks to Dagmar for being my supervisor during the secondment in Dresden, and especially thanks for cell lines provided for this project and the knowledge about 3D cell culturing. Thanks to Roland, my third Melplex supervisor, for immensely helping me with animal work and production and purification of the ligand.

Melplex, my second scientific family, thanks for all the good moments, friendship and support. Especially thanks to Cristiano for helping me with this project, Jan–for being my co-author and Biswa – for being everyday Melplex support in the lab.

Many thanks to Dani and Cathrin for their help with this thesis, I truly appreciate it. I would also like to thank Alex and Bea from Tierhaltung and Oli and Nadine for teaching me and helping with mouse work. Thanks to all the members of the Rehm/Morrison group, both in Dublin and Stuttgart, for being wonderful companions throughout this PhD.

And now the muggles...

I would like to thank my pole teachers and friends in Stuttgart and Dublin for keeping me in accordance with the saying „Mens sana in corpore sano". You played an important role in this PhD by motivating me and pushing my physical limits. There was no better way to complement the hard work done in the lab. Thanks for being wonderful friends. I am very lucky to have met you!

Napokon, hvala mojim najdražima, Marija, Željka, Frane, Alen, Mirna, Katja, Adrijana, Kruno, na dubokoumnim razgovorima, malo manje dubokoumnim razgovorima, znanstvenim i životnim raspravama, usklađivanju aviona i rasporeda u cilju dijasporskih druženja, ispijenim kavama i pivama. Sve znate! Hvala i mojim Trogirkama, Marijani, Marti, Ivani Č.Š. i Ivani V. za podršku i cjeloživotno prijateljstvo koje je ostalo i unatoč tome što ne živimo ni u istoj državi, a kamoli u istom gradu. Najveće hvala mojoj obitelji, mami Albini, ocu Andru, bratu

ACKNOWLEDGMENTS

Erklärung

Hiermit erkläre ich, dass die vorliegende Arbeit von mir persönlich ohne unrechtmäßige Hilfe angefertigt wurde. Verwendete Daten, Grafiken und Informationen, die nicht von mir stammen wurden entsprechend gekennzeichnet.

Declaration

I hereby declare, that this thesis was prepared by myself without illegal help. Where information has been derived from other sources, I confirm that this has been elucidated in the thesis.

Vesna Vetma

Publications, courses, conference contributions, secondments

Publications

Vetma, Vesna, Jan Rožanc, Emilie M Charles, Christian T Hellwig, Leonidas G Alexopoulos, and Markus Rehm. 2017. "Examining the In Vitro Efficacy of the IAP Antagonist Birinapant as a Single Agent or in Combination With Dacarbazine to Induce Melanoma Cell Death." *Oncology Research Featuring Preclinical and Clinical Cancer Therapeutics* 25 (9): 1489–94.

Rožanc J, Sakellaropoulos T, Antoranz A, Gutta C, Podder B, **Vetma V**, Rufo N, Agostinis P, Pliaka V, Sauter T, Kulms D, Rehm M, Alexopoulos LG. 2018. 'Phosphoprotein Patterns Predict Trametinib Responsiveness and Optimal Trametinib Sensitization Strategies in Melanoma'. *Cell Death & Differentiation* 26: 1365–1378.

(in print) **Vetma V**, Gutta C, Peters N, Praetorius C, Hutt M, Meier F, Kontermann R, Kulms D, Rehm M. Convergence of pathway analysis and pattern recognition predicts sensitization to latest generation TRAIL therapeutics by IAP antagonism. *Cell Death and Differentiation*

Conferences

12th PhD Workshop on Molecular Mechanisms and Therapeutic Approaches in Cancer, Freudenstadt, Germany (09/2018)

Poster: Data-driven modelling predicts responsiveness to TRAIL/SMAC mimetic combinations in malignant melanoma

11th European Workshop in Cell death (EWCD), Fiuggi, Italy (05/2018)
Poster: Data-driven modelling predicts responsiveness to TRAIL/SMAC mimetic combinations in malignant melanoma

11th PhD Workshop on Molecular Mechanisms and Therapeutic Approaches in Cancer, Freudenstadt, Germany (09/2017)

Talk: Development and validation of tools that can predict cell death induced by 2nd generation TRAIL ligand

10th European Workshop in Cell death (EWCD), Fiuggi, Italy (04/2016)
Poster: Examining the efficacy of DTIC/Birinapant and IZI1551/Birinapant combination treatments in melanoma cell lines
5th Irish Melanoma Forum, Dublin, Ireland (12/2015)
Abstract: Examining the efficacy of DTIC and Birinapant in melanoma cell lines

Courses

Commercialisation Bootcamp (10/2017), University College Dublin (UCD), Dublin, Ireland

Quantitative Biophotonics for Translational Systems Biology (01/2017), Danish Cancer Society, Copenhagen, Denmark

Summer school "Putting your research into context" (07/2016), King's College London (KCL), London, UK

Transferable skills course (Biomedical writing, Conflict Management, Statistics in Biomedical Research, Gender balance in Science; 05/2016), Katholieke Universiteit Leuven (KUL), Leuven, Belgium

Workshop in Systems Biology and Systems Medicine (10/2016), University of Luxembourg, Luxembourg

Innovative approaches in Translational Melanoma Research (05/2015), Royal College of Surgeons in Ireland (RCSI), Dublin, Ireland

Secondments

04/2015 – 05/2016 Royal College of Surgeons in Ireland, Dublin, Ireland
Group: Prof. Dr. Markus Rehm

05/2016-11/2016 Centre for Regenerative therapies, TU Dresden, Dresden, Germany
Group: Prof. Dr. Dagmar Kulms